INFORMATION TO USERS

This manuscript has been reproduced from the microfilm master. UMI films the text directly from the original or copy submitted. Thus, some thesis and dissertation copies are in typewriter face, while others may be from any type of computer printer.

The quality of this reproduction is dependent upon the quality of the copy submitted. Broken or indistinct print, colored or poor quality illustrations and photographs, print bleedthrough, substandard margins, and improper alignment can adversely affect reproduction.

In the unlikely event that the author did not send UMI a complete manuscript and there are missing pages, these will be noted. Also, if unauthorized copyright material had to be removed, a note will indicate the deletion.

Oversize materials (e.g., maps, drawings, charts) are reproduced by sectioning the original, beginning at the upper left-hand corner and continuing from left to right in equal sections with small overlaps.

Photographs included in the original manuscript have been reproduced xerographically in this copy. Higher quality 6" x 9" black and white photographic prints are available for any photographs or illustrations appearing in this copy for an additional charge. Contact UMI directly to order.

Bell & Howell Information and Learning
300 North Zeeb Road, Ann Arbor, MI 48106-1346 USA
800-521-0600

UMI®

PROPERTIES OF LIGHT MESONS IN A GENERALIZED NAMBU – JONA-LASINIO MODEL

By

BO HUANG

A dissertation submitted to the Graduate Faculty in Physics in partial fulfillment of the requirements for the degree of Doctor of Philosophy, The City University of New York

2000

This manuscript has been read and accepted for the Graduate Faculty in Physics in satisfaction of the dissertation requirement for the degree of Doctor of Philosophy.

12/16/99
Date

Chair of Examining Committee

12/16/99
Date

Executive Officer

Carl M. Shakin

Louis S. Celenza

Ming-Kung Liou

Peter Lesser

V Parameswaran Nair

Supervisory Committee

The City University of New York

Abstract

PROPERTIES OF LIGHT MESONS IN A GENERALIZED NAMBU – JONA-LASINIO MODEL

By

BO HUANG

Advisor: Distinguished Professor Carl M. Shakin

We present results for the spectra and other properties of a full range of light mesons making use of a generalized Nambu – Jona-Lasinio (NJL) model that includes a covariant model of confinement. Since the model also exhibits chiral symmetry, there is no difficulty in treating the pseudoscalar octet of mesons. Like other effective theories, the NJL model is not renormalizable. Therefore, we also describe the regularization schemes used in our work. We discuss the calculation of the leading vacuum polarization functions of order n_c, as well as functions of order 1 that describe decay to various two meson continuum channels. The calculation of the latter set of functions requires methods for the calculation of quark loops with three vertices. We describe how such calculations may be made in a fully covariant manner.

Acknowledgements

To Professor Carl M. Shakin, my thesis advisor, I wish to express my deepest gratitude for his valuable guidance and constant encouragement throughout this thesis work.

I would also like to express my sincere gratitude to Professor Louis S. Celenza of Brooklyn College of CUNY for many useful discussion and for help given to me during the course of this work.

My thanks also go to Mr. Huangsheng Wang for the help given to me during the course of this work.

I wish to acknowledge with gratitude the Department of Physics of Brooklyn College and the Research Foundation of CUNY for the financial support during the course of this work, and the Brooklyn College Computer Center for allowing me to use their facilities.

CONTENTS

List of Tables

List of Figures

Chapter 1

Introduction

This dissertation deals with the development and application of a model that may be used to study the spectra of all light mesons. The model is based upon that of Nambu – Jona-Lasinio (NJL) model, supplemented by a covariant model of confinement. Therefore, the model features chiral symmetry, confinement and covariance. We have also developed methods for the calculation of meson decay amplitudes at one (quark) loop order.

In the second chapter we discuss the scalar, vector, pseudoscalar, axial-vector nonets and calculate the various spectra up to about 2 GeV in energy. That in itself is a great improvement over the NJL model without confinement, since that model is limited to energies less than about 700 MeV. (The functions calculated in the standard NJL model exhibit spurious singularities when the quark and antiquark go on mass shell. These singularities appear if the energy is greater than twice the constituent quark mass. Our technique eliminates such singularities.) As we will see the model exhibits predictive power even though a number of parameters must be specified.

In the third chapter we consider the f_2 tensor meson. Here we have to extend the interactions of the NJL model to include terms that contain gradients of the quark field. Our results are quite successful in reproducing the main features of the spectrum

of these mesons.

The most challenging project is that discussed in Chapter 4, where we consider the properties of the scalar-isoscalar f_0 mesons. Satisfactory results are obtained for the spectrum and some insight is gained with respect to the $f_0(400\text{-}1200)$ resonance, which may be described, in part, as a complex threshold effect due to the rapid opening of the $\pi\pi$ and $K\bar{K}$ decay channels. (Another feature needed when we attempt to understand the nature of the $f_0(400\text{-}1200)$ is a consideration of the t-channel ρ exchange, although we do not discuss that matter here.)

Chapter 2

Covariant Confinement Model for the Study of the Properties of Light Mesons

2.1 Introduction

In a number of recent works [1-5] we have been developing a relativistic quark model that includes a covariant model of confinement. The Lagrangian of the model is

$$\begin{aligned}\mathcal{L} = \bar{q}\,(i\partial\!\!\!/ - m^0)q + \frac{G_S}{2}\sum_{i=0}^{8}\left[(\bar{q}\lambda^i q)^2 + (\bar{q}i\gamma_5\lambda^i q)^2\right] \\ -\frac{G_V}{4}\sum_{i=0}^{8}\left[(\bar{q}\gamma^\mu\lambda^i q)^2 + (\bar{q}\gamma^\mu\gamma_5\lambda^i q)^2\right] + \mathcal{L}_{conf}\ ,\end{aligned} \tag{2.1.1}$$

where $\mathcal{L}_{conf}$ denotes our model of confinement. In Eq.(2.1.1) m^0 is the current quark mass matrix, $m^0 = \mathrm{diag}(m_u^0, m_d^0, m_s^0)$, the $\lambda_i\,(i = 1, \ldots 8)$ are the Gell-Mann matrices, and $\lambda_0 = \sqrt{2/3}\,\mathbf{I}$, with $\mathbf{I}$ being the unit matrix in flavor space. In some calculations we have supplemented the Lagrangian of Eq.(2.1.1) with the 't Hooft interaction [6]. We remark that in the absence of our model of confinement, our Lagrangian is that of the Nambu – Jona-Lasinio (NJL) model [6].

In Ref.[1], we studied $\omega - \phi$ and $\eta - \eta'$ mixing and the radial excitations of these mesons. Reference [2] was concerned with the radial excitations of the pion and

included a detailed treatment of $\pi - a_1$ mixing. Application was made to the decay of the $\pi(1300)$ to the $\pi + \sigma$ and $\pi + \rho$ channels. Reference [3] concerned the form of the T matrices of our model. With the confinement model in place, it was shown that the T matrix is represented only in terms of bound states, as might be expected. That work also contains a rather detailed discussion of meson-quark vertex functions of the confining model in the presence of singlet-octet and pseudoscalar – axial-vector mixing. In references [4] and [5] we calculated the rates for the decays $\pi^0 \to \gamma\,\gamma$, $\eta \to \gamma\,\gamma$ and $\eta' \to \gamma\,\gamma$ with satisfactory results. In the present study we extend our analysis to the strange mesons, which requires that we consider quarks and antiquarks of different constituent mass.

Chapter 2 is organized as follows. In Section 2.2 we comment on our treatment confinement. In Section 2.3 we discuss the pseudoscalar nonet. In Section 2.4, we provide a short discussion concerning the choice of parameters made for this chapter. In Section 2.5 we discuss the vector nonet of states, using ideal mixing for the ϕ and ω mesons. In Section 2.6, we consider the scalar nonet of states and in Section 2.7 we describe the ${}^3P_1$ and ${}^1P_1$ nonets of axial-vector mesons and ${}^3P_1$ - ${}^1P_1$ mixing, as that mixing appears in the NJL model. Since the standard NJL interaction hardly affects ${}^1P_1$ states, in Section 2.8 we consider an extended NJL model, with an additional chirally-symmetric interaction that acts in ${}^1P_1$ states. Finally, Section 2.9 contains some further discussion and conclusions.

2.2 Model of Confinement

In this chapter we will calculate a number of vertex functions that sum a "ladder" of confining interaction. [For example, see Eq.(2.3.4).] For Euclidean-space calculations we may write

$$\mathcal{L}_{conf}(x) = \int d^4y\, \bar{q}(x)\,\gamma^\mu\, q(x)\, V^C(x-y)\, \bar{q}(y)\,\gamma_\mu\, q(y) \qquad (2.2.1)$$

where, in momentum-space, V^C describes four-momentum transfer. However, for the Minkowski-space calculations, we find it useful to neglect energy transfer by the confining field in the meson rest frame. For example, if we start with $V^C(r) = \kappa\, r \exp[-\mu r]$ and form the Fourier transform, we have

$$V^C(\vec{k}-\vec{k}') = -8\pi\kappa \left[\frac{1}{\left[(\vec{k}-\vec{k}')^2+\mu^2\right]^2} - \frac{4\mu^2}{\left[(\vec{k}-\vec{k}')^2+\mu^2\right]^3} \right] . \qquad (2.2.2)$$

Here μ is a small parameter used to soften the infrared singularities of V^C. If μ is small enough, the potential approximates a linear potential with "string tension" κ over the range of r relevant to our problem. The potential of Eq.(2.2.2) may be put in a covariant form [2], if we use the four-vectors $\hat{k}^\mu$ and $\hat{k}'^\mu$, where

$$\hat{k}^\mu(P) = k^\mu - \frac{(k\cdot P)\, P^\mu}{P^2} \quad , \qquad (2.2.3a)$$

and

$$\hat{k}'^{\mu}(P) = k'^{\mu} - \frac{(k'\cdot P)\,P^{\mu}}{P^2} \quad . \tag{2.2.3b}$$

since, when $\vec{P} = 0$, we have $\hat{k}^{\mu} = [0\,,\ \vec{k}]$ and $\hat{k}'^{\mu} = [0\,,\ \vec{k}']$.

The calculation of confining vertex functions using Eq.(2.2.2), and the calculation of vacuum polarization integrals that incorporate such vertex functions, is described in detail in Refs.[1-5] and in Chapter 4. The reader who is particularly interested in a detailed description of the calculation of polarization functions, including confinement vertex functions, may wish to read Section 4.2 and 4.3 before reading the next section.

2.3 The Pseudoscalar Nonet

Since we have studied the radial excitations of the pion, including pseudoscalar – axial-vector mixing, in some detail [2], we only comment upon the results here. In the confining field, considered in isolation, we find a series of doublets. One state of each doublet corresponds to the pseudoscalar vertex $i\gamma^5$ and the other corresponds to the axial-vector vertex $\gamma^0\gamma^5$, when $\vec{P} = 0$. When we include the NJL interaction, one member of each doublet moves down in energy. The member of each doublet that moves down in energy to the greatest degree shows little mixing and can be identified as either the $\pi(1S)$, the $\pi(2S)$, or the $\pi(3S)$ state. The other three states exhibit significant mixing. (The details of our calculation for the pion and its

radial-excitations are given in Ref.[2].) For the results of the calculations made in this work, see Table 1 and Fig.1.

In Ref.[1] we studied $\eta - \eta'$ mixing and the radial excitations of that system of states. In that case, we included both singlet-octet and pseudoscalar – axial-vector mixing, leading to the study of quark T matrices of dimension four. The general form of the equation for the T matrix is

$$(1 - GJ)T = -G \quad . \tag{2.3.1}$$

The form of the matrices G and J may be found in the Appendix of Ref.[7]. (Note, however, that the sign of our functions $J^{PA}(P^2)$ and $J^{AA}(P^2)$ is the opposite of that used in Ref.[7].) The T matrix of Eq.(2.3.1) has singularities at the energies of the bound states of the quark and antiquark. In Fig.2 we show the eigenvalue of the T matrix with the largest magnitude that is found at each value of P^2. (The calculations here differ from those of Ref.[1], since we now use $m_s = 565$ MeV, rather than the value 480 MeV used in that work. We have also used $\mu = 0.01$ GeV rather than the value $\mu = 0.02$ GeV used previously.) In Fig.2 we see ten states below 2.0 GeV. The mass values of these states are shown in Fig.1 as dotted lines. The calculated energies are 0.551, 1.039, 1.204, 1.406, 1.530, 1.543, 1.726, 1.749, 1.803 and 1.819 in GeV units. We have used $G_S = 12.46$ GeV^{-2} for the strength of the interaction in the octet states and $G_S - \delta$ for the strength in the singlet states. Here we use $\delta = 2.0$ GeV^{-2}, rather than the value of 4.0 GeV^{-2} used in Ref.[1]. (Details of these calculations may be found in that reference.)

We now turn to a study of the K meson. In this case, we have not included pseudoscalar – axial-vector mixing, so that we only have to generalize our calculations of the vertex functions and polarization functions, $\bar{\Gamma}_5(P, k)$ and $J^{PP}(P^2)$, to the case of different mass values for the up, down and strange quarks. (Here, we take $m_u = m_d$.) To carry out this program, we define

$$\Lambda_a^{(+)}(\vec{k}) = \frac{\not{k}_a + m_a}{2 m_a} \quad , \tag{2.3.2}$$

and

$$\Lambda_b^{(-)}(-\vec{k}) = \frac{\not{\tilde{k}}_b + m_b}{2 m_b} \quad , \tag{2.3.3}$$

with $k_a^\mu = [E_a(\vec{k}), \vec{k}]$ and $\tilde{k}_b^\mu = [-E_b(\vec{k}), \vec{k}]$. Here $E_a(\vec{k}) = [\vec{k}^2 + m_a^2]^{1/2}$, etc. The vertex function for pseudoscalar mesons is given by the equation

$$\bar{\Gamma}_{5,ab}(P,k) = \gamma_5 - i\int \frac{d^4k'}{(2\pi)^4}\left[\gamma^\rho S_a(P/2+k')\bar{\Gamma}_{5,ab}(P,k')S_b(-P/2+k')\gamma_\rho\right] \times V^C(k-k') \quad , \tag{2.3.4}$$

where $S_a(P) = [\not{P} - m_a + i\epsilon]^{-1}$, etc. The analysis proceeds by multiplying Eq.(2.3.4) from the left by $\gamma_5 \Lambda_a^{(+)}(\vec{k})$ and from the right by $\Lambda_b^{(-)}(-\vec{k})$ and forming the trace. If we neglect coupling between $\Gamma^{+-}_{5,ab}$ and $\Gamma^{-+}_{5,ab}$, we find

$$\Gamma^{+-}_{5,ab}(P^0, |\vec{k}|) = 1 - \int \frac{d^3k'}{(2\pi)^3} \frac{B(\vec{k},\vec{k}')\Gamma^{+-}_{5,ab}(P^0, |\vec{k}'|)V^C(\vec{k}-\vec{k}')}{P^0 - E_a(\vec{k}') - E_b(\vec{k}')} \quad , \tag{2.3.5}$$

with

$$
\begin{aligned}
B(\vec{k},\,\vec{k}') = {} & \frac{1}{2E_a(\vec{k}')E_b(\vec{k}')\,[\,m_a m_b + E_a(\vec{k})\,E_b(\vec{k}) + \vec{k}^{\,2}\,]} \\
& \times \{\, m_a m_b\,[\,E_a(\vec{k})E_b(\vec{k}') + E_b(\vec{k})\,E_a(\vec{k}') + 2\,\vec{k}\cdot\vec{k}' \\
& - 2E_a(\vec{k}')\,E_b(\vec{k}') - 2E_a(\vec{k})E_b(\vec{k}) - 2\vec{k}^{\,2} - 2\vec{k}'^{\,2}\,] \\
& + m_b^2\,[\,E_a(\vec{k})\,E_a(\vec{k}') - \vec{k}\cdot\vec{k}'\,] \\
& + m_a^2\,[E_b(\vec{k})E_b(\vec{k}') - \vec{k}\cdot\vec{k}'] \\
& - 2\,[(E_a(\vec{k})\,E_b(\vec{k}) + \vec{k}^{\,2})\,(E_a(\vec{k}')E_b(\vec{k}') + \vec{k}'^{\,2}\,] \\
& - 2\,m_a^2\,m_b^2\,\}\quad .
\end{aligned}
\tag{2.3.6}
$$

Note that $\Gamma^{-+}_{5,ab}(P,\,k)$ satisfies the equation

$$
\Gamma^{-+}_{5,ab}(P^0,\,|\vec{k}|) = 1 - \int \frac{d^3k'}{(2\pi)^3}\,\frac{B(\vec{k},\,\vec{k}')\Gamma^{-+}_{5,ab}(P^0,\,|k'|)\,V^C(\vec{k}-\vec{k}')}{P^0 + E_a(\vec{k}') + E_b(\vec{k}')}\ , \tag{2.3.7}
$$

These equations are much simpler when $m_a = m_b$. In that case, we have

$$
\begin{aligned}
\Gamma^{+-}_5(P^0,\,|\vec{k}|) = 1 - \int \frac{d^3k'}{(2\pi)^3}\,\left[\frac{m^2 - 2E(\vec{k})\,E(\vec{k}')}{E(\vec{k})\,E(\vec{k}')}\right] \\
\times \frac{\Gamma^{+-}_5(P^0,\,|\vec{k}'|)\,V^C(\vec{k}-\vec{k}')}{P^0 - 2E(\vec{k}')}\ ,
\end{aligned}
\tag{2.3.8}
$$

and

$$\Gamma_5^{-+}(P^0, |\vec{k}|) = 1 + \int \frac{d^3k'}{(2\pi)^3} \left[\frac{m^2 - 2E(\vec{k})E(\vec{k}')}{E(\vec{k})E(\vec{k}')} \right] \times \frac{\Gamma_5^{-+}(P^0, |\vec{k}'|) V^C(\vec{k}-\vec{k}')}{P^0 + E(\vec{k}')} , \tag{2.3.9}$$

We see from Eqs.(2.3.8) and (2.3.9) that these are significant relativistic kinematic corrections to $V^C(\vec{k}-\vec{k}')$ that are represented by the terms in square brackets.

For $m_a \neq m_b$, we define the polarization function

$$-iJ_{ab}^{PP}(P) = -2n_c \int \frac{d^4k}{(2\pi)^4} \mathrm{Tr}\left[iS_a(P/2+k) i\bar{\Gamma}_{5,ab}(P,k) iS_b(-P/2+k) i\gamma_5 \right], \tag{2.3.10}$$

where the factor of 2 arises from the flavor trace. We obtain

$$J_{ab}^{PP}(P^2) = -2n_c \int \frac{d^3k}{(2\pi)^3} \frac{[E_a(\vec{k})E_b(\vec{k}) + \vec{k}^2 + m_a m_b]}{P^0 - E_a(\vec{k}) - E_b(\vec{k})} \frac{\Gamma_{5,ab}^{+-}(P^0, |\vec{k}|)}{E_a(\vec{k})E_b(\vec{k})} , \tag{2.3.11}$$

if we neglect the contribution from the $\Gamma_{5,ab}^{-+}(P,k)$ term. Note, however, that for the study of the $\pi(138)$, we use the form [2]

$$J^{PP}(P^2) = -4n_c \int \frac{d^3k}{(2\pi)^3} \left[\frac{1}{P^0 - 2E(\vec{k})} - \frac{1}{P^0 + 2E(\vec{k})} \right] . \tag{2.3.12}$$

since we have neglected confinement in that case.

For the kaon and its radially-excited states, the mass values may be obtained from the solution of the equation

$$G_S^{-1} - J_{us}^{PP}(P^2) = 0 , \tag{2.3.13}$$

where now $m_a = m_u$ and $m_b = m_s$. The results of our calculations for the K meson are

given in Table 1, where we also provide mass values for the pion and its radial excitations. We note that the mass of the $K(1460)$ and $K(1830)$ are quite uncertain and these states need further confirmation [8]. However, we do see that after fitting the mass of the $K(495)$, we obtain the 2^1S_0 and 3^1S_0 states in the vicinity of the $K(1460)$ and $K(1830)$ states.

2.4 Choice of Parameters

In this section, we indicate how we have chosen the parameters for our calculation. There are ten parameters, but we only search for the best values of seven of these: G_S, G_V, κ, G_K, G_{KA}, δ and m_s. We fix $m_u = m_d = 0.364$ GeV, $\Lambda_3 = 0.622$ GeV and $\mu = 0.010$ GeV. [The value of 0.364 GeV for the mass of the up and down quarks was used in the extensive study reported in Ref.[7] and we adopt that value here.] Ideally, we should solve the Bethe-Salpeter equation in conjunction with the Schwinger-Dyson equation to obtain the quark self-energy. Since we perform our calculations in Minkowski space, that program is extremely difficult to implement. Therefore, we adopt a more phenomenological approach in our Minkowski-space calculations and use constant values for the constituent quark masses. We note that solutions in Euclidean space of the coupled Schwinger-Dyson and Bethe-Salpeter have been made using the global color model [10]. The constituent quark masses found in that model are rather similar to the ones used here, $m_u = m_d = 0.364$ GeV and $m_s = 0.565$ GeV.

We obtain G_S, G_V, κ and m_s by the following procedure. We use the energies of the $\omega(1S)$ and $\omega(2S)$ states to fix $G_V = 12.46$ GeV^{-2} and $\kappa = 0.055$ GeV^2. We then use the mass of the $\phi(1020)$ to fix m_s at 0.565 GeV. Finally, we fix G_S at 12.46 GeV^{-2} by fitting the mass of the $K(495)$. The parameters G_K and G_{KA} are determined in our study of the K_1 and b_1 mesons and their specification will be described at later point in our discussion. (The various parameters used here are listed in Table 2 for ease of reference.)

2.5 The Vector Nonet of Mesons

The treatment of the vector nonet of mesons is simpler than that of the pseudoscalar nonet, since we may use ideal mixing for the ω and ϕ mesons. As noted earlier, the ω and ϕ mesons were discussed in Ref.[1]. We have repeated those calculations with the parameters used in this work: $G_V = 12.46$ GeV^{-2} , $\kappa = 0.055$ GeV^2 and $\mu = 0.010$ GeV. The results are given in Table 3 and included in Fig.1. We see that the 1^3D_1 state of the ω found here coincides in energy with the state designated as $^3D_1$ in Table 12.2 of Ref.[8].

We define a vector vertex *via* the equation

$$\bar{\Gamma}^{\mu}(P,k) = \hat{\gamma}^{\mu} - i\int \frac{d^4k'}{(2\pi)^4}\left[\gamma^{\rho} S(P/2+k')\bar{\Gamma}^{\mu}(P,k')S(-P/2+k')\gamma_{\rho} V^C(k-k')\right], \quad (2.5.1)$$

where $\hat{\gamma}^{\mu} = \gamma^{\mu} - P^{\mu}\not{P}/P^2$. The solution of this equation is described in Ref.[1]. We now define the tensor

$$-iJ_u^{\mu\nu}(P) = (-1)n_c \int \frac{d^4k}{(2\pi)^4} \mathrm{Tr}\left[iS_u(P/2+k)\bar{\Gamma}_u^{\mu}(P,k)iS_u(-P/2+k)\hat{\gamma}^{\nu}\right] , \qquad (2.5.2)$$

for the up quark and put

$$J_u^{\mu\nu}(P) = -\tilde{g}^{\mu\nu}(P) J_u^V(P^2) \quad . \qquad (2.5.3)$$

with $\tilde{g}^{\mu\nu} = g^{\mu\nu} - P^{\mu}P^{\nu}/P^2$. We then define $J_\omega(P^2) = 2J_u^V(P^2)$. The mass of the ω and the masses of its radially-excited states are obtained by solving the equation

$$G_V^{-1} - J_\omega(P^2) = 0 \ . \qquad (2.5.4)$$

The solution of this equation is exhibited in Fig.3, where the horizontal line represents $G_V^{-1} = (12.46\ \mathrm{GeV}^{-2})^{-1}$. The mass values obtained from Eq.(2.5.4) are exhibited in Table 3. It may be seen in Fig.3 that the $2S$ state in the confining field is accompanied by the $1D$ state. (The splitting of these states is quite small, indicating that a very small tensor force is generated by our Lorentz-vector confinement model.) Further, the $2D$ state is found just above the $3S$ state, etc. Because of the short range of the NJL interaction, the $^3D_1$ states are hardly affected by that interaction.

The treatment of the ϕ meson is similar. We define $J_s^{\mu\nu}(P)$ in analogy to $J_u^{\mu\nu}(P)$ of Eq.(2.5.2) and then define

$$J_s^{\mu\nu}(P) = -\tilde{g}^{\mu\nu}(P) J_s^V(P^2) \qquad (2.5.5)$$

and $J_\phi(P^2) = 2J_s^V(P^2)$. Figure 4 shows the solution of the equation

$$G_V^{-1} - J_\phi(P^2) = 0 \ . \qquad (2.5.6)$$

The mass values obtained in this manner are given in Table 3.

We now need to generalize the results given in Ref.[1] to treat the case of differing quark and antiquark masses. We again consider $\hat{k}_\mu$ of Eq.(2.2.3) and recall the definition of $\hat{\gamma}^\mu$,

$$\hat{\gamma}^\mu = \gamma^\mu - P^\mu \not{P}/P^2 \ . \tag{2.5.7}$$

We also define

$$\gamma^\mu_{\perp,k} = \hat{\gamma}^\mu - \frac{\hat{k}^\mu \not{\hat{k}}}{\hat{k}^2} \ . \tag{2.5.8}$$

We see that $\hat{k}\cdot P = \gamma_{\perp,k}\cdot P = \hat{k}\cdot\gamma_{\perp,k} = 0$. The set $\hat{k}^\mu$, $\gamma^\mu_{\perp,k}$ and P^μ is useful in setting up the equations for the vertex functions.

We now generalize Eq.(2.5.1) to read

$$\begin{aligned}\bar{\Gamma}^\mu_{ab}(P,k) = \hat{\gamma}^\mu - i\int \frac{d^4k'}{(2\pi)^4}\Big[\gamma^\rho S_a(P/2+k')\bar{\Gamma}^\mu_{ab}(P,k')S_b(-P/2+k')\gamma_\rho\Big] \\ \times V^C(k-k') \ ,\end{aligned} \tag{2.5.9}$$

where we have introduced the possibility that m_a is unequal to m_b. We also define functions $\Gamma^{+-}_{1,ab}(P,k)$ and $\Gamma^{+-}_{2,ab}(P,k)$ in the frame where $\vec{P}=0$,

$$\begin{aligned}\Lambda^{(+)}_a(\vec{k})\bar{\Gamma}^\mu_{ab}(P,k)\Lambda^{(-)}_b(-\vec{k}) = \Gamma^{+-}_{1,ab}(P,k)\hat{k}^\mu\Lambda^{(+)}_a(\vec{k})\Lambda^{(-)}_b(-\vec{k}) \\ + \Gamma^{+-}_{2,ab}(P,k)\Lambda^{(+)}_a(\vec{k})\gamma^\mu_{\perp,k}\Lambda^{(-)}_b(-\vec{k}) \ .\end{aligned} \tag{2.5.10}$$

We introduce two additional functions

$$\gamma_1^{+-}(P,k) = \frac{-\vec{k}^2(m_a+m_b)}{2m_a m_b}\Gamma^{+-}_{1,ab}(P,k) \ , \tag{2.5.11}$$

and

$$\gamma_2^{+-}(P, k) = \Gamma_{2,ab}^{+-}(P, k) \quad . \tag{2.5.12}$$

A rather lengthy calculation yields coupled equations for γ_1^{+-} and γ_2^{+-}. For $\alpha = 1, 2$ we have, with $k = |\vec{k}|$ and $k' = |\vec{k}'|$,

$$\gamma_\alpha^{+-}(P, k) = C_\alpha + \sum_{\alpha'=1,2} \int dk' \frac{t_{\alpha\alpha'}(k, k')\, \gamma_{\alpha'}^{+-}(P, k')}{P^0 - E_a(k') - E_b(k')} \quad . \tag{2.5.13}$$

Here

$$C_1 = \frac{\vec{k}^2 (m_a + m_b)^2}{2 m_a m_b [E_a(k) E_b(k) + \vec{k}^2 - m_a m_b]} \tag{2.5.14}$$

and

$$C_2 = 1 \quad . \tag{2.5.15}$$

Now we use the notation $E_a = E_a(\vec{k})$, $E_a' = E_a(\vec{k}')$, etc., to write

$$\begin{aligned} t_{11}(k, k') = {} & \frac{k k'}{E_a' E_b' [E_a E_b + \vec{k}^2 - m_a m_b]} \\ & \times \{ a_1(k, k') [(E_a' E_b' + \vec{k}'^2)(E_a E_b + \vec{k}^2) \\ & - m_a m_b (E_a E_b + E_a' E_b' + \vec{k}^2 + \vec{k}'^2 - m_a m_b \\ & - \frac{1}{2} E_a E_b' - \frac{1}{2} E_a' E_b) - \frac{1}{2} m_a^2 E_b E_b' - \frac{1}{2} m_b^2 E_a E_a'] \\ & + a_2(k, k') k k' [m_a m_b + \frac{1}{2} m_a^2 + \frac{1}{2} m_b^2] \} \quad , \end{aligned} \tag{2.5.16}$$

$$t_{12}(k,\ k') = \frac{\vec{k}^2\,\vec{k}'^2}{4m_a m_b E'_a E'_b}\,\frac{[E'_a E'_b + \vec{k}'^2 + m_a m_b]}{[E_a E_b + \vec{k}^2 - m_a m_b]} \times (a_0(k,k') - a_2(k,k')) \quad , \tag{2.5.17}$$

$$t_{21}(k,k') = \frac{\vec{k}'^2\, m_a m_b}{2E'_a E'_b}(a_0(k,k') - a_2(k,k')) \ , \tag{2.5.18}$$

and

$$\begin{aligned} t_{22}(k,\ k') = {} & \frac{\vec{k}'^2}{4E'_a E'_b[E_a E_b + \vec{k}^2 + m_a m_b]} \\ & \times \{a_1(k,k')[E'_a E_b + E_a E'_b + E_a E'_a + E_b E'_b] \\ & + (a_0(k,k') + a_2(k,k'))[(E_a E_b + \vec{k}^2)(E'_a E'_b + \vec{k}'^2) \\ & + m_a m_b(E_a E_b + E'_a E'_b + \vec{k}^2 + \vec{k}'^2 + m_a m_b)]\} \ . \end{aligned} \tag{2.5.19}$$

In these equations

$$a_i(k,\ k') = \frac{1}{(2\pi)^3}\int_{-1}^{1} dx\, V^C(\vec{k} - \vec{k}')\, x^i \quad , \tag{2.5.20}$$

with $x = \cos\theta$.

We also introduce the tensor

$$-iJ^{\mu\nu}_{ab}(P) = -2n_c \int \frac{d^4k}{(2\pi)^4}\,\mathrm{Tr}\left[iS_a(P/2+k)\,\bar{\Gamma}^{\mu}_{ab}(P,k)\,iS_b(-P/2+k)\,\hat{\gamma}^{\nu}\right] \tag{2.5.21}$$

and put

$$J^{\mu\nu}_{ab}(P) = -\bar{g}^{\mu\nu}(P)\, J^{V}_{ab}(P^2) \quad . \tag{2.5.22}$$

We obtain

$$\begin{aligned} J^{V}_{ab}(P^2) = \frac{-2\,n_c}{3} \int \frac{d^3k}{(2\pi)^3} \{ & -\overline{k}^2 (m_a + m_b)\, \Gamma^{+-}_{1,ab}(P,k) \\ & + 2\,(m_a m_b + \overline{k}^2 + E_a E_b)\, \Gamma^{+-}_{2,ab}(P,k) \} \\ & \times \frac{1}{E_a E_b\, [\, P^0 - E_a - E_b \,]} \quad , \end{aligned} \tag{2.5.23}$$

where the factor of 2 originates from the flavor trace.

We now in a position to study the K^* mesons. In Fig.5 we exhibit $J^{V}_{us}(P^2)$ and include a horizontal line representing $G_V^{-1} = (12.46\ \text{GeV}^{-2})^{-1}$. In this manner we find states with the energies 0.870, 1.590, 1.732 and 1.893 GeV, where the third state is a D state - see Table 3 and Fig.1. With no new parameters, we find that the energy of the $K^*(892)$ is fit rather well, while our state at 1.590 GeV is too high to provide a good fit the $K^*(1410)$. On the other hand, if the $K^*(1680)$ is indeed a $^3D_1$ state [8], we fit its energy quite well. (See Table 12.2 of Ref.[8].)

2.6 The Scalar Nonet

The scalar nonet of states is depicted in Fig.6. We have studied the nonstrange isoscalar states, in the presence of singlet-octet mixing, in Ref.[11]. The situation is made complex by the very strong coupling of the scalar-isoscalar states to the $\pi\pi$ and $\bar{K}K$ channels. (It has also been suggested that there is a 0^{++} glueball state with energy

about 1.5 GeV, which further complicates the picture.) Therefore, in the present work, we will concentrate on the properties of the K_0^* and a_0 mesons. To study the K_0^* states we again need to define the confining vertex and polarization functions for unequal masses of the quark and antiquark. We define $\bar{\Gamma}^S_{ab}(P,k)$ to be the solution of the equation

$$\bar{\Gamma}^S_{ab}(P,k) = 1 - i\int \frac{d^4k'}{(2\pi)^4}\left[\gamma^\rho S_a(P/2+k')\bar{\Gamma}^S_{ab}(P,k')S_b(-P/2+k')\gamma_\rho\right] \times V^C(k-k') \ . \tag{2.6.1}$$

We also introduce $\Gamma^{+-}_{S,ab}$ and $\Gamma^{-+}_{S,ab}$:

$$\Lambda_a^{(+)}(\vec{k})\bar{\Gamma}^S_{ab}(P,k)\Lambda_b^{(-)}(-\vec{k}) = \Gamma^{+-}_{S,ab}(P,k)\ \Lambda_a^{(+)}(\vec{k})\,\Lambda_b^{(-)}(-\vec{k}) \tag{2.6.2}$$

and

$$\Lambda_b^{(-)}(-\vec{k})\bar{\Gamma}^S_{ab}(P,k)\Lambda_a^{(+)}(\vec{k}) = \Gamma^{-+}_{S,ab}(P,k)\ \Lambda_b^{(-)}(-\vec{k})\,\Lambda_a^{(+)}(\vec{k}) \ . \tag{2.6.3}$$

We obtain the equation

$$\Gamma^{+-}_{S,ab}(P^0,|\vec{k}|) = 1 - \frac{1}{(2\pi)^2}\int k'^2dk'\int_{-1}^{1}dx\frac{A_1(k,k',x)}{E_a(\vec{k}')E_b(\vec{k}')}\frac{1}{B(\vec{k})} \times \frac{\Gamma^{+-}_{S,ab}(P^0,|\vec{k}'|)\,V^C(\vec{k}-\vec{k}')}{P^0-E_a(\vec{k}')-E_b(\vec{k}')} \ , \tag{2.6.4}$$

with $x=\cos\theta$,

$$B(k) = [\ -E_a(\vec{k})E_b(\vec{k}) - \vec{k}^2 + m_a m_b\ ] \tag{2.6.5}$$

and

$$
\begin{aligned}
A_1(k, k') = \{ & (E_a(\vec{k}')E_b(\vec{k}') + \vec{k}'^2)(E_a(\vec{k})E_b(\vec{k}) + \vec{k}^2) \\
& - m_a m_b (E_a(\vec{k})E_b(\vec{k}) + E_a(\vec{k}')E_b(\vec{k}') + \vec{k}^2 + \vec{k}'^2 \\
& - m_a m_b - \frac{1}{2}E_a(\vec{k})E_b(\vec{k}') - \frac{1}{2}E_a(\vec{k}')E_b(\vec{k})) \\
& - \frac{1}{2}m_a^2 E_b(\vec{k}')E_b(\vec{k}) - \frac{1}{2}m_b^2 E_a(\vec{k})E_a(\vec{k}') \\
& + \vec{k}\cdot\vec{k}'[m_a m_b + \frac{1}{2}m_a^2 + \frac{1}{2}m_b^2]\} .
\end{aligned}
\tag{2.6.6}
$$

Further,

$$
\begin{aligned}
\Gamma^{-+}_{S,ab}(P^0, |\vec{k}|) = 1 + \frac{1}{(2\pi)^2}\int k'^2 dk' \int_{-1}^{1} dx \frac{\tilde{A}_1(k, k', x)}{E_a(\vec{k}')E_b(\vec{k}')}\frac{1}{B(\vec{k})} \\
\times \frac{\Gamma^{-+}_{S,ab}(P^0, |\vec{k}'|)V^C(\vec{k}-\vec{k}')}{P^0 + E_a(\vec{k}') + E_b(\vec{k}')} ,
\end{aligned}
\tag{2.6.7}
$$

where $\tilde{A}_1(k, k', x)$ is obtained from $A_1(k, k', x)$ by the replacements $E_a(\vec{k}) \to -E_a(\vec{k})$, $E_b(\vec{k}) \to -E_b(\vec{k})$, $E_a(\vec{k}') \to -E_a(\vec{k}')$ and $E_b(\vec{k}') \to -E_b(\vec{k}')$.

The result simplifies if $m_a = m_b$, such that

$$
\begin{aligned}
\Gamma^{+-}_S(P^0, k) = 1 + 4\pi \int_0^{\Lambda_3} \frac{k'^2 dk'}{(2\pi)^3} \frac{[2k'^2k^2V_0(k, k') + m^2kk'V_1(k, k')]}{k^2E^2(k')} \\
\times \frac{\Gamma^{+-}_S(P^0, k')}{P^0 - 2E(\vec{k}')} ,
\end{aligned}
\tag{2.6.8}
$$

where

$$
V_i(k, k') = \frac{1}{2}\int_{-1}^{1} dx P_i(x) V^C(\vec{k} - \vec{k}') . \tag{2.6.9}
$$

Here $P_i(x)$ is a Legendre function. We do not include $\Gamma^{-+}_{S,ab}(P, k)$ in our calculations, since the effect of including this function is small.

As a next step, we define

$$-iJ^S_{ab}(P^2) = (-2)n_c \int \frac{d^4k}{(2\pi)^4} \mathrm{Tr}\left[iS_a(P/2+k)\,\bar{\Gamma}^S_{ab}(P,k)\,iS_b(-P/2+k)\right], \qquad (2.6.10)$$

where the factor of 2 again arises from the flavor trace. We obtain

$$J^S_{ab}(P^2) = -2n_c \int \frac{d^3k}{(2\pi)^3} \frac{[E_a(\vec{k})E_b(\vec{k}) + \vec{k}^2 - m_a m_b]}{E_a(\vec{k})E_b(\vec{k})} \times \left[\frac{\Gamma^{+-}_{S,ab}(P,k)}{P^0 - E_a(\vec{k}) - E_b(\vec{k})} - \frac{\Gamma^{-+}_{S,ab}(P,k)}{P^0 + E_a(\vec{k}) + E_b(\vec{k})}\right]. \qquad (2.6.11)$$

This result is quite simple, if $m_a = m_b$

$$J^S(P^2) = -4n_c \int \frac{d^3k}{(2\pi)^3} \frac{k^2}{E^2(\vec{k})} \left[\frac{\Gamma^{+-}_S(P,k)}{P^0 - 2E(\vec{k})} - \frac{\Gamma^{-+}_S(P,k)}{P^0 + 2E(\vec{k})}\right] . \qquad (2.6.12)$$

We show $J^S_{ud}(P^2)$ for the equal mass case in Fig.7 and include a line representing $G_S^{-1} = (12.46\ \mathrm{GeV}^{-2})^{-1}$. The intersection of that line with the line representing the function $J^S_{ud}(P^2)$ determines the energy of the states $a_0(1S)$, $a_0(2S)$ and $a_0(3S)$. These energies are given in Table 4.

In Fig.8 we show the function $J^S_{us}(P^2)$ and a horizontal line representing G_S^{-1}. We find K_0^* states at 1.412 GeV, 1.738 GeV and 1.999 GeV. (See Table 4.) There are two states given in the data tables [8], the $K_0^*(1430)$ and $K_0^*(1950)$. We find a 2^3P_0 state between these states, suggesting that the $K_0^*(1950)$ may be a 3^3P_0 state.

(Note that we fit the mass of the $K_0^*(1430)$ without the introduction of any additional parameters.)

2.7 Axial-Vector Nonets

In Fig.9 we exhibit the $^3P_1$ and $^1P_1$ axial-vector nonets, as described in the constituent quark model. When using the NJL model in relativistic calculations, it is somewhat more convenient to characterize the nonets by the NJL interaction for that nonet. For example, we will use the NJL interaction that gives rise to the vertices $\gamma^\mu \gamma_5$ to calculate the properties of what is usually called the $^3P_1$ nonet. At a later point in the discussion, we will introduce another interaction that we use to perform dynamical calculation for what is the $^1P_1$ nonet in the constituent quark model. Since, the vertex $\gamma^\mu \gamma_5$ acts to a small degree in $^1P_1$ states, we do not have an exact separation into $^3P_1$ and $^1P_1$ states. However, our procedure is particularly convenient when we perform fully relativistic calculations using the NJL model. This aspect of our calculations will become more apparent as we continue our presentation. Although the axial current is not conserved, we need not consider vertices that depend upon P^μ when working in the meson rest frame. Thus, we consider the vertex associated with the matrix $\hat{\gamma}^\mu \gamma_5$ and define $\Gamma^{+-}_{A,1}(P,k)$ and $\Gamma^{+-}_{A,2}(P,k)$, such that

$$\Lambda_a^{(+)}(\vec{k})\bar{\Gamma}^\mu_{A,ab}(P,k)\Lambda_b^{(-)}(-\vec{k}) = \Gamma^{+-}_{A,1,ab}(P,k)\hat{k}^\mu \Lambda_a^{(+)}(\vec{k})\gamma_5\Lambda_b^{(-)}(-\vec{k}) + \Gamma^{+-}_{A,2,ab}(P,k)\Lambda_a^{(+)}(\vec{k})\gamma^\mu_{\perp,k}\gamma_5\Lambda_b^{(-)}(-\vec{k}) \ . \tag{2.7.1}$$

We note that $\bar{\Gamma}^\mu_A(P,k)$ satisfies the equation

$$\bar{\Gamma}^{\mu}_{A}(P,k) = \hat{\gamma}^{\mu}\gamma_5 - i\int \frac{d^4k'}{(2\pi)^4}\Big[\gamma^{\rho} S_a(P/2+k')\bar{\Gamma}^{\mu}_{A}(P,k')S_b(-P/2+k')\gamma_{\rho}\Big] \times V^{C}(k-k') \ . \tag{2.7.2}$$

For $\alpha = 1, 2$, we have

$$\Gamma^{+-}_{A,\alpha}(P,k) = D_{\alpha} + \sum_{\alpha'=1,2}\int dk' \frac{t_{\alpha\alpha'}(k,k')\,\Gamma^{+-}_{A,\alpha'}(P,k')}{P^0 - E_a(k') - E_b(k')} \ , \tag{2.7.3}$$

with

$$D_1 = \frac{m_b - m_a}{E_a E_b + \vec{k}^2 + m_a m_b} \ , \tag{2.7.4}$$

and

$$D_2 = 1 \ . \tag{2.7.5}$$

Here we have put $E_a = E_a(\vec{k})$, $E'_a = E'_a(\vec{k})$ etc. We have

$$\begin{aligned} t_{11}(k,\,k') = {} & \frac{\vec{k}'^3}{\vec{k}E'_aE'_b[E_aE_b + \vec{k}^2 + m_am_b]} \\ & \times\{a_1(k,k')[(E'_aE'_b + \vec{k}'^2)(E_aE_b + \vec{k}^2) \\ & + m_am_b(E_aE_b + E'_aE'_b + \vec{k}^2 + \vec{k}'^2 + m_am_b \\ & - \frac{1}{2}E_aE'_b - \frac{1}{2}E'_aE_b) - \frac{1}{2}m_a^2E_bE'_b - \frac{1}{2}m_b^2E_aE'_a] \\ & + a_2(k,k')kk'[-m_am_b + \frac{1}{2}m_a^2 + \frac{1}{2}m_b^2]\} \ , \end{aligned} \tag{2.7.6}$$

$$t_{12}(k,\,k') = \frac{-\overline{k}'^2\,(m_a - m_b)}{2E_a'E_b'}\,\frac{[\,E_a'E_b' + \overline{k}'^2 - m_a m_b\,]}{[\,E_a E_b + \overline{k}^2 + m_a m_b\,]} \times (\,a_0(k,k') - a_2(k,k')\,)\quad , \tag{2.7.7}$$

$$t_{21}(k,\,k') = \frac{\overline{k}'^4\,(m_b - m_a)}{4E_a'E_b'}\,(\,a_0(k,k') - a_2(k,k')\,)\quad , \tag{2.7.8}$$

and

$$\begin{aligned} t_{22}(k,\,k') = {} & \frac{\overline{k}'^2}{4E_a'E_b'[\,E_aE_b + \overline{k}^2 - m_a m_b\,]} \\ & \times \{\,a_1(k,k')[\,E_a'E_b + E_aE_b' + E_aE_a' + E_bE_b'\,] \\ & + (a_0(k,k') + a_2(k,k'))[\,(E_aE_b + \overline{k}^2)(E_a'E_b' + \overline{k}'^2) \\ & - m_a m_b(E_aE_b + E_a'E_b' + \overline{k}^2 + \overline{k}'^2 - m_a m_b)\,]\,\}\quad , \end{aligned} \tag{2.7.9}$$

Note that when $m_a = m_b$, the inhomogeneous term $D_1 = 0$. That feature has its origin in the fact that we can write

$$\hat{\gamma}^\mu \gamma_5 = \gamma_{\perp,k}^\mu \gamma_5 + \frac{\hat{k}^\mu \hat{k}}{\hat{k}^2}\gamma_5\ , \tag{2.7.10}$$

and note that $\bar{u}(\overline{k},\,s')\,\hat{k}\,v(-\overline{k},\,-s) = 0$ in the equal-mass case. The remaining matrix, $\gamma_{\perp,k}^\mu \gamma_5$ governs the interaction in ${}^3P_1$ states.

We will also need to define

$$-iJ_{A,ab}^{\mu\nu}(P^2) = (-2)n_c \int \frac{d^4k}{(2\pi)^4}\,\mathrm{Tr}\left[iS_a(P/2+k)\,\bar{\Gamma}_{A,ab}^\mu(P,\,k)\,iS_b(-P/2+k)\,\hat{\gamma}^\nu\gamma_5\right]\ , \tag{2.7.11}$$

We write

$$J^{\mu\nu}_{A,ab}(P) = -\bar{g}^{\mu\nu}(P)\, J^{A}_{ab}(P^2) \ , \tag{2.7.12}$$

with $\bar{g}^{\mu\nu}(P) = g^{\mu\nu} - P^{\mu}P^{\nu}/P^2$, and find that

$$\begin{aligned} J^{A}_{ab}(P^2) = \frac{-2n_c}{3} \int \frac{d^3k}{(2\pi)^3} \{ & -\overline{k}^2 (m_a - m_b)\, \Gamma^{+-}_{A,1,ab}(P,k) \\ & + 2(-m_a m_b + \overline{k}^2 + E_a E_b)\, \Gamma^{+-}_{A,2,ab}(P,k) \} \\ & \times \frac{1}{E_a E_b [\, P^0 - E_a - E_b \,]} \ , \end{aligned} \tag{2.7.13}$$

Using this formalism, we obtained the values of $J^{A}_{us}(P^2)$ given in Fig.10. We interpret the figure as follows. The pair of vertical lines at about 2.5 GeV^2 and 3.4 GeV^2 represent the energies of the 1^3P_1 and 1^1P_1 states and the 2^3P_1 and 2^1P_1 states, respectively, in the absence of the NJL interaction. It is then found that the 1^3P_1 moves down to 1.41 GeV and the $2\,^3P_1$ state moves down to 1.75 GeV when the NJL interaction is considered. On the other hand, the 1^1P_1 and 2^1P_1 states move hardly at all from their original position. (One may say that the two $^1P_1$ states are "trapped" between the pairs of vertical lines.) This behavior follows from the structure of the NJL model, since there is no interaction term that acts on the $^1P_1$ states, except for the second term in Eq.(2.7.10), which yields quite small effects. Since it is known that there is significant $^3P_1$ and $^1P_1$ mixing for the strange axial-vector mesons [12], we need to modify the NJL Lagrangian to deal with this problem. We take up that matter in Section 2.8.

For the equal mass case, the $^3P_1$ and $^1P_1$ states are uncoupled. Therefore, we

can use the equation for $\Gamma^{+-}_{A,2}(P,k)$ and the values of $J^A(P^2)$ for the equal mass case, to find the energies of the a_1 meson and its radially-excited states. We find a state at 1239 MeV which can be identified as the $a_1(1260)$. (That state is assigned an energy of 1230 ± 40 MeV in the data tables [8].) The radial excitations of the a_1, 2^3P_1 and 3^3P_1 states, are at 1600 and 1895 MeV, respectively. (See Fig.10 and Table 5.) Note that this analysis is quite consistent with the fact that the $b_1(1235)$, which is assigned an energy of 1231 ± 10 MeV in the data tables [8], is essentially degenerate with the $a_1(1260)$. (Recall that the $a_1(1260)$ has an energy of 1230 ± 40 MeV in the data tables and 1239 MeV in our calculations.) This aforementioned degeneracy appears in the NJL model, since there is no $^3P_1$ - $^1P_1$ mixing for $m_a = m_b$, which is the case for the $^3P_1$ a_1 mesons and the $^1P_1$ b_1 mesons.

2.8 An Extended NJL Model for the Study of $^3P_1$ - $^1P_1$ Mixing

The NJL model has only a very weak interaction in $^1P_1$ states, as may be seen in Fig.10. Whatever interaction exists arises from the small coupling of the $^1P_1$ states to the $^3P_1$ states that appears in the coupled equations for $\Gamma^{+-}_{A,1,ab}$ and $\Gamma^{+-}_{A,2,ab}$ given in the last section. (We recall that the coupling term and D_1 vanish when $m_a = m_b$.)

Since it is believed that the $^3P_1$ and $^1P_1$ states are mixed with a mixing angle of about $45°$ in the case of the strange axial-vector mesons [12], we wish to extend the NJL model to treat such coupling. The natural choice for such a generalization is an interaction Lagrangian that preserves the chiral symmetry of the original

Lagrangian:

$$\mathcal{L}_{\rm int} = \frac{G_K}{4M^2}\sum_{i=0}^{8}\Big[(i\bar{q}\lambda^i\partial_\mu q)(-i\partial_\mu\bar{q}\lambda^i q) - (\bar{q}\lambda^i\gamma_5 i\partial_\mu q)(-i\partial_\mu\bar{q}\lambda^i\gamma_5 q)\Big] \ . \tag{2.8.1}$$

Such a interaction actually appears in a natural fashion, if we consider a gradient expansion of the effective quark interaction. (One can envision a series of terms which have varying numbers of gradients.) In Eq.(2.8.1) we have inserted a factor of $1/M^2$ so that G_K has the same dimension as G_S and G_V. For our convenience, we take $M = 1.0$ GeV, although any other value will do.

It is now natural to consider an additional vertex equation with an inhomogeneous term $\hat{k}^\mu\gamma_5$. Thus, we define

$$\bar{\Gamma}^\mu_{B,ab}(P,k) = \hat{k}^\mu\gamma_5 - i\int\frac{d^4k'}{(2\pi)^4}\Big[\gamma^\rho S_a(P/2+k')\bar{\Gamma}^\mu_{B,ab}(P,k')S_b(-P/2+k')\gamma_\rho\Big] \times V^C(k-k') \ . \tag{2.8.2}$$

and also write

$$\Lambda_a^{(+)}(\overline{k})\bar{\Gamma}^\mu_{B,ab}(P,k)\Lambda_b^{(-)}(-\overline{k}) = \Gamma^{+-}_{B,1,ab}(P,k)\hat{k}^\mu\Lambda_a^{(+)}(\overline{k})\gamma_5\Lambda_b^{(-)}(-\overline{k}) + \Gamma^{+-}_{B,2,ab}(P,k)\Lambda_a^{(+)}(\overline{k})\gamma^\mu_{\perp,k}\gamma_5\Lambda_b^{(-)}(-\overline{k}) \ . \tag{2.8.3}$$

We obtain the equation

$$\Gamma^{+-}_{B,\alpha,ab}(P,k) = E_\alpha + \sum_{\alpha'=1,2} \int dk' \frac{t_{\alpha\alpha'}(k,k')\,\Gamma^{+-}_{B,\alpha',ab}(P,k')}{P^0 - E_a(k') - E_b(k')} \,, \tag{2.8.4}$$

with $E_1 = 1$ and $E_2 = 0$. This equation is the same as that given previously for $\bar{\Gamma}^{+-}_A$ except that D_1 is replaced by E_1 and D_2 is replaced by E_2. Note that, since the homogeneous equations for $\bar{\Gamma}^{\mu}_A$ and $\bar{\Gamma}^{\mu}_B$ are the same, these functions will have the singularities at the same energies. These energies represent the energies of the bound states in the confining field set up by $V^C(\vec{k} - \vec{k}')$.

We now define four polarization functions. First, we introduce

$$-iJ^{\mu\nu}_{11}(P^2)_{ab} = (-2)n_c \int \frac{d^4k}{(2\pi)^4} \mathrm{Tr}\Big[iS_a(P/2+k)\,\bar{\Gamma}^{\mu}_{B,ab}(P,k) \times iS_b(-P/2+k)\,\hat{k}^{\nu}\gamma_5\Big] \,, \tag{2.8.5}$$

and put

$$J^{\mu\nu}_{11}(P)_{ab} = -\tilde{g}^{\mu\nu}(P)\,J^{A}_{11}(P^2) \,. \tag{2.8.6}$$

We find that $J^{A}_{11}(P^2)$ does not depend upon $\Gamma^{+-}_{B,2,ab}$,

$$J^{A}_{11}(P^2) = -\frac{2}{3}n_c \int \frac{d^3k}{(2\pi)^3} \frac{\vec{k}^2}{E_a(\vec{k})E_b(\vec{k})} \frac{[E_a(\vec{k})E_b(\vec{k}) + \vec{k}^2 + m_a m_b]}{P^0 - E_a(\vec{k}) - E_b(\vec{k})} \times \Gamma^{+-}_{B,1,ab}(P,k) \,. \tag{2.8.7}$$

We also define

$$-iJ_{12}^{\mu\nu}(P^2)_{ab} = (-2)n_c \int \frac{d^4k}{(2\pi)^4} \mathrm{Tr}\left[iS_a(P/2+k)\,\bar{\Gamma}^{\mu}_{B,ab}(P,k)\,iS_b(-P/2+k)\,\hat{\gamma}^{\nu}\gamma_5 \right] . \tag{2.8.8}$$

With

$$J_{12}^{\mu\nu}(P)_{ab} = -\bar{g}^{\mu\nu}(P)\,J_{12}^{A}(P^2) . \tag{2.8.9}$$

we obtain

$$\begin{aligned} J_{12}^{A}(P^2) = \frac{-2n_c}{3} \int \frac{d^3k}{(2\pi)^3} \{ & -\overline{k^2}(m_a - m_b)\,\Gamma^{+-}_{B,1,ab}(P,k) \\ & + 2(-m_a m_b + \overline{k^2} + E_a E_b)\,\Gamma^{+-}_{B,2,ab}(P,k) \} \\ & \times \frac{1}{E_a E_b [\,P^0 - E_a - E_b\,]} , \end{aligned} \tag{2.8.10}$$

which is of the form of Eq.(2.7.13) with the replacement $\Gamma^{+-}_{A,1,ab}(P,k) \rightarrow \Gamma^{+-}_{B,1,ab}(P,k)$ and $\Gamma^{+-}_{A,2,ab}(P,k) \rightarrow \Gamma^{+-}_{B,2,ab}(P,k)$.

We also note that $J_{21}^{A}(P^2) = J_{12}^{A}(P^2)$, where the definition of $J_{21}^{A}(P^2)$ is straightforward. The polarization function $J_{22}^{A}(P^2)$ may be identified with our result for $J_{ab}^{A}(P^2)$ given in Eq.(2.7.13). We also see that J_{11}^{A}, J_{12}^{A} and J_{22}^{A} will have singularities at the same values of P^2. Values of $J_{11}^{A}(P^2)$ are given in Fig.11 and $J_{12}^{A}(P^2)$ is shown in Fig.12.

We now define a T matrix for the coupled $^3P_1$ - $^1P_1$ system, which we organize in a matrix form,

$$\hat{T} = (\hat{k}_\mu \gamma_5 , \hat{\gamma}_\mu \gamma_5) \begin{bmatrix} T_{11}^{\mu\nu}(P) & T_{12}^{\mu\nu}(P) \\ T_{21}^{\mu\nu}(P) & T_{22}^{\mu\nu}(P) \end{bmatrix} \begin{bmatrix} \hat{k}_\nu \gamma_5 \\ \hat{\gamma}_\nu \gamma_5 \end{bmatrix} , \tag{2.8.11}$$

and put $T_{11}^{\mu\nu}(P) = -g^{\mu\nu} T_{11}(P^2)$, $T_{12}^{\mu\nu}(P) = -g^{\mu\nu} T_{12}(P^2)$, $T_{21}^{\mu\nu}(P) = -g^{\mu\nu} T_{21}(P^2)$ and $T_{22}^{\mu\nu}(P) = -g^{\mu\nu} T_{22}(P^2)$.

We introduce the matrices

$$G = \begin{bmatrix} -G_K & 0 \\ 0 & -G_V \end{bmatrix} , \tag{2.8.12}$$

$$J(P^2) = \begin{bmatrix} J_{11}^A(P^2)/M^2 & J_{12}^A(P^2)/M \\ J_{21}^A(P^2)/M & J_{22}^A(P^2) \end{bmatrix} , \tag{2.8.13}$$

and

$$T(P^2) = \begin{bmatrix} T_{11}(P^2) & T_{12}(P^2) \\ T_{21}(P^2) & T_{22}(P^2) \end{bmatrix} . \tag{2.8.14}$$

We then have the matrix equation

$$T(P^2) = G - G J(P^2) T(P^2) , \tag{2.8.15}$$

or

$$[\, 1 + G J(P^2) \,] T(P^2) = G , \tag{2.8.16}$$

so that $T(P^2) = D^{-1}(P^2) G$, with

$$D(P^2) = \begin{bmatrix} 1 - G_K J_{11}^A(P^2)/M^2 & -G_K J_{12}^A(P^2)/M \\ -G_V J_{12}^A(P^2)/M & 1 - G_V J_{22}^A(P^2) \end{bmatrix} . \tag{2.8.17}$$

Thus

$$T_{11}(P^2) = -\frac{G_K[\,1 - G_V J_{22}^A(P^2)\,]}{\det D(P^2)} , \tag{2.8.18}$$

$$T_{12}(P^2) = \frac{-G_V G_K J_{12}^A(P^2)/M}{\det D(P^2)} , \tag{2.8.19}$$

and

$$T_{22}(P^2) = \frac{-G_V[\,1 - G_K J_{11}^A(P^2)/M^2\,]}{\det D(P^2)} , \tag{2.8.20}$$

where

$$\begin{aligned} \det D(P^2) = {} & [\,1 - G_K J_{11}^A(P^2)/M^2\,][\,1 - G_V J_{22}^A(P^2)/M\,] \\ & - G_K G_V [\,J_{12}^A(P^2)/M\,]^2 . \end{aligned} \tag{2.8.21}$$

We may obtain the spectrum of the coupled system from the equation

$$\det D(P^2) = 0 . \tag{2.8.22}$$

Alternately, we may bring the T matrix to diagonal form at each value of P^2, such that

$$M(\phi)T(P^2)M^{-1}(\phi) = \begin{bmatrix} T_1(P^2) & 0 \\ 0 & T_2(P^2) \end{bmatrix} , \tag{2.8.23}$$

with

$$M(\phi) = \begin{bmatrix} \cos\phi & -\sin\phi \\ \sin\phi & \cos\phi \end{bmatrix} , \qquad (2.8.24)$$

where ϕ is a function of P^2. Resonances or bound states appear as singularities of $T_1(P^2)$ and $T_2(P^2)$.

We may first consider the case where $J_{12}^A(P^2) = 0$. We determine the parameter G_K by fitting the energy of the $b_1(1235)$ meson by solving the equation

$$G_K^{-1} - J_{11,ud}^A(P^2) = 0 , \qquad (2.8.25)$$

where $J_{11,ud}^A(P^2)$ is $J_{11}^A(P^2)$ calculated in the equal-mass case with $m_a = m_b = 0.364$ GeV. [See Fig.13.] Here we are assuming that we have ideal mixing for the b_1 mesons. We find that $G_K = 78.13$ GeV^{-2} yields the mass values given in Table 6.

We now consider the $^3P_1$ and $^1P_1$ K_1 mesons in the uncoupled case. The mass values obtained from the solution of the equations

$$G_K^{-1} - J_{11}^A(P^2) = 0 \qquad (2.8.26)$$

and

$$G_V^{-1} - J_{22}^A(P^2) = 0 \qquad (2.8.27)$$

are given in Fig.14a and 14b, respectively. (Recall that J_{11}^A and J_{22}^A are defined with $m_a = m_u$ and $m_b = m_s$.)

We now proceed to discuss $^3P_1$ - $^1P_1$ mixing for the strange axial-vector mesons. Our first observation is that $J_{12}^A(P^2)$ is quite small and leads to relatively little mixing. We note that if we do not use the energy of the $b_1(1235)$ to fix G_K, we may

put $G_K = 93.0$ GeV^{-2} and provide a rather good fit to the masses of the K_1 mesons. However, we continue to maintain $G_K = 78.13$ GeV^{-2} and consider another model for $^3P_1$ - $^1P_1$ mixing. We replace the matrix G of Eq.(2.8.12) by

$$G = - \begin{bmatrix} G_K & G_{KA} \\ G_{KA} & G_V \end{bmatrix} . \tag{2.8.28}$$

It is clear that G_{KA} couples the $^3P_1$ and $^1P_1$ channels directly. (The equations for the T matrix have to be modified appropriately.) We find that $G_{KA} = 8.00$ GeV^{-2} gives rise to the K_1 energies given in Table 7 and shown in Fig.14c.

We now turn to a discussion of the mixing angle, coupling constant, and form factors, as defined in our covariant formulation. Near a singularity of $T_1(P^2)$ at $P^2 = m_1^2$ we may define

$$\langle k' \mid \hat{T}(P^2) \mid k \rangle = -F_\mu^A(k') \frac{\tilde{g}^{\mu\nu}}{P^2 - m_1^2} F_\nu^A(k) \tag{2.8.29}$$

with

$$F_A^\mu(k) = g_1 \left[\frac{\hat{k}^\mu \gamma_5}{M} \cos\phi - \hat{\gamma}^\mu \gamma_5 \sin\phi \right] . \tag{2.8.30}$$

In Eq.(2.8.30), g_1 is a coupling constant.

We may also modify the vertex form factor, $F_A^\mu(k)$, to include the effects of confinement using the methods developed in Ref.[3]. (With that procedure, we are able to show that $\hat{T}(P^2)$ is represented by bound states only, if the potential V^C is absolutely confining. Note that we have already modified the vacuum polarization

integrals to include confinement effects.) To include confinement effects in the numerator of the T matrix of Eq.(2.8.29), we replace Eq.(2.8.30) by [3]

$$\bar{F}^{\mu}(P,k) = g_1 \left[\frac{\bar{\Gamma}^{\mu}_{B}(P,k)}{M} \cos\phi - \bar{\Gamma}^{\mu}_{A}(P,k) \sin\phi \right] , \qquad (2.8.31)$$

where $P^2 = m_1^2$. The mixing angle, ϕ, is given in Table 7 for the first two states of Fig.14c. However, that angle is particular to our method of calculation and does not correspond to the angle introduced to describe mixing of ${}^3P_1$ and ${}^1P_1$ octets in Ref.[12], for example.

One interesting feature of the $K_1(1270)$ and the $K_1(1400)$ mesons is that they have differing predominant decay channels. For example, the decay width for $K_1(1400) \to K^* + \pi$ is much larger than the width for $K_1(1400) \to K + \rho$. On the other hand, the $K_1(1270)$ decays predominantly to $K + \rho$, with weaker decay to the $K^* + \pi$ channel. This feature suggests approximately equal mixtures of ${}^3P_1$ and ${}^1P_1$ states in these K_1 mesons, as discussed by Suzuki, for example [12], where a single mixing angle is used for the $K_1(1270)$ and $K_1(1400)$. However, in the case of composite mesons, the mixing angle is P^2-dependent, as is the case here. (To use the formalism used in Ref.[12], one must assume that the $K_1(1270)$ and $K_1(1400)$ are elementary particles.)

Finally, we calculate the mass values for the $s\bar{s}$ states of the f_1 and h_1 mesons, under the assumption of ideal mixing. For the f_1 we consider the equation

$$G_V^{-1} - J^A_{22,ss}(P^2) = 0 \ , \tag{2.8.32}$$

where $J^A_{22,ss}(P^2)$ has $m_a = m_b = m_s$. For the h_1 meson, we solve

$$G_K^{-1} - J^A_{11,ss}(P^2) = 0 \ , \tag{2.8.33}$$

where $J^A_{11,ss}(P^2)$ also has $m_a = m_b = m_s$. Mass values obtained in this manner are given in Table 8. It is uncertain as to whether ideal mixing is appropriate for the f_1 and h_1 mesons and an analysis similar to that made for the $\eta - \eta'$ system, with a reduced attraction in singlet states, may be most appropriate. (Recall that in our study of $\eta - \eta'$ mixing, we used $G_S - \delta$ for the interaction in singlet states and G_S for the interaction in the octet states [1].)

2.9 Discussion

In this chapter we have calculated the energy of fifty-four $q\bar{q}$ states using the parameters listed in Table 2. The parameters Λ_3, μ and m_u were fixed at the outset and m_s, G_S, G_V and κ were adjusted to fit the masses of the $\omega(782)$, $\omega(1420)$, $K(495)$ and $\phi(1020)$. There are three other parameters, δ, G_K and G_{KA}. The parameter δ was chosen when fitting the $\eta(547)$ and $\eta'(958)$ mass values. That parameter is meant to take into account the effect of the gluon fields upon the singlet state η^0. The value of G_K was introduced to create a significant interaction in the $^1P_1$ states and G_{KA} was introduced to create significant $^3P_1$ - $^1P_1$ mixing for the strange axial-vector mesons. (Without such terms, the standard NJL interaction has a very

small interaction in ${}^1P_1$ states and quite small ${}^3P_1$ - ${}^1P_1$ mixing.) We note that the parameters are largely determined from our study of the pseudoscalar and vector nonets. Therefore, our predictions for states such as the $K_0^*(1430)$, $a_1(1260)$ and $K^*(892)$ require no parameter fitting. Our prediction for the mass of the $a_0(980)$ is too high by about 80 MeV. However, the non-strange scalar states are known to have quite strong coupling to channels such as $\pi\pi$, $K\bar{K}$ and $\pi\eta$, so that one can expect a significant shift in energy arising from the real part of the meson self-energy that describes the decay to the various open channels [11, 13].

A particular advantage of our formalism is that we combine chiral symmetry, covariance and a model of confinement in the same model. While our Lagrangian has chiral symmetry, the approximations made in our Minkowski-space calculation violate chiral symmetry to some degree. Since the properties of the $\pi(138)$ are very sensitive to small violation of chiral symmetry, we neglect confinement in that case. Alternately, the pion may be studied in a Euclidean momentum space, where it is easier to maintain exact chiral symmetry in the presence of a model of confinement [9].

In the present chapter, we have not emphasized the covariance of our formulation. That feature played an important role in our studies of the decays of the $\pi(1300)$ to $\pi+\sigma$ and $\pi+\rho$ channels [2]. For example, if the $\pi(1300)$ is taken to be at rest, the final-state mesons (σ, ρ or π) have finite three-momentum. Therefore, to describe the confinement vertex for these mesons, we have to make use of the covariance of the model. The decay amplitude then becomes independent of the frame chosen for its evaluation. We have also shown that the various vacuum polarization

functions, such as $J^P(P^2)$, $J^V_{\mu\nu}(P^2)$, $J^S(P^2)$ and $J^A_{\mu\nu}(P^2)$, may be calculated in any Lorentz frame with the same result.

The extension of our Lagrangian to include gradient terms is a novel feature of our work. We consider this aspect of our work somewhat preliminary to a more complete study of the effects of such terms upon the full range of mesons. It remains to be seen whether our model can explain the decay widths of $K_1(1270)$ and $K_1(1400)$ to various open channels, such as $K^* + \pi$ and $K + \pi$.

There exist several approaches to the study of light mesons. A model for the calculation of radial excitations of mesons in a generalized NJL is presented in Ref.[14]. Also, extensive studies of hadron properties have been made using the global color model and we list several useful works in Ref.[15]. In addition, there is a body of work that makes use of the potential models of the kind that are used in the study of heavy mesons. That body of work is reviewed in Ref.[16].

The overestimate by about 200 MeV of the energy of the $K^*(1410)$ seen in Fig.5 is quite similar feature to that exhibited in Fig.14 of Ref.[16], where theoretical and experimental values for meson masses are shown. (In Section 4.2.2 of Ref.[16], it is suggested that the low energy of the 2^3S_1 $K^*(1410)$, when compared to the shell-model prediction, may be due to the mixing of two states *via* decay channels that lowers the energy of one state and increases the energy of the other. Alternatively, we may suggest a large shift due to the real part of the meson self-energy that describes the effects due to the coupling of the $K^*(1410)$ to the various open channels.) We may note that our value for the mass of the $K_0^*(1430)$, given in the data tables as $1412 \pm$

6 MeV, is better than the predicted value given in Ref.[16], which is about 170 MeV too small.

Chapter 3

Covariant Calculation of the Properties of f_2 Mesons in a Generalized Nambu – Jona-Lasinio Model

3.1 Introduction

In this chapter we continue our study of our generalized Nambu – Jona-Lasinio (NJL) model [6]. A natural extension of the calculations of Chapter 2 is a consideration of tensor mesons. As we will see, we have to further generalize the NJL model to include short-range interactions that affect the states of such mesons. These new interactions contain gradients of the quark fields and may be thought of as being part of a more comprehensive expansion of the quark-antiquark interaction than that which appears in the standard form of the SU(3)-flavor NJL Lagrangian.

In this chapter we will study the f_2 mesons, which have $I^G(J^{PC}) = 0^+(2^{++})$, where I is the isospin and G is the G parity. To further motivate this study, we refer to Table 9, where the states of the f_2 mesons are listed [8]. (We have not listed the $f_J(1710)$, although it is possible that state has $J = 2$.) We see that there are a large number of states, with eight states below 2.0 GeV. This large number of states creates a problem for the standard constituent quark shell model. This matter is discussed on

page 1671 of Ref.[8], where it is suggested that the $f_2(1270)$ and $f_2'(1525)$ are probably the two 1^3P_2 $q\bar{q}$ states of the quark model. It is remarked that there are a large number of possible non-$q\bar{q}$ candidates with $J^{PC}=2^{++}$: $f_2(1430)$, $f_2(1520)$, $f_J(1710)$, $f_2(1810)$, $f_2(2010)$, $f_2(2300)$ and $f_2(2340)$. It is stated that the $f_2(1810)$ is likely to be the 2^3P_2 state and the three f_2 mesons above 2 GeV could be the 2^3P_2 $s\bar{s}$, 1^3F_2 $s\bar{s}$ and 1^3P_2 $s\bar{s}$ states. As we will see, our fully relativistic calculation can readily account for the full range of states seen below 2 GeV. That is, in part, due to the fact the spacing of levels in the relativistic confinement potential is quite different from that in the quark shell model, with the $1S$, $2S$ and $3S$ $n\bar{n}$ states and the $1S$ and $2S$ $s\bar{s}$ states bound by the relativistic confining field at energies less that 2 GeV. (Here, $n\bar{n}$ stands for the $(u\bar{u}+d\bar{d})/\sqrt{2}$ states.) Since the search for exotic, hybrid, or gluonium states is an important part of meson spectroscopy [10, 15], we believe our formalism will be of value in identifying states of $q\bar{q}$ structure that can then be eliminated in the search for non-$q\bar{q}$ states.

The organization of this chapter is as follows. In Section 3.2 we discuss some of the successes and limitation of our model and compare our approach to other models. In Section 3.3 we exhibit additional interaction terms that allow us to treat 2^{++} states in our generalized NJL model. In Section 3.4, we describe the T matrix used in our study of the f_2 mesons. This T matrix allows for a general study of singlet-octet mixing, however, in this chapter we limit our investigation to a model with "ideal mixing". In Section 3.5 we present the results of our numerical calculations, while Section 3.6 contains some further discussion and conclusions.

3.2 A Generalized NJL model with a Covariant Model of Confinement

In order to understand the merits and the limitations of our model, we will discuss the relation of our model to three models to be found in the literature. These are the extensively-studied global color model [10, 15], the constituent quark model [16], and the work of Münz and collaborators [18-22].

We consider our work somewhat complementary to the studies using the global color model (GCM). That model uses a phenomenological form for the nonperturbative part of the gluon propagator in an Abelian approximation to QCD. The high-energy behavior is taken to be the same as that obtained in perturbative QCD. In that body of work [10, 15], one solves the Schwinger-Dyson equation in conjunction with the Bethe-Salpeter equation and obtains momentum-dependent quark mass values. All calculations are made in Euclidean momentum space, where the theory is defined. Results in Minkowski space may be obtained by analytic continuation, but such procedures are subject to significant uncertainties. Alternatively, one may calculate mass values for hadrons by studying hadronic current correlation functions in Euclidean space. (The recent work of Meissner and Kisslinger reports a Euclidean-space calculation of the vector hadronic correlation function that yields a value for the ρ mass of 590 MeV [23].) Since the global color model is only formulated in Euclidean space, it is quite difficult to study radial excitations of mesons, since the large Euclidean-time behavior of hadronic correlators is dominated by the properties of the hadronic ground state in the relevant channel. Therefore, the GCM is not very useful for the study of light

meson spectroscopy.

The treatment of confinement in the GCM differs from that in our work. In the GCM the parameterization of the gluon propagator in the infrared is such that the quark propagator does not have an on-mass-shell pole. Thus, the quark is not a propagating mode in the vacuum. On the other hand, in our model, confinement is a property of the $q\bar{q}$ system, such that, while a quark (or antiquark) may go on mass shell, the amplitude for the quark and antiquark to both go on-mass-shell at the same time vanishes. These features of the two models are such that the GCM must be formulated in Euclidean space, while our generalized NJL model may be used in either Euclidean or Minkowski space.

The model that we use in our work takes the form of an effective (nonrenormalizable) theory. In contrast to the work of the global color model, we do not solve the Schwinger-Dyson equation, but use constant values for the constituent quark masses. On the other hand, our parameterization of the Lorentz-vector confining potential is somewhat analogous to the parameterization of the infrared part of the gluon propagator in the GCM.

As we have seen in our earlier work, our model provides quite good fits to the full range of light-meson spectra in terms of a number of phenomenological parameters. In the few cases that our fit is not particularly good, we find that the physical meson state appears very close to a threshold for a two-meson decay channels. An example is the $a_0(980)$, which lies directly below the threshold for the $K\bar{K}$ channel at 990 MeV. In this case we overestimate the mass of the $a_0(980)$ by 80 MeV. This

suggest that a study of the influence of the decay channels in modifying the theoretical values of the masses of various mesons is in order.

Another attempt to study the full range of light meson states is reviewed by Godfrey and Napolitano [16]. Their review contains a description of results obtained using a "relativized" version of the potential models that are highly successful in obtaining fits the spectra of heavy mesons. Since that model does not describe chiral symmetry breaking, it is not suited to the description of the pseudoscalar nonet of states. (One can use a spin-spin interaction to obtain correct pion mass, with the consequence that the ρ mass is not given correctly [16].) Also, the nonrelativistic nature of the model leads to a poor description of the density of states in the low-energy spectrum. For example, in Ref.[16], we find two $^3P_2$ states and one $^3F_2$ state below 2 GeV in a study of tensor mesons. As discussed in the Introduction, we find ten f_2 states below 2.0 GeV. The first seven of these states can be put into correspondence with the first seven experimentally determined states. Problems in obtaining the correct number states in a nonrelativistic formulation can also be seen when we study pseudoscalar – axial-vector mixing for the pion and its radial excitations, as well as for the $\eta - \eta'$ system of states. For example, in the meson rest frame we may discuss states with vertex structure of the form $i\gamma_5$ or $\gamma^0\gamma_5$. That immediately doubles the number of states we have to consider in a fully relativistic formalism. In our study of the pion, the states in the confining field appear as doublets, which are then split when the NJL interaction is included. This feature leads to an interesting interpretation of the data in the region of the $\pi(1300)$, which is

presented in Ref.[2]. In that work, the covariant nature of our formalism is particularly important, since we calculate meson decay amplitudes at one-loop order. For example, in the decays $\pi' \to \rho + \pi$, or $\pi' \to \sigma + \pi$, the final-state mesons have finite momentum, requiring a covariant model of the confining vertex for a consistent description [2]. While we have made extensive calculations of light meson spectra, we have only calculated meson decay amplitudes in a few cases. Our recent work has included a description of the decays $\pi \to \gamma + \gamma$, $\eta \to \gamma + \gamma$, $\eta' \to \gamma + \gamma$. We have found that our description of pseudoscalar-axialvector mixing is quite important in obtaining a consistent picture of these decay rates [4, 5].

Another model which may be used to make a comprehensive fit to the properties of light mesons is a model based upon the six-quark interaction of the 't Hooft, that has it origin in the study of instantons [18]. That model described in Ref.[18] also includes an (instantaneous) linear confining potential, which is used when solving the Salpeter equation. However, the model is not covariant, since only the timelike part of the potential, which is proportional to $\gamma^0(1)\,\gamma^0(2)$, is used, rather than the $\gamma^\mu(1)\,\gamma_\mu(2)$ form that we have used in our work. The model of Ref.[18] can provide a good fit to various spectra, however, the predications for the decays widths are quite poor. Another choice of parameters yields good values for the decay rates, however, the fit to the spectra is then poor [18].

We have found that it is useful to neglect confinement for the $\pi(138)$ in our Minkowski-space calculations, since the properties of the pion are very sensitive to small violations of chiral symmetry that appear in our analysis. On the other hand, we

have studied the pion using our model in a Euclidean-space calculation, where it is easy to maintain chiral symmetry (in the absence of a current-quark mass matrix). In that work, we found that the Goldstone theorem was satisfied, with the pion as the Goldstone boson [9].

Some discussion of our choice of parameters is in order. We define the parameters G_S and G_V in Eq.(2.1.1). In addition, there is the "string tension", κ, and a Minkowski-space momentum cut off, Λ_3, which is usually chosen so that the pion decay constant, f_π, is given correctly. We begin by fixing $m_u = m_d = 0.364$ GeV. That is the value used in the extensive calculations of Vogl and Weise [6]. We then chose G_V and κ so that the mass of the ω and the mass of the first radial excitation of the ω are given correctly. At that point, we fix $m_s = 0.565$ GeV, so that the mass of the ϕ meson is reproduced, when using the value of κ already determined. Finally, we fix G_S by fitting the mass of the $K(495)$. (When studying the η - η' system [17], we used a smaller value of G_S in singlet states to take into account effects due to the coupling to gluonic intermediate states. That procedure may be seen to be equivalent to the use of the 't Hooft interaction, which affects both singlet and octet states [6].) Once the parameters of the model are fixed by fitting the energies of the $\omega(782)$, $\omega(1420)$, $K(495)$ and $\phi(1020)$, we find that the model has significant predictive power. For example, the masses of the $K^*(892)$, $K_0^*(1430)$ and $a_1(1260)$ are predicted correctly [17]. In the present chapter, we introduce two additional parameter that are defined in Eq.(3.3.4). The values are determined so as to yield a good fit to the masses of the f_2 mesons.

3.3 Tensor Mesons in a Generalized NJL Model

The standard NJL Lagrangian that is exhibited as part of Eq.(2.1.1) describes interactions in the scalar, pseudoscalar, vector and axialvector nonets. If we are to study the f_2 tensor mesons, we need to add various interactions to the Lagrangian of Eq.(2.1.1). That may be done in a manner that preserves the chiral symmetry of the Lagrangian.

We now consider the following interaction Lagrangian

$$\mathcal{L}_Q^{int} = g_{T_1} \sum_{a=0}^{8} \{ [\bar{q} \lambda^a (3\partial^\mu \partial^\nu - g^{\mu\nu} \Box) q] \times [\bar{q} \lambda_a (3\bar{\partial}_\mu \bar{\partial}_\nu - g_{\mu\nu} \bar{\Box}) q] + c.p. \} , \tag{3.3.1}$$

where *c.p.* stands for the "chiral partner" of the first term. Rather than work with Eq.(3.3.1), we go directly to the momentum-space interaction and consider two new terms. We define two dimensionless tensors

$$Q^{\mu\nu}(k) = \frac{3\hat{k}^\mu \hat{k}^\nu - \tilde{g}^{\mu\nu} \hat{k}^2}{-2\hat{k}^2} \tag{3.3.2}$$

and

$$P^{\mu\nu}(k) = \frac{\hat{k}^\mu \gamma_{\perp,k}^\nu + \hat{k}^\nu \gamma_{\perp,k}^\mu}{\sqrt{-\hat{k}^2}} . \tag{3.3.3}$$

[See Eq.(2.2.3a) and Eqs.(2.5.7) - (2.5.8).] Note that $Q_\mu^\mu = P_\mu^\mu = 0$. Since we have chosen to make these tensors dimensionless by dividing by $\hat{k}^2$ in Eq.(3.3.2) and

$(-\hat{k}^2)^{1/2}$ in Eq.(3.3.3), $Q^{\mu\nu}$ is not in direct correspondence with Eq.(3.3.1), however, Eq.(3.3.1) could be modified to achieve that correspondence. We may also write a coordinate space version of Eq.(3.3.3), but we will not need that form of the interaction Lagrangian for the present chapter. We will carry out our analysis in the meson rest frame, where $\vec{P} = 0$ and $\hat{k}^\mu = [0, \vec{k}]$. Thus, we only need to use the spacial components of the tensors, Q^{ij} and P^{ij}. However, it is best to maintain the complete relativistic notation, since calculations are simpler in that case.

We now extend the NJL momentum-space interaction to include two attractive interactions and write

$$V_T(P, k', k) = -\frac{G_{T_1}}{4} Q^{\mu\nu}(k')\, g_{\mu\nu\alpha\beta}\, Q^{\alpha\beta}(k) - \frac{G_{T_2}}{4} P^{\mu\nu}(k')\, g_{\mu\nu\alpha\beta}\, P^{\alpha\beta}(k) \ . \tag{3.3.4}$$

Here, $g_{\mu\nu\alpha\beta}$, which depends upon P^μ, is defined to be

$$g^{\mu\nu\alpha\beta} = \frac{1}{2}\left\{ \tilde{g}^{\mu\alpha}\tilde{g}^{\nu\beta} + \tilde{g}^{\mu\beta}\tilde{g}^{\nu\alpha} - \frac{2}{3}\tilde{g}^{\mu\nu}\tilde{g}^{\alpha\beta} \right\} \ . \tag{3.3.5}$$

Note that $g^{\mu\nu}{}_{\alpha\beta}\ g^{\alpha\beta\rho\sigma} = g^{\mu\nu\rho\sigma}$. Following our standard procedure [1-2, 17], we introduce equations for the tensor vertex functions

$$\bar{\Gamma}^{\mu\nu}_{T_1}(P, k) = Q^{\mu\nu}(k) - i\int \frac{d^4k'}{(2\pi)^4}\, V^C(k-k') \times \left[\gamma^\rho S(P/2 + k')\bar{\Gamma}^{\mu\nu}_{T_1}(P, k') S(-P/2 + k')\gamma_\rho\right] , \tag{3.3.6}$$

and

$$\bar{\Gamma}^{\mu\nu}_{T_2}(P,k) = P^{\mu\nu}(k) - i\int \frac{d^4k'}{(2\pi)^4} V^C(k-k') \times \left[\gamma^\rho S(P/2+k')\bar{\Gamma}^{\mu\nu}_{T_2}(P,k')S(-P/2+k')\gamma_\rho\right] . \tag{3.3.7}$$

The Dirac matrices γ^ρ and γ_ρ appear since we use Lorentz-vector confinement. (Equations (3.3.6) and (3.3.7) may be generalized to describe a quark and antiquark of different constituent mass values. However, for our study of the f_2 mesons, we only need these equations for $n\bar{n}$ or $s\bar{s}$ states. The more general form is needed in a study of strange mesons.)

We proceed as usual, and define four functions for the case $\vec{P} = 0$:

$$\Lambda^{(+)}(\vec{k})\bar{\Gamma}^{\mu\nu}_{T_1}(P,k)\Lambda^{(-)}(-\vec{k}) = \Gamma^{+-}_{T_1,1}(P,k)Q^{\mu\nu}\Lambda^{(+)}(\vec{k})\Lambda^{(-)}(-\vec{k}) + \Gamma^{+-}_{T_1,2}(P,k)\Lambda^{(+)}(\vec{k})P^{\mu\nu}\Lambda^{(-)}(-\vec{k}) \tag{3.3.8}$$

and

$$\Lambda^{(+)}(\vec{k})\bar{\Gamma}^{\mu\nu}_{T_2}(P,k)\Lambda^{(-)}(-\vec{k}) = \Gamma^{+-}_{T_2,1}(P,k)Q^{\mu\nu}\Lambda^{(+)}(\vec{k})\Lambda^{(-)}(-\vec{k}) + \Gamma^{+-}_{T_2,2}(P,k)\Lambda^{(+)}(\vec{k})P^{\mu\nu}\Lambda^{(-)}(-\vec{k}) . \tag{3.3.9}$$

The equations that may be used to determine the four functions defined in Eqs.(3.3.8) and (3.3.9) are given in the Appendix.

We now need to define a number of vacuum polarization functions. We write

$$-iJ^{\mu\nu\alpha\beta}_{QQ,ab}(P) = -n_c\mathrm{Tr}\int \frac{d^4k}{(2\pi)^4} \times \left[\lambda_a iS(P/2+k)\bar{\Gamma}^{\mu\nu}_{T_1}(P,k)iS(-P/2+k)Q^{\alpha\beta}(k)\lambda_b\right] , \tag{3.3.10}$$

where a and b are 0 or 8 in an analysis of singlet-octet mixing. We also define

$$-iJ^{\mu\nu\alpha\beta}_{QP,ab}(P) = -n_c \mathrm{Tr} \int \frac{d^4k}{(2\pi)^4} \times \left[\lambda_a iS(P/2+k)\bar{\Gamma}^{\mu\nu}_{T_1}(P,k)iS(-P/2+k)P^{\alpha\beta}(k)\lambda_b\right], \tag{3.3.11}$$

with a corresponding definition of $-iJ^{\mu\nu\alpha\beta}_{PQ,ab}$. We also write

$$-iJ^{\mu\nu\alpha\beta}_{PP,ab}(P) = -n_c \mathrm{Tr} \int \frac{d^4k}{(2\pi)^4} \times \left[\lambda_a iS(P/2+k)\bar{\Gamma}^{\mu\nu}_{T_2}(P,k)iS(-P/2+k)P^{\alpha\beta}(k)\lambda_b\right]. \tag{3.3.12}$$

Now we define

$$J^{\mu\nu\alpha\beta}_{QQ,ab}(P) = g^{\mu\nu\alpha\beta} J^{QQ}_{ab}(P^2), \tag{3.3.13}$$

$$J^{\mu\nu\alpha\beta}_{PQ,ab}(P) = g^{\mu\nu\alpha\beta} J^{PQ}_{ab}(P^2), \tag{3.3.14}$$

and

$$J^{\mu\nu\alpha\beta}_{PP,ab}(P) = g^{\mu\nu\alpha\beta} J^{PP}_{ab}(P^2), \tag{3.3.15}$$

with $J^{QP}_{ab}(P^2) = J^{PQ}_{ab}(P^2)$.

We obtain, for a quark of mass m_u and with $k = |\vec{k}|$,

$$J^{QQ}_u(P^2) = -\frac{3}{10\pi^2} n_c \int^{\Lambda_3} k^2\,dk\, \frac{k^2}{E^2(k)} \frac{\Gamma^{+-}_{T_1,1}(P,k)}{P^0 - 2E_u(k)}, \tag{3.3.16}$$

where $E_u(k) = [k^2 + m_u^2]^{1/2}$. [Note that the various functions $\Gamma^{+-}(P,k)$ depend upon the mass of the quark.] There is a corresponding equation for $J^{QQ}_s(P^2)$. The values of $J^{QQ}_{ab}(P^2)$ are obtained from the knowledge of $J^{QQ}_u(P^2)$ and $J^{QQ}_s(P^2)$.

We find that

$$J_u^{PP}(P^2) = -\frac{4}{5\pi^2} n_c \int^{\Lambda_3} k^2 dk \, \frac{\Gamma^{+-}_{T_1,2}(P, k)}{P^0 - 2E_u(k)} , \tag{3.3.17}$$

and

$$J_u^{QP}(P^2) = -\frac{4}{5\pi^2} n_c \int^{\Lambda_3} k^2 dk \, \frac{\Gamma^{+-}_{T_1,2}(P, k)}{P^0 - 2E_u(k)} , \tag{3.3.18}$$

etc. In obtaining these results we have used the relation $g_{\mu\nu\alpha\beta} g^{\mu\nu\alpha\beta} = 5$ and have neglected small terms proportional to $[P^0 + 2E(k)]^{-1}$.

3.4 T Matrices for the Study of f_2 Mesons

We now construct the matrices that enable us to study singlet-octet and $Q_{\mu\nu}(k) - P_{\mu\nu}(k)$ mixing. [We remark that the latter mixing occurs due to the nonzero values of $J_{ab}^{PQ}(P^2) = J_{ab}^{QP}(P^2)$.] We define the matrix

$$J(P^2) = \begin{bmatrix} J_{00}^{QQ} & J_{08}^{QQ} & J_{00}^{QP} & J_{08}^{QP} \\ J_{80}^{QQ} & J_{88}^{QQ} & J_{80}^{QP} & J_{88}^{QP} \\ J_{00}^{PQ} & J_{08}^{PQ} & J_{00}^{QQ} & J_{08}^{QQ} \\ J_{80}^{PQ} & J_{88}^{PQ} & J_{80}^{QQ} & J_{88}^{QQ} \end{bmatrix} , \tag{3.4.1}$$

where all the elements depend upon P^2. We also put the T matrix into a 4×4 matrix form, using the basis vector

$$\Phi^{\mu\nu}(k) = \begin{bmatrix} Q^{\mu\nu}(k)\,\lambda_0 \\ Q^{\mu\nu}(k)\,\lambda_8 \\ P^{\mu\nu}(k)\,\lambda_0 \\ P^{\mu\nu}(k)\,\lambda_8 \end{bmatrix} \tag{3.4.2}$$

and its transpose. Thus, we write

$$\hat{T}(P^2, k', k) = \Phi^T_{\mu\nu}(k')\,\hat{T}^{\mu\nu\alpha\beta}(P^2)\,\Phi_{\alpha\beta}(k)\ , \tag{3.4.3}$$

where $\hat{T}^{\mu\nu\alpha\beta}(P) = g^{\mu\nu\alpha\beta}\,\tilde{T}(P)$. Here $\tilde{T}(P^2)$ is also a 4×4 matrix.

We also define the matrix

$$G = -\begin{bmatrix} G_{T_1} & 0 & 0 & 0 \\ 0 & G_{T_1} & 0 & 0 \\ 0 & 0 & G_{T_2} & 0 \\ 0 & 0 & 0 & G_{T_2} \end{bmatrix}\ . \tag{3.4.4}$$

We then solve the matrix equation

$$(\,1 + GJ(P^2)\,)\,\tilde{T}(P^2) = G\ , \tag{3.4.5}$$

and write

$$\tilde{T}(P^2) = (\,1 + GJ(P^2)\,)^{-1}\,G\ . \tag{3.4.6}$$

Theoretical values for the masses of the f_2 mesons may be determined by finding the values of P^2 for which $\tilde{T}(P^2)$ is singular. Near a singularities of $\tilde{T}(P^2)$ we may write

$$(k' \mid \tilde{T}(P^2) \mid k) = -F^{\mu\nu}(k')\frac{g_{\mu\nu\alpha\beta}}{P^2 - m_i^2}F^{\alpha\beta}(k)\ , \tag{3.4.7}$$

where m_i^2 is the theoretical value of the squared mass of one of our f_2 mesons. Here,

we have defined the form factor

$$F^{\mu\nu}(k) = g\,Q^{\mu\nu}(k)[\cos\hat{\theta}\,\lambda_0 - \sin\hat{\theta}\,\lambda_8] + g'\,P^{\mu\nu}(k)[\cos\tilde{\theta}\,\lambda_0 - \sin\tilde{\theta}\,\lambda_8]\ . \qquad (3.4.8)$$

We may include confinement effects in the numerator of the T matrix [3], if we replace $F^{\alpha\beta}(k)$ by

$$\begin{aligned} F_c^{\mu\nu}(k) = {} & g\,\bar{\Gamma}_{T_1}^{\mu\nu}(P,\,k)[\cos\hat{\theta}\,\lambda_0 - \sin\hat{\theta}\,\lambda_8] \\ & + g'\bar{\Gamma}_{T_2}^{\mu\nu}(P,\,k)[\cos\tilde{\theta}\,\lambda_0 - \sin\tilde{\theta}\,\lambda_8]\ , \end{aligned} \qquad (3.4.9)$$

where $P^2 = m_i^2$. The presence of the confinement vertices $\bar{\Gamma}_{T_1}^{\mu\nu}(P,k)$ and $\bar{\Gamma}_{T_2}^{\mu\nu}(P,k)$ allows us to show that the T matrix is represented by bound states only, if the potential V^C is absolutely confining [3]. Recall that equations for $\bar{\Gamma}_{T_1}^{\mu\nu}(P,k)$ and $\bar{\Gamma}_{T_2}^{\mu\nu}(P,k)$ were presented in Eqs.(3.3.6) and (3.3.7).

If the matrix G is of the form given in Eq.(3.4.4), we find ideal mixing. If a state has the structure $(\bar{u}u + \bar{d}d)/\sqrt{2}$, the mixing angles are $\hat{\theta} = \tilde{\theta} = -35.26°$ and, for a $\bar{s}s$ state, $\hat{\theta} = \tilde{\theta} = 54.74°$. Deviations from ideal mixing can be obtained if we use different interactions for singlet and octet states. Such effects may be found if one takes into account coupling of states through the gluon field, a feature which only affects the strength of the interaction in singlet states.

3.5 Results of Numerical Calculations

As noted earlier, the spectrum of states may be obtained by studying the singularities of the T matrix. Result of our calculations are found in Fig.15 and Table

10. In Fig.15a we show the positions of the bound states in the confining field in the absence of the NJL interaction. The 1S $\bar{n}n$ state is at 1520 MeV, with the 2S and 3S states at about 1755 and 1970 MeV, respectively. The 1S and 2S $s\bar{s}$ states are at 1790 MeV and 1998 MeV. These states all have a degeneracy factor of 2, since they may be associated with the vertex governed by either $Q^{\mu\nu}$ or $P^{\mu\nu}$. Since the NJL forces are attractive, we expect to find at least ten states below 2 GeV. We show these ten states in Fig.15. [See Fig.16 and Table 11.]

The 1S $n\bar{n}$ state gives rise two states at 1254 and 1429 MeV, if we take G_{T_1} = 47.0 GeV^{-2} and G_{T_2} = 6.8 GeV^{-2}. The next state at 1527 MeV seen in Fig.15c originates from the 2S $n\bar{n}$ state. The fourth state at 1551 MeV is a 1S $s\bar{s}$ state and may be identified with the $f_2'(1525)$. (We see that we have overestimated the energy of that state by about 25 MeV.) There are two f_2' states at 1745 and 1767 MeV. [See Fig.16.] The first of these states, which is nodeless, may be identified with the $f_J(1750)$ if $J^{PC} = 2^{++}$ for that state [24]. (The 2S $s\bar{s}$ state at 1767 MeV may mix with the 1S state at 1745 MeV to some degree.)

The 2S $n\bar{n}$ state bound in the confining field gives rise to the states at 1524 and 1685 MeV. The second of these states may be identified with the $f_2(1640)$. We note that the two 2S $n\bar{n}$ states at 1524 and 1685 MeV in Table 10 have small values of g and g', when compared with the three 1S states listed in the table. That is as expected, since the coupling constants for meson-quark coupling (g and g') decrease rapidly with increase of the number of nodes in the meson wave function. [We remark that the phase of the form factor, $F^{\mu\nu}(k)$ or $F_c^{\mu\nu}(k)$, is arbitrary, however, the relative phase

of g and g' is meaningful.]

3.6 Discussion

As may be seen in Fig.15, we predict one or two more states than are seen in experiment. That suggests that there is little evidence in our study for non-$q\bar{q}$ states below 2 GeV. Since some of the states shown in Fig.15c are quite close in energy, there could be a good deal of additional configuration mixing, since the states can be coupled to each other via their decay channels. However, the first four states appear reasonably well isolated from the other groupings and their characterization may survive further coupling interactions such as that mentioned above.

We have also remarked that the spacing of levels in the confining field is radically different than that obtained from a harmonic oscillator potential. For example, in our model, states that differ by a single node in the wave function are separated by about 225 MeV. (See Fig.15a.) However, if we consider the 1S $n\bar{n}$ state at about 1520 MeV and subtract $2\,m_u = 728$ MeV, we are left with an excitation in the potential of approximately 800 MeV, a value that may be compared to the 225 MeV level separation mentioned above. We conclude that the covariant confinement model places the states in the confining field (Fig.15a) in a quite satisfactory arrangement, so that the introduction of two new terms in the short-range (NJL) interaction brings the theoretical spectrum into overall agreement with the f_2 states obtained from experiment.

Chapter 4

Covariant Confinement Model for the Calculation of the Properties of Scalar Mesons

4.1 Introduction

In our previous work and in Chapters 2 and 3, we studied properties of a broad range of light mesons, with the exception of the scalar-isoscalar f_0 mesons [17,25]. In this chapter, we extend our calculations to study the spectrum of the f_0 mesons. Such calculations are complicated by the fact that one expects to find a low-lying scalar glueball among the f_0 states. Also, the f_0 states exhibit significant coupling to the $\pi\pi$ and $K\bar{K}$ channels and the four-pion continuum. Coupling to the $\eta\eta$ and $\eta\eta'$ channels appears to play a less important role. In this chapter we calculate the effects of coupling to the $\pi\pi$, $K\bar{K}$, $\eta\eta$ and $\eta\eta'$ channels and treat decay to the four-pion and other meson channels by introducing a single parameters into our analysis. In addition, there is another parameter that determines the form of the regularization of loop diagrams with three vertices. The other parameters used have been fixed in our earlier work [17].

We remind the reader that our model is a relativistic quark model whose form is suggested by the SU(3)-flavor Nambu – Jona-Lasinio (NJL) model. Since we have

applied our model to study spectra up to 2.4 GeV in a recent work [26], we see that our model may not be directly identified with NJL model, which is usually considered to be applicable up to energies of the order of the cutoff, which is about 900 MeV for Euclidean-space calculations and about 700 MeV for Minkowski-space calculations. [See reference [6] for reviews of the NJL model.]

Our model has a number of good features which include chiral symmetry of the Lagrangian and a covariant model of confinement. While we usually study mesons in their rest frame, our calculations may be shown to be covariant. The Lagrangian of our model is

$$\begin{aligned}\mathcal{L} = &\bar{q}(i\partial - m^0)q + \frac{G_S}{2}\sum_{i=0}^{8}\left[(\bar{q}\lambda^i q)^2 + (\bar{q}i\gamma_5\lambda^i q)^2\right] \\ &- \frac{G_V}{4}\sum_{i=0}^{8}\left[(\bar{q}\gamma^\mu\lambda^i q)^2 + (\bar{q}\gamma^\mu\gamma_5\lambda^i q)^2\right] \\ &+ \frac{G_D}{2}\left\{\det[\bar{q}(1+\gamma_5)q] + \det[\bar{q}(1-\gamma_5)q]\right\} \\ &+ \mathcal{L}_{tensor} + \mathcal{L}_{conf}\ ,\end{aligned} \tag{4.1.1}$$

Here, the fourth term is the 't Hooft interaction [6], $\mathcal{L}_{tensor}$ denotes interactions added to study tensor mesons, while $\mathcal{L}_{conf}$ denotes our model of confinement [25].

The organization of this chapter is as follows. In Section 4.2 we review the calculation of the leading vacuum-polarization diagram of the NJL model and show how confinement vertices are introduced in the calculation. The leading vacuum polarization diagram is of order of n_c, where n_c is the number of colors. In Section 4.3 we discuss a class of polarization diagrams of order 1 that describe the effect of

decay to various continuum meson channels. These diagrams yield complex functions $K(P^2)$, that allow us to obtain energy shifts and decay width of the f_0 states. In Section 4.4 we show how $q\bar{q}$ T matrices may be constructed in terms of the vacuum polarization functions. The spectrum of f_0 states may be obtained by studying the singularities of the T matrix. In Section 4.5 we present some results of our numerical calculations. Our most satisfactory treatment of the problem is reserved for the discussion given in Section 4.6. Finally, Section 4.7 contains some further discussion and concluding remarks.

4.2 Vacuum Polarization Diagrams and Confinement Vertex Functions

In calculations made using the Nambu – Jona-Lasinio model one calculates the vacuum polarization function represented in Fig.17a. For this work we need to consider the functions involving scalar vertices, $J^S_{88}(P^2)$, $J^S_{80}(P^2) = J^S_{08}(P^2)$ and $J^S_{00}(P^2)$. We define

$$-iJ^S_{ij}(P^2) = -n_c \int \frac{d^4k}{(2\pi)^4} \mathrm{Tr}\left[iS(P/2+k)\lambda_i iS_b(-P/2+k)\lambda_j\right], \qquad (4.2.1)$$

where λ_i and λ_j are the Gell-Mann matrices and $S(P) = [\not{P} - m + i\eta]^{-1}$ is the quark propagator for a quark of constituent mass m. The function defined in Eq.(4.2.1) has a cut for $P^2 > (2m)^2$ corresponding to the quark of momentum $P/2 + k$ and the antiquark of momentum $P/2 - k$ both going on mass shell. In our model that cut is eliminated by introducing a model of confinement. That is accomplished by inserting

a vertex for the confining interaction, as shown in Fig.17b, where we also show a perturbative expansion of the confining vertex. The inhomogeneous equation for that vertex is shown in Fig.18.

The scalar vertex is a solution of the equation

$$\bar{\Gamma}^S(P,k) = 1 - i\int \frac{d^4k'}{(2\pi)^4}\left[\gamma^\rho S(P/2+k')\bar{\Gamma}^S(P,k')S(-P/2+k')\gamma_\rho\right] \times V^C(\vec{k}-\vec{k}') \tag{4.2.2}$$

in the meson rest frame ($\vec{P} = 0$). It is also useful to introduce the functions Γ_S^{+-} and Γ_S^{-+}. We first define the projection operators

$$\Lambda^{(+)}(\vec{k}) = \frac{\not{k} + m}{2m} \quad , \tag{4.2.3}$$

and

$$\Lambda^{(-)}(-\vec{k}) = \frac{\tilde{\not{k}} + m}{2m} \quad , \tag{4.2.4}$$

with $k^\mu = [E(\vec{k}), \vec{k}]$ and $\tilde{k}^\mu = [-E(\vec{k}), \vec{k}]$. Then, we write

$$\Lambda^{(+)}(\vec{k})\bar{\Gamma}^S(P,k)\Lambda^{(-)}(-\vec{k}) = \Gamma_S^{+-}(P,k)\Lambda^{(+)}(\vec{k})\Lambda^{(-)}(-\vec{k}) \tag{4.2.5}$$

and

$$\Lambda^{(-)}(-\vec{k})\bar{\Gamma}^S(P,k)\Lambda^{(+)}(\vec{k}) = \Gamma_S^{-+}(P,k)\Lambda^{(-)}(-\vec{k})\Lambda^{(+)}(\vec{k}) \ . \tag{4.2.6}$$

For a study of the a_0 mesons only a single function $J^S(P^2)$ was needed [18]. In that case we found

$$J^S(P^2) = -2n_c \int \frac{d^3k}{(2\pi)^3} \frac{\vec{k}^2}{E^2(\vec{k})} \left[\frac{\Gamma_S^{+-}(P,k)}{P^0 - 2E(\vec{k})} - \frac{\Gamma_S^{-+}(P,k)}{P^0 + 2E(\vec{k})} \right] , \qquad (4.2.7)$$

where the factor of 2 arose from the flavor trace. Similar integrals for up, down and strange quarks are needed when constructing $J_{88}^S(P^2)$, $J_{08}^S(P^2)$ and $J_{00}^S(P^2)$ for our study of the f_0 mesons. We use the notation $J_{ud}^S(P^2)$, if Eq.(4.2.7) is evaluated for an up (or down) quark. If a strange quark appears in Eq.(4.2.7), we use the notation $J_{ss}^S(P^2)$ for the function defined in Eq.(4.2.7). We show values calculated for $J_{ud}^S(P^2)$ and $J_{ss}^S(P^2)$ in Figs.19 and 20. Note that these functions are singular when $\bar{\Gamma}_S(P,k)$ is singular. That occurs when the homogeneous version of Eq.(4.2.2) has a solution. The energies at which such singularities appear are the energies of bound states in the confining yield. [See Figs.19 and 20.] (We remark that Eq.(4.2.2) does not require a momentum cutoff for large values of $|\vec{k}|$. We have made calculations for $|\vec{k}|_{max}$ = 2 GeV and 4 GeV in our earlier work.) Note that $J_{00}^S(P^2)$, $J_{08}^S(P^2)$ and $J_{88}^S(P^2)$ are readily obtained in terms of $J_{ud}^S(P^2)$ and $J_{ss}^S(P^2)$.

4.3 Vacuum Polarization Diagrams Describing Coupling to States of Two or More Mesons

In this section we discuss the calculation of vacuum polarization diagrams such as that shown in Fig.21a. There, the wavy lines denote mesons. Such diagrams serve to define functions $K_{ij}(P^2)$. The quark-loop integrals are calculated using the notation given in Fig.22. In Fig.22 we only show the $\pi\pi$ and $K\bar{K}$ channels. However, we have

calculated $K_{ij}(P^2)$ for the $\eta\eta$ and $\eta\eta'$ channels as well. Since $K_{ij}(P^2)$ is found to be small for the $\eta\eta$ and $\eta\eta'$ channels, we do not present our results for those channels. Confining vertex functions are neglected for the pion, as in Fig.22a. However, such vertex functions are included for all other mesons.

The treatment of the scalar vertex in Fig.22 requires a detailed discussion. In the last section, we introduced the functions Γ_S^{+-} and Γ_S^{-+}. We now also define the function Γ_S^{++} and Γ_S^{--} for $\vec{P} = 0$:

$$\Lambda^{(+)}(\vec{k})\,\bar{\Gamma}^S(P,k)\,\Lambda^{(+)}(\vec{k}) = \Gamma_S^{++}(P,k)\Lambda^{(+)}(\vec{k})\Lambda^{(+)}(\vec{k}) \tag{4.3.1}$$

and

$$\Lambda^{(-)}(-\vec{k})\,\bar{\Gamma}^S(P,k)\,\Lambda^{(-)}(-\vec{k}) = \Gamma_S^{--}(P,k)\Lambda^{(-)}(-\vec{k})\,\Lambda^{(-)}(-\vec{k})\ . \tag{4.3.2}$$

A general expression for the scalar vertex $\bar{\Gamma}^S(P,k)$ was given in Ref.[11]. If both the quark and the antiquark at the scalar vertex have the same mass, we saw that we could write

$$\bar{\Gamma}_S(P,k) = a_1(P,k) + \hat{k}\,a_2(P,k)\ , \tag{4.3.3}$$

where the four-vector

$$\hat{k}^\mu = k^\mu - \frac{(k\cdot P)\,P^\mu}{P^2} \tag{4.3.4}$$

was defined previously. We find that

$$\Gamma_S^{+-}(P,k) = a_1(P,k) + m_q\,a_2(P,k)\ , \tag{4.3.5}$$

and

$$\Gamma_S^{++}(P,k) = a_1(P,k) - \frac{\vec{k}^2}{m_q} a_2(P,k) \ . \tag{4.3.6}$$

We have the following equation for $\Gamma_S^{+-}(P,k)$ when $\vec{P} = 0$ [11],

$$\Gamma_S^{+-}(P^0,k) = 1 - 4\pi \int \frac{k'^2 dk'}{(2\pi)^2} \left[V_0^C(k,k') + \frac{m_q^2}{2kk'} V_1^C(k,k') \right] \times \frac{-8\vec{k}'^2}{E(k')} \frac{\Gamma_S^{+-}(P^0,k')}{(P^0)^2 - [2E(k')]^2} \ . \tag{4.3.7}$$

The function $\Gamma_S^{++}(P,k)$ may be obtained once $\Gamma_S^{+-}(P,k)$ is known by evaluating the following integral

$$\Gamma_S^{++}(P^0,k) = 1 - 4\pi \int \frac{k'^2 dk'}{(2\pi)^2} \left[V_0^C(k,k') - \frac{k}{2k'} V_1^C(k,k') \right] \times \frac{-8\vec{k}'^2}{E(k')} \frac{\Gamma_S^{+-}(P^0,k')}{(P^0)^2 - [2E(k')]^2} \ . \tag{4.3.8}$$

In Eqs.(4.3.7) and (4.3.8) $k = |\vec{k}|$, $k' = |\vec{k}'|$, and

$$V_l^C(k,k') = \frac{1}{2} \int_{-1}^{1} dx \, P_l(x) \, V_c(\vec{k}^2 + \vec{k}'^2 - 2kk'x) \ . \tag{4.3.9}$$

Using Eq.(4.3.3) we may show that $\Gamma_S^{+-} = \Gamma_S^{-+}$ and $\Gamma_S^{++} = \Gamma_S^{--}$. The more general case, in which the quark masses at the vertex are unequal, is discussed in Ref.[17].

As noted earlier, $\bar{\Gamma}_S(P,k)$ is singular when the homogeneous version of Eq.(4.3.7) has a solution. That feature gives rise to singularities in both $J^S(P^2)$ and $K_{ij}(P^2)$. [See Figs.19 and 20.] The singularities of $J^S(P^2)$ create no problem for the analysis. However, the corresponding singularities of $K_{ij}(P^2)$ can be seen to lead to

a double-counting of diagrams and must be removed. A satisfactory procedure is to calculate $K_{ij}(P^2)$ using a Hilbert space for the quark and antiquark that is orthogonal to the space spanned by all the bound state wave functions of the confining field. In this chapter, we approximated Eq.(4.3.7) by the equation

$$\Gamma_S^{+-}(P^0,k) = 1 - 4\pi \int \frac{k'^2 dk'}{(2\pi)^2} \left[V_0^C(k,k') + \frac{m_q^2}{2kk'} V_1^C(k,k') \right] \times \frac{-8\overline{k}'^2}{E(k')} \frac{1}{4E(k')} \frac{\Gamma_S^{+-}(P^0,k')}{P^0 - 2E(k')} \tag{4.3.10}$$

and defined a "wave function"

$$\psi(P,k) = \frac{\Gamma_S^{+-}(P,k)}{P^0 - 2E(k)} \tag{4.3.11}$$

which is finite, since $\Gamma_S^{+-}(P,k) = 0$ when $P^0 = 2E(\overline{k})$. We note that for large $|\overline{k}|$, $\psi(P,k) \to -1/(2|\overline{k}|)$, since $\Gamma_S^{+-}(P,k) \to 1$ for large $|\overline{k}|$.

It is useful to symmetrize the homogeneous version of Eq.(4.3.10) by first multiplying Eq.(4.3.10) by $k^2/E(k)$. We can then write the homogenous version of Eq.(4.3.10) as a standard bound-state problem of the form

$$[E_i - 2E(k)]\overline{\phi}_i(k) = -4\pi \int dk' H_1(k,k')\,\overline{\phi}_i(k') \ , \tag{4.3.12}$$

where $H_1(k,k')$ is symmetric. We solve Eq.(4.3.12) for bound states $\overline{\phi}_i(k)$ which have energies E_i. We then define the set of states

$$\phi_i(k) = \frac{E(k)}{k^2}\overline{\phi}_i(k) \ . \tag{4.3.13}$$

We start with $\phi_1(k)$ and normalize that function by requiring that

$$\langle \phi_1^N | \phi_1^N \rangle \equiv \int dk \phi_1^N(k) \phi_1^N(k) \tag{4.3.14a}$$

$$= 1 \ . \tag{4.3.14b}$$

We then construct

$$| \phi_2' \rangle = | \phi_2 \rangle - \langle \phi_1^N | \phi_2 \rangle \ | \phi_1^N \rangle \tag{4.3.15}$$

such that $\langle \phi_1^N | \phi_2' \rangle = 0$. We normalize $| \phi_2' \rangle$ as in Eq.(4.3.14), and denote the normalized function as $| \phi_2^N \rangle$. As a next step we construct

$$| \phi_3' \rangle = | \phi_3 \rangle - \langle \phi_2^N | \phi_3 \rangle \ | \phi_2^N \rangle - \langle \phi_1^N | \phi_3 \rangle \ | \phi_1^N \rangle \ . \tag{4.3.16}$$

This procedure is continued for all the bound states, yielding a set $| \phi_i^N \rangle$ that is used to construct the project operator

$$Q(k, k') = \sum_{i=1}^{n} \phi_i^N(k) \phi_i^N(k') \ . \tag{4.3.17}$$

We then define a function that is orthogonal to all the bound state wave functions

$$\Phi(P, k) = \psi(P, k) - \int dk' Q(k, k') \psi(P, k') \ . \tag{4.3.18}$$

Next, we introduce a modified vertex function

$$\hat{\Gamma}_S^{+-}(P, k) = [P^0 - 2E(\overline{k})] \Phi(P, k) \ , \tag{4.3.19}$$

and $\hat{\Gamma}_S^{-+}(P, k) = \hat{\Gamma}_S^{+-}(P, k)$. We obtain $\hat{\Gamma}_S^{++}(P, k) = \hat{\Gamma}_S^{--}(P, k)$ by using Eq.(4.3.8) with $\Gamma_S^{+-}(P, k)$ replaced by $\hat{\Gamma}_S^{+-}(P, k)$ on the right-hand side of Eq.(4.3.8). We then use Eqs.(4.3.5) and (4.3.6), with Γ_S^{+-} and Γ_S^{++} replaced by $\hat{\Gamma}_S^{+-}$ and $\hat{\Gamma}_S^{++}$. In this manner, we obtain

$$\hat{a}_1(P,k) = \frac{1}{2}\left[\hat{\Gamma}_S^{++}(P,k) + \frac{\overline{k}^2}{m_q^2}\hat{\Gamma}_S^{+-}(P,k)\right] \qquad (4.3.20)$$

and

$$\hat{a}_2(P,k) = \frac{m_q}{E(k)}\left[\hat{\Gamma}_S^{+-}(P,k) - \hat{\Gamma}_S^{++}(P,k)\right] . \qquad (4.3.21)$$

This entire procedure may be made covariant [17] leading to the definition of the invariants $\hat{a}_1(\sqrt{P^2}\,, \sqrt{-\hat{k}_c^2}\,)$ and $\hat{a}_2(\sqrt{P^2}\,, \sqrt{-\hat{k}_c^2}\,)$, where $k_c^\mu = k^\mu - (k\cdot P)P^\mu/P^2$. Thus, we may use

$$\hat{\Gamma}^S(P,k) = \hat{a}_1(\sqrt{P^2}\,, \sqrt{-k_c^2}\,) + \hat{\not{k}}\,\hat{a}_2(\sqrt{P^2}\,, \sqrt{-k_c^2}\,) \qquad (4.3.22)$$

as the scalar vertex. This procedure completely eliminates singularities that would otherwise occur in $K_{ij}(P^2)$.

In our calculations, we neglect confinement for the pion and use a coupling constant $g_{\pi qq} = 4.57$ with a mixing angle of $\theta = -3.09°$. For the kaon vertices, we include confinement and pseudoscalar – axial-vector coupling. In general, we have [28]

$$f(P,k_c) = i\,g_{Kqq}\{\gamma_5\cos\theta\,[\,b_0 + b_1\not{P} + b_2\hat{\not{k}}_c] + \sin\theta\frac{\not{P}\gamma_5}{\sqrt{P^2}}[d_0 + \not{P}\,d_1\,]\}\,. \qquad (4.3.23)$$

For the kaon we found $g_{Kqq} = 8.09$ and $\theta = -7.04°$ [28]. The functions b_0, b_1, b_2, d_0 and d_1, which depend upon $\sqrt{P^2}$ and $\sqrt{-k_c^2}$, implement our model of confinement. It is worth noting that, if the meson of momentum P is leaving the vertex, we need to change the signs of b_1, b_2 and d_0 in Eq.(4.3.23). While confinement might be neglected for the kaon, it is essential for the η'. Since the formalism is fully covariant, the

singularities that would otherwise appear when calculating decay amplitudes, such as those shown in Fig.22, are automatically removed for an η' meson of any momentum present in the decay channel.

We use the notation $M_i(P^2)$, with $i = 0$ or 8, for the decay amplitude of Fig.22. A particularly important feature of the calculation of these decay amplitudes is the regularization of the quark-loop integrals representing the processes seen in Fig.22. The choice of such a regulator was first discussed in Ref.[27]. The regulator we use for the first part of our study is given by

$$R(k_c^2, P^2) = \sqrt{\frac{2}{3}}\, \exp[k_c^2/\alpha_1^2]\{\, 1 - \exp[P^2 - m_{th}^2)/\beta^2]\} \ . \qquad (4.3.24)$$

With $m_{th} = 2\,m_\pi$ for two-pion decay, $m_{th} = 2\,m_K$ for $K\bar{K}$ decay, etc. We use $\alpha_1 = 0.325$ GeV and $\beta^2 = 0.434$ GeV^2 [27]. Again, $k_c^\mu = k^\mu - (k\cdot P)P^\mu/P^2$, so that $k_c^\mu = [0, \vec{k}]$ when $\vec{P} = 0$. The parameters α_1 and β^2 were fixed in Ref.[27] and the values obtained there are used here. The factor $[1 - \exp[-(P^2 - m_{th}^2)/\beta^2]$ in Eq.(4.3.24) has been introduced to soften the cusplike behavior of $\mathrm{Re}K_{ij}(P^2)$ at the various thresholds. Without that factor we can obtain bound states below the energy of the $f_0(980)$. This problem is solved when we introduce $\mathrm{Im}K_{ij}(P^2)$ at a later point in this chapter. However, $R(k_c^2, P^2)$ of Eq.(4.3.24) is quite useful for studying the spectrum of states in the approximation in which we include $\mathrm{Re}K_{ij}(P^2)$ and neglect $\mathrm{Im}K_{ij}(P^2)$. That approximation is maintained until the last part of Section 4.4, at which point we introduce $\mathrm{Im}K_{ij}(P^2)$, while keeping the form of Eq.(4.3.24). In Section 4.6, we describe our results when the P^2-dependent factor of Eq.(4.3.24) is

removed. As we will see, the main effect of removing that factor is to provide a "background" for the $f_0(980)$, which is probably closely related to the introduction of the $f_0(400\text{-}1200)$ "meson", which now appear in the data tables. We also find satisfactory values for the $\Gamma(K\bar{K})/[\Gamma(\pi\pi)+\Gamma(K\bar{K})]$ branching ratio for the $f_0(980)$ in the calculation reported in Section 4.6. It is instructive, however to proceed with $R(k_c^2, P^2)$ of Eq.(4.3.24) and we will do so through Section 4.5. [The use of $R(k_c^2, P^2)$, with and without the P^2-dependent factor, clarifies the role of the cusplike behavior found for $\mathrm{Re}K_{ij}(P^2)$ at the opening of the $\pi\pi$ and $K\bar{K}$ thresholds and leads to some understanding of the origin of the $f_0(400-1200)$, as noted above.]

The factor $\sqrt{2/3}$ in Eq.(4.3.24) sets the overall scale for $\mathrm{Im}K_{ij}(P^2)$ and is adjusted so that the width of the $f_0(980)$ is reasonable. (With the factor $\sqrt{2/3}$ in place, we obtain $\Gamma_{f_0}(980) = 56$ MeV in the calculation reported in Section 4.6.) There is one more new parameter in our analysis that we will introduce in the next section. An additional parameter is needed, since we have only calculated $\mathrm{Im}K_{ij}(P^2)$ for the $\pi\pi$, $K\bar{K}$, $\eta\eta$ and $\eta\eta'$ channels, while the decay of f_0 mesons to the four-pion continuum is known to be quite important for several states [29].

4.4 T Matrices for Scalar-Isoscalar Meson States: Quarkonium-Glueball Coupling

As noted in our earlier discussion, a procedure for finding the energies of the scalar states is to construct a $q\bar{q}$ T matrix and determine the energies at which the T matrix is singular [17]. The T matrix is written in terms of the vacuum polarization

functions defined in the previous sections. We have maintained the definition of $J_{ij}^{S}(P^2)$ given in Eq.(4.2.1) for ease of reference to our earlier work. However, for the study of singlet-octet mixing in this work, we will use as a basis the Gell-Mann matrices $\lambda_8/\sqrt{2}$ and $\lambda_0/\sqrt{2}$ rather than λ_8 and λ_0. Therefore, maintaining the notation of our earlier work, we will introduce factors of 1/2 for $J_{ij}^{S}(P^2)$ and $K_{ij}(P^2)$ when constructing the $q\bar{q}$ T matrix. Similarly, we will write $2G_{88}$ and $2G_{00}$ for the coupling constants. Thus, we define a matrix

$$G = \begin{bmatrix} 2G_{88} & 0 \\ 0 & 2G_{00} \end{bmatrix} , \tag{4.4.1}$$

where we have neglected the small term $G_{08} = G_{80}$. We also define the matrix

$$J(P^2) + \mathrm{Re}K(P^2) = \begin{bmatrix} \frac{1}{2}[J_{88}(P^2) + \mathrm{Re}K_{88}^{T}(P^2)] & \frac{1}{2}[J_{80}(P^2) + \mathrm{Re}K_{80}^{T}(P^2)] \\ \frac{1}{2}[J_{08}(P^2) + \mathrm{Re}K_{08}^{T}(P^2)] & \frac{1}{2}[J_{00}(P^2) + \mathrm{Re}K_{00}^{T}(P^2)] \end{bmatrix} , \tag{4.4.2}$$

where

$$K_{ij}^{T}(P^2) = K_{ij}^{\pi\pi}(P^2) + K_{ij}^{K\bar{K}}(P^2) + \ldots \quad . \tag{4.4.3}$$

In Eq.(4.4.3) the superscripts refer to the two-meson continuum channels. For example, in Figs.23 and 24, we exhibit the values calculated for the imaginary parts of $K_{88}^{\pi\pi}$, $K_{08}^{\pi\pi}$, $K_{00}^{\pi\pi}$, $K_{88}^{K\bar{K}}$, $K_{08}^{K\bar{K}}$ and $K_{00}^{K\bar{K}}$. We obtain the corresponding real parts by use of a dispersion relation. For example,

$$\mathrm{Re}K_{ij}^{\pi\pi}(P^2) = -\frac{\mathrm{P}}{\pi}\int_{(2m_\pi)^2}^{\Lambda^2} dP' \frac{\mathrm{Im}K_{ij}^{\pi\pi}(P'^2)}{P^2 - P'^2} \ , \qquad (4.4.4)$$

where the upper limit Λ^2 is taken to be 6.0 GeV^2 in this chapter. Contributions from mass values larger than Λ^2 appear as contributions to the parameter introduced in Eq.(4.4.6).

We now need to describe $\mathrm{Re}K_{ij}^{T}(P^2)$ appearing in Eq.(4.4.2) in greater detail. We write

$$\mathrm{Re}K_{ij}^{T}(P^2) = \mathrm{Re}K_{ij}^{\pi\pi}(P^2) + \mathrm{Re}K_{ij}^{K\bar{K}}(P^2) + \mathrm{Re}K_{ij}^{\pi\pi\pi\pi}(P^2) + \mathrm{Re}\Delta K_{ij}(P^2) \ , \qquad (4.4.5)$$

where $\mathrm{Re}K_{ij}^{\pi\pi\pi\pi}(P^2)$ refers to the contribution of coupling to the four-pion continuum channel and $\mathrm{Re}\Delta K_{ij}(P^2)$ refers to all other channels: $\eta\eta$, $\eta\eta'$, $\eta'\eta'$, $\rho\rho$, and multi-meson channels other the four-pion channel. As a first step, we approximate $\mathrm{Re}K_{ij}^{\pi\pi\pi\pi}(P^2) = \mathrm{Re}K_{ij}^{\pi\pi}(P^2) + \mathrm{Re}K_{ij}^{K\bar{K}}(P^2)$. For example, for the $f_0(1370)$, we find $\Gamma(4\pi)/\Gamma_{total} = 0.80 \pm 0.04$ [29]. (However, this last branching ratio is uncertain, since the quite broad $f_0(1370)$ overlaps the $f_0(400\text{-}1200)$ to some degree.) For the $f_0(1500)$, we find $\Gamma(K\bar{K})/\Gamma_{total} = 0.044 \pm 0.021$ and $\Gamma(2\pi)/\Gamma_{total} = 0.454 \pm 0.104$, suggesting that $\Gamma(4\pi)/\Gamma_{total} \sim 0.5$, if $\Gamma(\eta\eta)/\Gamma_{total}$ and $\Gamma(\eta\eta')/\Gamma_{total}$ are small, as they are in our model. We also suggest that $\mathrm{Re}\Delta K_{ij}^{T}(P^2) \sim \mathrm{Re}K_{ij}^{\pi\pi}(P^2) + \mathrm{Re}K_{ij}^{K\bar{K}}(P^2)$ so that we finally assume

$$\mathrm{Re}K_{ij}^{T}(P^2) = 3\,[\mathrm{Re}K_{ij}^{\pi\pi}(P^2) + \mathrm{Re}K_{ij}^{K\bar{K}}(P^2)] \ . \qquad (4.4.6)$$

The factor of 3 in Eq.(4.4.6) is an important parameter of our model, since the mass values predicted for the $f_0(980)$ and $f_0(1370)$ are sensitive to the value chosen for that

parameter. Figure 25 shows values of $\mathrm{Re}K_{ij}^{T}(P^2)$ obtained with the use of Eq.(4.4.4). (The factor of 3 in Eq.(4.4.6) is not included.)

We note that the detailed dependence on P^2 of $\mathrm{Re}K_{ij}^{****}(P^2)$ and $\Delta\mathrm{Re}K_{ij}(P^2)$ is not important, since only the energies of the $f_0(980)$ and $f_0(1370)$ are sensitive to the values of $\mathrm{Re}K_{ij}^{T}(P^2)$, as we will see. It is also important to understand that the contribution of all closed channels above 1500 MeV will make positive contributions to $\mathrm{Re}K_{ii}^{T}(P^2)$ in the region below 1500 MeV, where we find the $f_0(980)$ and $f_0(1370)$. That follows from the form of the dispersion relations, such as that given in Eq.(4.4.4), and the fact that $\mathrm{Im}K_{ii}(P^2)$ is positive. Ideally, it would be desirable to have calculations of the contribution to $\mathrm{Re}K_{ij}^{T}(P^2)$ of the channels other than $\pi\pi$, $K\bar{K}$, $\eta\eta$ and $\eta\eta'$, whose contributions to $\mathrm{Re}K_{ij}^{T}(P^2)$ have been calculated in this chapter.

A T matrix is obtained as a solution of the matrix equation

$$t^{S}(P^2) = -G + G[J(P^2) + \mathrm{Re}K(P^2)]\,t^{S}(P^2) \tag{4.4.7}$$

or

$$t^{S}(P^2) = -(1 - G[J(P^2) + \mathrm{Re}K(P^2)])^{-1}G\ . \tag{4.4.8}$$

We will use the notation

$$t^{S}(P^2) = \begin{bmatrix} t_{88}(P^2) & t_{80}(P^2) \\ t_{08}(P^2) & t_{00}(P^2) \end{bmatrix} \tag{4.4.9}$$

for $t^{S}(P^2)$ of Eq.(4.4.8).

The coupling constants of Eq.(4.4.1) may be expressed in terms of the

parameters G_S and G_D that appear in Eq.(4.1.1). We use a notation related to that of Vogl and Weise [6] and write

$$G_{88} = G_S - \frac{G_D}{2} c_{88} \ , \tag{4.4.10}$$

and

$$G_{00} = G_S - \frac{G_D}{2} c_{00} \ , \tag{4.4.11}$$

with c_{88} and c_{00} expressed in terms of the vacuum condensates

$$c_{88} = \frac{1}{3} (4 \langle \bar{u}u \rangle - \langle \bar{s}s \rangle) \tag{4.4.12}$$

and

$$c_{00} = - \frac{2}{3} (2 \langle \bar{u}u \rangle + \langle \bar{s}s \rangle) \ . \tag{4.4.13}$$

With $\langle \bar{u}u \rangle$ = - (0.248 GeV)^3 and $\langle \bar{s}s \rangle$ = -(0.258 GeV)^3, we have c_{88} = -0.0146 GeV^3 and c_{00} = 0.0317 GeV^3. With the choice G_S = 11.83 GeV^{-2} and G_D = 86.39 GeV^{-2}, we have G_{88} = 12.46 GeV^{-2} and G_{00} = 10.46 GeV^{-2}. These values of G_{88} and G_{00} are those used in the extensive studies reported in Ref.[17] and, therefore, do not represent new parameters.

A T matrix may also be written with an explicit representation of the flavor matrices:

$$\bar{t}^{S}(P^2) = \frac{\lambda_8}{\sqrt{2}} t_{88}(P^2) \frac{\lambda_8}{\sqrt{2}} + \frac{\lambda_8}{\sqrt{2}} t_{80}(P^2) \frac{\lambda_0}{\sqrt{2}} + \frac{\lambda_0}{2} t_{80}(P^2) \frac{\lambda_8}{\sqrt{2}} + \frac{\lambda_0}{2} t_{00}(P^2) \frac{\lambda_0}{\sqrt{2}} \,. \tag{4.4.14}$$

The basis $\lambda_8/\sqrt{2}$ and $\lambda_0/\sqrt{2}$ is useful since it is related by a unitary transformation to the basis spanned by the matrices λ_{nn} and λ_{ss}, with

$$\begin{bmatrix} \lambda_{nn} \\ \lambda_{ss} \end{bmatrix} = M \begin{bmatrix} \lambda_8/\sqrt{2} \\ \lambda_0/\sqrt{2} \end{bmatrix} \,. \tag{4.4.15}$$

Here,

$$M = \begin{bmatrix} \sqrt{\frac{1}{3}} & \sqrt{\frac{2}{3}} \\ -\sqrt{\frac{2}{3}} & \sqrt{\frac{1}{3}} \end{bmatrix} \,, \tag{4.4.16}$$

so that

$$\lambda_{nn} = \frac{\lambda_8}{\sqrt{6}} + \frac{\lambda_0}{\sqrt{3}} \,, \tag{4.4.17}$$

and

$$\lambda_{ss} = -\frac{\lambda_8}{\sqrt{3}} + \frac{\lambda_0}{\sqrt{6}} \,. \tag{4.4.18}$$

This transformation is useful since our results are rather close to "ideal mixing" with the T matrix approximately diagonal in the basis given by λ_{nn} and λ_{ss}.

To include the glueball in our formalism we extend the definition of G to read

$$G = \begin{bmatrix} 2G_{88} & 0 & 0 \\ 0 & 2G_{00} & g' \\ 0 & g' & g'' \end{bmatrix} , \qquad (4.4.19)$$

where we have used the fact that the glueball only couples to singlet states, with g' a measure of such coupling. The matrix elements $[J(P^2) + \mathrm{Re}K(P^2)]_{ij}$ with $i = 1, 2, 3$ and $j = 1, 2, 3$ are now obtained by adding the element $\delta_{3,i}\delta_{3,j}J_{gg}(P^2)$ to the elements given in Eq.(4.4.2). We write

$$J_{gg}(P^2) = -\frac{a^2}{P^2 - m_g^2} , \qquad (4.4.20)$$

where a^2 is a parameter and m_g is the "bare mass" of the glueball. In the absence of quarkonium-glueball mixing, the mass of the glueball is $m_G^2 = m_g^2 - g''a^2$. Since, in this work, g'' and a are taken to be quite small, we have $m_G^2 \simeq m_g^2$.

As we will see, when g' is small the glueball is hardly mixed into other states. Therefore, we will work with 2×2 matrices when describing some of our results. It is useful to define the matrices of dimension two

$$\hat{J}^S(P^2) = M J(P^2) M^{-1} , \qquad (4.4.21)$$

$$\hat{K}^S(P^2) = M K(P^2) M^{-1} , \qquad (4.4.22)$$

$$\hat{G}^S(P^2) = M G M^{-1} , \qquad (4.4.23)$$

and

$$\hat{t}^S(P^2) = M t^S(P^2) M^{-1} \ . \tag{4.4.24}$$

We note that

$$\hat{J}^S(P^2) = \begin{bmatrix} J^S_{nn}(P^2) & J^S_{ns}(P^2) \\ J^S_{sn}(P^2) & J^S_{ss}(P^2) \end{bmatrix} \ , \tag{4.4.25}$$

with

$$J^S_{nn}(P^2) = \frac{1}{2}\left[\frac{1}{3} J^S_{88}(P^2) + \frac{2}{3} J^S_{00}(P^2) + \frac{2\sqrt{2}}{3} J^S_{08}(P^2) \right] \ , \tag{4.4.26}$$

$$J^S_{ss}(P^2) = \frac{1}{2}\left[\frac{2}{3} J^S_{88}(P^2) + \frac{1}{3} J^S_{00}(P^2) - \frac{2\sqrt{2}}{3} J^S_{08}(P^2) \right] \tag{4.4.27}$$

and $J_{ns}(P^2) = J_{sn}(P^2) = 0$. There are similar relations for $K^T_{nn}(P^2)$, $K^T_{ss}(P^2)$ and $K^T_{ns}(P^2)$. However, $K^T_{ns}(P^2) \neq 0$, as may be seen in Fig.26, where we exhibit values of $\mathrm{Re}K^T_{nn}(P^2)$, $\mathrm{Re}K^T_{ss}(P^2)$ and $\mathrm{Re}K^T_{ns}(P^2)$.

We use a notation similar to that of Eq.(4.4.25) for $\hat{G}^S$ and $\hat{t}^S(P^2)$. It is also worth noting that $\hat{G}^S$ of Eq.(4.4.23) is given by

$$\hat{G}^S = \begin{bmatrix} 22.25 & -1.88 \\ -1.88 & 23.68 \end{bmatrix} \tag{4.4.28}$$

for our choice of G_S and G_D. We remark that it is the nonzero values of G_{ns} and $\mathrm{Re}K^T_{ns}(P^2)$ that lead to nonzero values of $t_{ns}(P^2)$. Since $t_{ns}(P^2)$ is small, it is useful to consider the functions

$$T_{nn}(P^2) = -\frac{\mathrm{Im}K_{nn}^{\pi\pi}(P^2)}{G_{nn}^{-1} - [J_{nn}(P^2) + \mathrm{Re}K_{nn}^{T}(P^2)] - i\,\mathrm{Im}K_{nn}^{T}(P^2)} \tag{4.4.29}$$

and

$$T_{ss}(P^2) = -\frac{\mathrm{Im}K_{ss}^{K\bar{K}}(P^2)}{G_{ss}^{-1} - [J_{ss}(P^2) + \mathrm{Re}K_{ss}^{T}(P^2)] - i\,\mathrm{Im}K_{ss}^{T}(P^2)}\ , \tag{4.4.30}$$

which may also be written in terms of phase shifts and absorption parameters

$$T_{nn}(P^2) = -e^{i\delta_{nn}(P^2)-\eta_{nn}(P^2)}\sin[\delta_{nn}(P^2) + i\,\eta_{nn}(P^2)] \tag{4.4.31}$$

and

$$T_{ss}(P^2) = -e^{i\delta_{nn}(P^2)-\eta_{nn}(P^2)}[\sin\delta_{ss}(P^2) + i\eta_{ss}(P^2)]\ . \tag{4.4.32}$$

In the next section we will exhibit values of the functions

$$|T_{nn}|^2 = \frac{[\mathrm{Im}K_{nn}^{\pi\pi}(P^2)]^2}{\left[G_{nn}^{-1} - [J_{nn}(P^2) + \mathrm{Re}K_{nn}^{T}(P^2)]\right]^2 + [ImK_{nn}^{T}(P^2)]^2} \tag{4.4.33}$$

and

$$|T_{ss}|^2 = \frac{[\mathrm{Im}K_{ss}^{\pi\pi}(P^2)]^2}{\left[G_{ss}^{-1} - [J_{ss}(P^2) + \mathrm{Re}K_{ss}^{T}(P^2)]\right]^2 + [ImK_{ss}^{T}(P^2)]^2} \tag{4.4.34}$$

Note that for those states that have $\mathrm{Im}K_{nn}^{\pi\pi}(P^2) = \mathrm{Im}K_{nn}^{T}(P^2)$ in Eq.(4.4.33), we have unity as the maximum value of $|T_{nn}|^2$, *etc.*

4.5 Results of Numerical Calculations

As a first step in our analysis, we found the energies of the $n\bar{n}$ and $s\bar{s}$ states in the confining field, in the absence of the NJL interaction and glueball couplings. The $n\bar{n}$ states are shown in Fig.27a and the $s\bar{s}$ states are shown Fig.27c. Recall that the energies of these states may be found from the position of the singularities seen in Figs.19 and 20. We do not have absolute confinement in our model, with the continuum for $n\bar{n}$ states starting at 2.75 GeV. (That value may be obtained by noting that $V_{max} = \kappa/\mu e$ and $2m_u + V_{max} = 2.75$ GeV, when $m_u = 0.364$ GeV, $\kappa = 0.055$ GeV^2 and $\mu = 0.010$ GeV.) Below 2.75 GeV, we find eight $n\bar{n}$ states and seven $s\bar{s}$ states. (There are additional bound $s\bar{s}$ states, since the continuum for those states starts at 3.15 GeV. See Fig.20.)

As a next step we consider the role of the NJL interaction, but with $\mathrm{Re}K_{ij}^T(P^2) = 0$. (Here, we continue to use $G_{88} = 12.46$ GeV^{-2} and $G_{00} = 10.46$ GeV^{-2}.) The results for the mass values are given in Fig.27b, where the dotted lines denote the $s\bar{s}$ states. Note that the states with the least of number of nodes are most strongly affected by the NJL interaction, since such states have wave functions that are large at the origin in coordinate space.

We now include $\mathrm{Re}K_{88}^T(P^2)$, $\mathrm{Re}K_{80}^T(P^2)$, $\mathrm{Re}K_{08}^T(P^2)$ and $\mathrm{Re}K_{00}^T(P^2)$ in the calculation, making use of Eq.(4.4.6). We also introduce a glueball with $m_G \simeq m_g = 1.70$ GeV. (Here we consider matrices of dimension 3.) In Fig.27d, we see that only the nodeless $s\bar{s}$ and $n\bar{n}$ states are moved down to significant extent with the

inclusion of $\mathrm{Re}K_{ij}^{T}(P^2)$. There is relatively little deviation from ideal mixing as may be seen in Table 12. We write the eigenfunctions resulting from the diagonalization of the T matrix as

$$|\psi_n\rangle = c_1 |n\bar{n}\rangle + c_2 |s\bar{s}\rangle + c_3 |G\rangle \ . \tag{4.5.1}$$

For the choice $g' = g'' = 0.1$ GeV^{-2} and $a = 0.1$ GeV^2, we obtain the results given in Table 12, where we also show the coupling constant g for a few states. These meson-quark coupling constants are defined after diagonalizing the T matrix. Near a singularity of one of the eigenvalues, $T_1(P^2)$, we define

$$T_1(P^2) = \frac{g_1^2}{P^2 - m_1^2} \ , \tag{4.5.2}$$

etc. For the $f_0(980)$ we have $g = 5.77$ and for the $f_0(1370)$ we have $g = 8.15$. [Note that we have neglected $\mathrm{Im}K(P^2)$ in our matrix diagonalization.] Since the effect on any state of $\mathrm{Re}K_{ij}^{T}(P^2)$ is approximately proportional to the square of the coupling constant for that state, we can see why only the two nodeless states, which have large coupling constants, are affected. In order to clarify this observation, we may consider a simple, single-channel model for which

$$t(P^2) = -\frac{1}{G^{-1} - [J(P^2) + \mathrm{Re}K(P^2)]} \ . \tag{4.5.3}$$

We then expand $J(P^2)$ about the resonance value obtained form the equation

$$G^{-1} - J(m_R^2) = 0 \ . \tag{4.5.4}$$

We write

$$J(P^2) \simeq J(m_R^2) + (P^2 - m_R^2) \left.\frac{\partial J(P^2)}{\partial P^2}\right|_{P^2 = m_R^2} . \qquad (4.5.5)$$

(Here, we are treating $\mathrm{Re}K(P^2)$ as a perturbation.) We identify the coupling constant as

$$g^{-2} = \left.\frac{\partial J(P^2)}{\partial P^2}\right|_{P^2 = m_R^2} , \qquad (4.5.6)$$

so that

$$t(P^2) = \frac{g^2}{P^2 - m_R^2 + g^2 \,\mathrm{Re}K(P^2)} . \qquad (4.5.7)$$

Therefore, we see that we only obtain large shifts away from m_R if g is large, as it is for the nodeless states found near 980 MeV and 1370 MeV in this chapter. Using a similar analysis, we can see that

$$m_R \Gamma_R = g^2 \,\mathrm{Im}K(m_R^2) , \qquad (4.5.8)$$

where Γ_R is the width of the state.

In this section we calculated the eigenstates of the 3×3 T matrix while neglecting $\mathrm{Im}K_{ij}(P^2)$. [See Table 12.] Since the glueball was hardly mixed with the $q\bar{q}$ states, we turn to a consideration of 2×2 matrices. However, in this case we include $\mathrm{Im}K_{ij}(P^2)$ and diagonalize the resulting complex 2×2 matrices. That is, we bring the matrix $t(P^2)$ to diagonal form, with eigenvalues $t_1(P^2)$ and $t_2(P^2)$:

$$t_{diag} = \begin{bmatrix} t_1(P^2) & 0 \\ 0 & t_2(P^2) \end{bmatrix} \quad . \tag{4.5.9}$$

Consider the $f_0(980)$ resonance which appears in $t_1(P^2)$. We may write

$$t_1(P^2) = \frac{g_1^2}{P^2 - m_1^2 + i\, m_1\, \Gamma_1} \quad , \tag{4.5.10}$$

or, incorporating the eigenvectors, we have

$$\hat{T}(P^2) = |e_1\rangle\ t_1(P^2)\ \langle e_1| \quad , \tag{4.5.11}$$

with

$$|e_1\rangle = 0.300\, \frac{\lambda_8}{\sqrt{2}} + 0.950\, \frac{\lambda_0}{\sqrt{2}} \quad . \tag{4.5.12}$$

(In Eq.(4.5.12) we have neglected a quite small imaginary part of one eigenvalue, which is about 0.05 in magnitude.) The eigenvector in Eq.(4.5.12) corresponds to about a 10 % strange quark content in the $f_0(980)$.

Note that one way to obtain g_1 is to calculate $|\, t(m_1^2)\,|^2$ and put

$$g_1^4 = m_1^2\, \Gamma_1^2\, |\, t_1(m_1^2)\,|^2 \quad , \tag{4.5.13}$$

once the (total) width of the state is known. We find $g_1 = 5.96$ for the $f_0(980)$, with $\Gamma_{f_0}(980) = 99$ MeV, as before. For the $f_0(1370)$, we have

$$t_2(P^2) = \frac{g_2^2}{P^2 - m_2^2 + i\, m_2\, \Gamma_2} \quad , \tag{4.5.14}$$

with $g_2 = 8.58$ and $\Gamma_{f_0}(1370) = 225$ MeV. Further, near the $\Gamma_{f_0}(1370)$ resonance

$$\hat{T}(P^2) = |e_2\rangle\, t_2(P^2)\, \langle e_2| \ , \tag{4.5.15}$$

with

$$|e_2\rangle = -0.870\,\frac{\lambda_8}{\sqrt{2}} + 0.490\,\frac{\lambda_0}{\sqrt{2}} \ . \tag{4.5.16}$$

In this case we only have about 1 % of the nodeless $n\bar{n}$ state present. Note that the inclusion of $\mathrm{Im}K_{ij}(P^2)$ in the T matrix, and the use of the approximation represented by Eqs.(4.5.10) and (4.5.14), leads to slightly larger values of the coupling constants for the $f_0(980)$ and $f_0(1370)$ than those given in Table 12.

The spectrum obtained with the neglect of $\mathrm{Im}K_{ij}(P^2)$ was exhibited in Fig.27d. In Fig.28 we compare our results for the a_0 meson spectrum with that for the f_0 mesons. Since, we have approximate ideal mixing, we see the ($T = 0$) f_0 spectrum may be obtained from the ($T = 1$) a_0 spectrum by inserting a number of what are largely $s\bar{s}$ states plus the glueball.

At this point we proceed to exhibit various T matrices calculated in different approximations. First, we show the results that follow, if we make the assumption of ideal mixing. In Fig.29 we exhibit values of $|T_{nn}(E)|^2$ of Eq.(4.4.33). The peaks of the resonances seen there are at 978, 1549, 1843, and 2064 MeV. The width of the $f_0(980)$ is $\Gamma_{f_0}(980) = 99$ MeV, while the other widths that measure decay to the $\pi\pi$ and $K\bar{K}$ channels are significantly smaller. In Fig.30 we show $|T_{ss}(E)|^2$ of Eq.(4.4.34). Here we see peaks at 1340, 1864 and 2108 MeV. There is a small peak at 1843 MeV and a very small peak at 2064 MeV, which is too small to be seen in the figure. Here the $f_0(1370)$ and the $f_0(2108)$ appear as elastic resonances with $\Gamma_{f_0}(1370)$

= 225 MeV. The width of the $f_0(1370)$ found in the data tables is 200 - 500 MeV [29]. As we will see, the approximation used to construct Eqs.(4.4.33) and (4.4.34) should be improved upon, since there are corrections to the results based upon ideal mixing.

We continue to study matrices of dimension 2 and use this formalism to obtain a T matrix for $\pi\pi$ or $K\bar{K}$ scattering. For example, from Fig.31, we see that

$$T_{\pi\pi}(P^2) = \frac{1}{S}\left[\frac{\mathrm{Im}K_{88}^{\pi\pi}(P^2)}{2}t_{88}(P^2) + \frac{\mathrm{Im}K_{00}^{\pi\pi}(P^2)}{2}t_{00}(P^2) + 2\frac{\mathrm{Im}K_{08}^{\pi\pi}(P^2)}{2}t_{08}(P^2)\right], \tag{4.5.17}$$

where we have used the fact that

$$\mathrm{Im}K_{ij}^{\pi\pi}(P^2) = \frac{\kappa^{\pi\pi}S}{8\pi P^0}M_i^{\pi\pi}(P^2)M_j^{\pi\pi}(P^2), \tag{4.5.18}$$

Here $S = 2$ is a statistical factor which is removed when calculating $T_{\pi\pi}(P^2)$ of Eq.(4.5.17). Also,

$$\kappa^{\pi\pi} = \left[\frac{(P^0)^2}{4} - m_\pi^2\right]^{1/2}. \tag{4.5.19}$$

We see that we may write

$$T_{\pi\pi}(P^2) = -e^{i\delta_{\pi\pi}(P^2)-\eta_{\pi\pi}(P^2)}\sin[\delta_{\pi\pi}(P^2) + i\eta_{\pi\pi}(P^2)], \tag{4.5.20}$$

so that for an elastic resonance $|T_{\pi\pi}(P^2)|^2$ takes on a maximum value of unity at the peak.

The calculation of $|T_{\pi\pi}(P^2)|^2$ of Eq.(4.5.17) yields a curve that is very similar

to that seen in Fig.29, where ideal mixing was assumed. However, when we calculate $|T_{K\bar{K}}(E)|^2$, using the analog of Eq.(4.5.17), we get the solid curve seen in Fig.32. There $|T_{K\bar{K}}(E)|^2$ is compared to $|T_{ss}(E)|^2$, which is shown as a dotted line. For $|T_{K\bar{K}}(E)|^2$ we find a maximum value of 1.0 at the $f_0(1370)$ energy and at the energy of the $f_0(1863)$. We note that the width of the $f_0(1370)$ for $\pi\pi$ plus $K\bar{K}$ emission is reduced to $\Gamma_{f_0}(1370) = 192$ MeV from the value 225 MeV obtained from $|T_{ss}(E)|^2$. It is worth noting that significant peaks are seen in Fig.32 for the (predominantly) $n\bar{n}$ states at 1549, 1843 and 2064 MeV. (These states have only small $s\bar{s}$ components. The values of $\mathrm{Im}K_{ij}^{K\bar{K}}(P^2)$ are larger than those of $\mathrm{Im}K_{ij}^{\pi\pi}(P^2)$. and that leads to significant (small) peaks in Fig.32 at the energies of the $n\bar{n}$ states.)

4.6 Threshold Effects in the Calculation of the Properties of the f_0 Mesons

Thus far we have made use of the regulator of Eq.(4.3.24). In this section, we consider our results when the factor $\{1 - \exp[-(P^2 - m_{th}^2)/\beta^2]\}$ is removed from the regulator. In this case, we obtain $\mathrm{Re}K_{ij}^{\pi\pi}(P^2)$ and $\mathrm{Re}K_{ij}^{K\bar{K}}(P^2)$ directly from $\mathrm{Im}K_{ij}^{\pi\pi}(P^2)$ and $\mathrm{Im}K_{ij}^{K\bar{K}}(P^2)$ using the dispersion relation given in Eq.(4.4.4). Thus, the real and imaginary parts of $K_{ij}(P^2)$ now have the threshold behavior obtained from the use of a regulator without any P^2 dependence. [See Figs.33 - 38.] However, we still need a parameter to describe the contribution of the four-pion channel and other two-meson, or multi-meson channels. To that end, we modify $\mathrm{Re}K_{ij}^{T}(P^2)$ to read

$$\mathrm{Re}K_{ij}^{T}(P^2) = \mathrm{Re}K_{ij}^{\pi\pi}(P^2) + \mathrm{Re}K_{ij}^{K\bar{K}}(P^2) + a_{ij} \qquad (4.6.1)$$

where $a_{00} = 0.020$ GeV^2, $a_{88} = 0.005$ GeV^2 and $a_{08} = -0.005$ GeV^2. There is only a single new parameter here, since we chose a value for a_{00} and then fixed the ratios a_{88}/a_{00} and a_{08}/a_{00} to correspond the ratios $\mathrm{Re}K_{88}^{T}(P^2)/\mathrm{Re}K_{00}^{T}(P^2)$ and $\mathrm{Re}K_{08}^{T}(P^2)/\mathrm{Re}K_{00}^{T}(P^2)$ seen in Fig.25 at about $P^2 = 1.0$ MeV. This procedure ensures that the rapid rise at threshold of $\mathrm{Im}K_{ij}^{\pi\pi}(P^2)$ and $\mathrm{Im}K_{ij}^{K\bar{K}}(P^2)$ only affects the threshold behavior of $\mathrm{Re}K_{ij}^{\pi\pi}(P^2)$ and $\mathrm{Re}K_{ij}^{K\bar{K}}(P^2)$. Recall that the only relevant values of a_{ij} are those in the region of the $f_0(980)$ and the $f_0(1370)$, so that the use of constant values for the a_{ij} is an acceptable approximation. In Figs.33-35, we show the values of $\mathrm{Re}K_{ij}^{\pi\pi}(P^2)$ and $\mathrm{Im}K_{ij}^{\pi\pi}(P^2)$ obtained when the regulator $R(k_c^2) = \sqrt{\frac{2}{3}}\exp[k_c^2/\alpha_1^2]$ is used. What is to be noted in these figures is the strong cusplike behavior seen in $\mathrm{Re}K_{ij}^{\pi\pi}(P^2)$. The values of $\mathrm{Im}K_{ij}^{\pi\pi}(P^2)$ shown in Figs.33-35 may be compared to the values shown in Fig.23 where the regulator of Eq.(4.3.24) was used. The functions shown in Fig.33-35 increase much faster with P^2 near threshold than those of Fig.23. The functions $\mathrm{Re}K_{ij}^{K\bar{K}}(P^2)$ and $\mathrm{Im}K_{ij}^{K\bar{K}}(P^2)$ show similar differences when calculated with the two different regulators. (See Fig.24 and Figs.36-38.)

We now calculate $T_{\pi\pi}(P^2)$ and $T_{K\bar{K}}(P^2)$ using Eq.(4.5.17) and its analog for $K\bar{K}$ scattering. The results found with the regulator $R(k_c^2) = \sqrt{\frac{2}{3}}\exp[k_c^2/\alpha_1^2]$ are shown in Figs.39 and 40. In Fig.39 we see peaks at 982, 1552, 1840 and 2062 MeV. The $f_0(980)$ has a width of 56 MeV at half-maximum. That resonance also exhibits a significant "background" starting near the two-pion threshold and continuing to about 1.2 GeV. In Fig.40 we show $|T_{K\bar{K}}(E)|^2$ and find peaks at 1040, 1410, 1552, 1840,

1858, 2062 and 2102 MeV. The peaks at 1040, 1552, 1840 and 2062 MeV have as their basis states that are largely of $n\bar{n}$ character. (The prominence of these peaks in Fig.40 is due to the relatively large values of $\mathrm{Im}K_{ij}^{K\bar{K}}(P^2)$ when compared to $\mathrm{Im}K_{ij}^{\pi\pi}(P^2)$.)

The excitation in the vicinity of 980 MeV in Fig.39 and that around 1040 MeV in Fig.40 should properly be thought of as arising from a single state, the $f_0(980)$. [See Fig.41.] That state would therefore show finite values for the branching ratio $\Gamma(K\bar{K})/[\Gamma(K\bar{K})+\Gamma(\pi\pi)] \simeq \Gamma(K\bar{K})/\Gamma_{total}(980)$. Values of 0.1 to 0.3 could be obtained for that ratio depending upon the energy range is assigned to the $f_0(980)$ in Fig.39. That is, the branching ratio will depend upon how one treats the "background" seen in the vicinity of the $f_0(980)$ in Fig.39. The experimental values of the branching ratio listed in the data tables are 0.67 ± 0.09, $0.81 \pm^{0.09}_{0.04}$ and 0.78 ± 0.03 [31]. Inspection of Figs.39 and 40 suggests that, if we were to use a Breit-Wigner form to represent the $f_0(980)$ resonance (with a width of about 56 MeV) we would then wish to account for the enhanced $\pi\pi$ interaction seen in the energy range of 400-1200 MeV. Clearly, there exists some motivation to introduce an excitation somewhat like the $f_0(400\text{-}1200)$ that appears in the data tables.

Finally, we remark that we have used $R(k_c^2) = \sqrt{2/3}\,\exp[k_c^2/\alpha_1^2]$ as the regulator for the calculations reported in this section. Alternatively, we could have used $R(k_c^2) = \exp[k_c^2/\alpha_1^2]$ if we put $\alpha_1 = 0.25$ GeV^2, instead of $\alpha_1 = 0.325$ GeV^2, which was the value used when the factor of $\sqrt{2/3}$ appeared in the regulator.

4.7 Discussion

The assignment of the states $f_0(980)$, $f_0(1370)$, $f_0(1500)$ and $f_0(1710)$ to specific quark model configurations, as well as the identification of the scalar glueball, is difficult and there is no agreement to be found in the literature. One is usually assisted in this matter by studying branching ratios, but given the absence of a satisfactory scheme for calculating decay widths, various contradictory conclusions may be drawn. There are also problems associated with the data itself. We take as an example the $f_0(1370)$. In the data tables, we find $\Gamma_{\pi\pi}/\Gamma_{total}$ to be either 0.26 ± 0.09, < 0.15 and < 0.2 depending upon the experiment [29]. (The determination of $\Gamma_{\pi\pi}/\Gamma_{total}$ for the $f_0(1370)$ is difficult, since the large width of the $f_0(1370)$ leads to an overlap with the $f_0(400\text{-}1200)$.) We also find $\Gamma(4\pi)/\Gamma_{total} = 0.80 \pm 0.04$ and $\Gamma(K\bar{K})/\Gamma_{total} = 0.35 \pm 0.13$ in the data tables. If we take the first value given for $\Gamma_{\pi\pi}/\Gamma_{total}$, and sum these ratios we find $140 \pm 26\,\%$, rather than $100\,\%$ of the total width. Therefore, we can assume that there are significant uncertainties associated with the values of the branching ratios. Our work suggests that $\Gamma(K\bar{K})/\Gamma_{total}$ may be about 0.5, with $\Gamma(4\pi)/\Gamma_{total}$ also about 0.5 and with very little two-pion emission. The fact that the $f_0(1370)$ is only weakly coupled to the two-pion channel has been reported by Bugg and supports our suggestion that the $f_0(1370)$ is a $s\bar{s}$ state. Since we have $\Gamma(K\bar{K}) \simeq 190$ MeV, the above argument suggests a total width of about 400 MeV for the $f_0(1370)$, while the data tables have $\Gamma_{Total}(1370) \simeq$ 200-500 MeV [29]. However, we should note that the most significant shortcoming of our analysis is the absence of a

model for decay to the four-pion channel.

As for the $f_0(1500)$, the small total width of 112 $\pm$ 10 MeV leads to the suggestion that the $f_0(1500)$ may be a glueball [30, 31]. However, in our model the width of the $f_0(1500)$ is quite small, since it is a radial excitation of the $f_0(980)$ with a single node and, therefore, it has a small coupling constant for coupling to quarks. In our calculation, we found $\Gamma(\pi\pi) \simeq \Gamma(K\bar{K}) \simeq 6$ MeV. That is consistent with $\Gamma(K\bar{K})/\Gamma_{total} = 0.044 \pm 0.021$ which appears in the data tables, but inconsistent with $\Gamma(K\bar{K})/\Gamma(2\pi) = 0.19 \pm 0.07$, which also appears in the tables [29]. The last branching ratio suggests that we have underestimated $\Gamma(2\pi)$ for the $f_0(1500)$ by a factor of 4 or 5. That may be due to our neglect of final-state interactions of the pions in the decay channel. The fact that $\Gamma(4\pi)/\Gamma(2\pi) = 3.4 \pm 0.8$ in one experiment suggests that one might have $\Gamma(2\pi) \simeq 30$ MeV, $\Gamma(K\bar{K}) \simeq 6$ MeV and $\Gamma(4\pi) \simeq$ 75 MeV for a $\Gamma_{Tot}(1500) = 111$ MeV (However, that suggestion leaves little room for $\Gamma(\eta\eta)$ which is thought to be significant in some experiments [29].) In Ref.[31] the width of the $f_0(1500)$ is given as $\Gamma = 111 \pm 12$ MeV, with decays to the $\pi\pi$, $\eta\eta$, $\eta\eta'$, $K\bar{K}$ and 4π channels, and with branching percentages of 29.5, 5, 1, 3 and 62%, respectively. That result again suggests that we have underestimated the $\pi\pi$ decay width for the $f_0(1500)$ by about a factor of 4 or 5. Our relative success in calculating $\Gamma(K\bar{K})$, while underestimating $\Gamma(\pi\pi)$ for the $f_0(1500)$, may be due to the fact that we are closer to the $K\bar{K}$ threshold than the $\pi\pi$ threshold when investigating the properties of the $f_0(1500)$.

It is of interest to note that our identification of the $f_0(1710)$ as the glueball is

in accord with the results of lattice QCD calculations [32-34]. The wave functions suggested by Lee and Weingarten have the percentages of $n\bar{n}$, $s\bar{s}$ and glueball configurations given in Table 13. There we see that the $f_0(1500)$ is mainly of $s\bar{s}$ character. However, we saw that this state had $\Gamma(K\bar{K})/\Gamma_{Total} = 0.044 \pm 0.021$, which is very hard to understand if the $s\bar{s}$ characterization is correct. In a similar fashion, since the $n\bar{n}$ content of the $f_0(1370)$ is given as 67.1 % in Table 13, one would expect a quite large value of $\Gamma(2\pi)/\Gamma_{Total}$ for the $f_0(1370)$. However, the value $\Gamma(2\pi)/\Gamma_{Total}$ is quite small. Therefore we believe our assignments of $s\bar{s}$ character to the $f_0(1370)$ and 2^3P_0 $n\bar{n}$ character to the $f_0(1500)$ is more in keeping with the implications of the experimental data.

Quarkonium-glueball mixing has also been studied in Refs.[36] and [37]. In Ref.[36] the following matrix is considered

$$H_1 = \begin{bmatrix} m_{G_0} & z & \sqrt{2}\,z \\ z & m_{s\bar{s}} & 0 \\ \sqrt{2}\,z & 0 & m_{n\bar{n}} \end{bmatrix}, \qquad (4.7.1)$$

where m_{G_0}, $m_{s\bar{s}}$ and $m_{n\bar{n}}$ are the masses in the absence of quarkonium-glueball mixing. Here $z = \langle G_0 | H_I | s\bar{s} \rangle = \langle G_0 | H_I | n\bar{n} \rangle / \sqrt{2}$, where $| G_0 \rangle$ is the "bare" glueball. The relation between the off-diagonal elements only pertains if they have the same configuration. However, in our model the $s\bar{s}$ state has a 1^3P_0 character and the nearby $n\bar{n}$ state is a 2^3P_0 state. Therefore, it might be more appropriate to consider the matrix

$$H_2 = \begin{bmatrix} m_{G_0} & z & \sqrt{2}\,z_1 & \sqrt{2}\,z \\ z & m_{s\bar{s}} & 0 & 0 \\ \sqrt{2}\,z_1 & 0 & m'_{n\bar{n}} & 0 \\ \sqrt{2}\,z & 0 & 0 & m_{n\bar{n}} \end{bmatrix} , \qquad (4.7.2)$$

where $m'_{n\bar{n}}$ is the "bare" mass of the 2^3P_0 $n\bar{n}$ state and $m_{n\bar{n}}$ is the mass of the 1^3P_0 $n\bar{n}$ state [the $f_0(980)$]. The relation between z and z_1 is unknown.

We solve for the eigenfunctions and eigenvalues of Eq.(4.7.1) putting z = 0.060 GeV, m_{G_0} = 1.55 GeV, $m_{s\bar{s}}$ = 1.400 GeV and $m_{n\bar{n}}$ = 1.550 GeV. We obtain the eigenvalues and eigenvectors shown in Table 14 and write the resulting state as

$$|\Psi\rangle = a_1 |G\rangle + a_2 |s\bar{s}\rangle + a_3 |(n\bar{n})'\rangle , \qquad (4.7.3)$$

where the a_i's are given in Table 14. If the glueball state has a large decay amplitude for four-pion decay and only a small amplitude for two-decay [37], we can still understand why the $f_0(1370)$ has little coupling to the two-pion channel. We can also understand why the $f_0(1500)$ has about a 0.6 branching ratio for decay to the 4π channel. Note that, since the $|(n\bar{n})'\rangle$ has a quite small width (~ 6 MeV) for decay to either the 2π or the $K\bar{K}$ channel, it is not important for our qualitative observations.

If we turn to Eq.(4.7.2), we see that there is an extra parameter to be considered. For simplicity, we put $z_1 = z$ and write the wave functions as

$$|\psi_n\rangle = b_1 |G\rangle + b_2 |s\bar{s}\rangle + b_3 |(n\bar{n})'\rangle + b_4 |n\bar{n}\rangle \ . \qquad (4.7.4)$$

We put $m_{n\bar{n}} = 1.00$ GeV and obtain the results given in Table 15. [See Fig.42.] (The values of m_{G_0}, $m'_{n\bar{n}}$ and $m_{s\bar{s}}$ are the same as those specified previously.

It is clear that a good deal of work is needed to understand the coupling of the glueball to the $q\bar{q}$ states calculated in this work. That is, the parameters z and z_1 should be calculated from first principles. Coupling constants for the glueball to decay to pairs of pseudoscalar $q\bar{q}$ states have already been reported in Ref.[38] and appear to favor the assignment of the $f_0(1710)$ as having the major glueball component. The fact that the glueball has a (small) finite decay to the two-pion continuum probably accounts for some part of our underestimate of the two-pion decay in the case of the $f_0(1500)$. Also, if the wave functions of Table 15 are to have some correspondence to reality, we would have to probably appeal to destructive interference between the decay amplitudes of the $s\bar{s}$ state and the glueball for decay to the $K\bar{K}$ channel. Otherwise, we would overestimate the $K\bar{K}$ decay of the $f_0(1500)$ by a large factor. This matter clearly requires further study.

Appendix A

In this Appendix we present equations that may be solved to obtain $\Gamma^{+-}_{T_1,1}$, $\Gamma^{+-}_{T_1,2}$, $\Gamma^{+-}_{T_1,1}$ and $\Gamma^{+-}_{T_1,2}$. These equations are obtained from Eqs.(3.3.6) and (3.3.7). One method that may be used is to multiply $\bar{\Gamma}^{\mu\nu}(P, k)$ from the right by $\Lambda^{(-)}(-\vec{k})$ and from the left by $\Lambda^{(+)}(\vec{k})$. One can then multiply from the left by either $Q_{\mu\nu}$ or $P_{\mu\nu}$ and then form the trace of both sides of the equation. We find, with $i = 1$ or 2,

$$\Gamma^{+-}_{T_1,i}(P,k) = C_i - \sum_{j=1}^{2} \int \frac{dk'}{(2\pi^2)} t_{ij}(k,k',x) \left[\frac{m}{E(k')} \right]^2 \times \frac{V^C(\vec{k}-\vec{k}')}{P^0 - 2E(k')} \Gamma^{+-}_{T_1,j}(P,k') \,, \tag{A.1}$$

Here $C_1 = 1$ and $C_2 = 0$. With $x = \cos\theta$, we have

$$t_{11}(k,\, k',x) = -\left[2\left[\frac{k'}{m} \right]^2 + \frac{k'x}{k} \right] P_2(x) \,, \tag{A.2}$$

$$t_{12}(k,\, k',x) = \left[\frac{E(k')}{m} \right]^2 2x(1-x^2)\frac{m}{k} \,, \tag{A.3}$$

$$t_{21}(k,\, k',x) = \frac{3}{4} x(1-x^2)\frac{k'}{m} \,, \tag{A.4}$$

and

$$t_{22}(k, k', x) = -\left[\frac{E(k')}{m}\right]^2 \left[x^3 + \frac{k k'}{E(k) E(k')} P_2(x)\right] . \qquad \text{(A.5)}$$

In Eqs.(A.2) and (A.5), $P_2(x)$ is a Legendre function. Also, $k = |\vec{k}|$, $k' = |\vec{k}'|$ in all the equations given above. Corresponding equations for $\Gamma^{+-}_{T_2,1}$ and $\Gamma^{+-}_{T_2,2}$ are obtained by replacing C_i by D_i where $D_1 = 0$ and $D_2 = 1$. We then see that the homogenous equations for the various Γ^{+-} are the same. Therefore, $\Gamma^{+-}_{T_1,1}$, $\Gamma^{+-}_{T_1,2}$, $\Gamma^{+-}_{T_2,1}$ and $\Gamma^{+-}_{T_2,2}$ have singularities at the same energies.

Table 1

Pseudoscalar mesons. The pion states designated as n^1S_0 have little pseudoscalar – axial-vector mixing [2]. Here $G_S = 12.46$ GeV^{-2} for states other than the $\pi(138)$. Also, $\kappa = 0$ for the $\pi(138)$, and $\kappa = 0.0575$ GeV^2 for all other states. We use $\mu = 0.01$ GeV and $\Lambda_3 = 0.622$ GeV.

Meson	Mass (Expt) [MeV]	Mass (Theory) [MeV]	Spectroscopic character
$\pi(138)$	π^0: 134.9764 ± 0.0006 $\pi^\pm$: 139.56995 ± 0.00035	138	$1\,^1S_0$
$\pi(1300)$	1300 ± 100	1202[b] 1400	mixed 2^1S_0
	-----	1539	mixed
$\pi(1800)$	1795 ± 10[a]	1746 1805	3^1S_0 mixed

a) Needs confirmation.

b) See Ref.[2] for a detailed study of this state.

Table 1 (continued)

Pseudoscalar mesons. The pion states designated as n^1S_0 have little pseudoscalar − axial-vector mixing [2]. Here $G_S = 12.46$ GeV^{-2} for states other than the $\pi(138)$. Also, $\kappa = 0$ for the $\pi(138)$, and $\kappa = 0.0575$ GeV^2 for all other states. We use $\mu = 0.01$ GeV and $\Lambda_3 = 0.622$ GeV.

Meson	Mass (Expt) [MeV]	Mass (Theory) [MeV]	Spectroscopic character
$K(495)$	$K^{\pm}$: 493.677 ± 0.016 K^0: 497.672 ± 0.031	495	$1\,^1S_0$
$K(1460)^a$	1400 - 1460	1557	2^1S_0
$K(1830)^a$	~ 1830	1879	3^1S_0

a) Needs confirmation.

b) See Ref.[2] for a detailed study of this state.

Table 2

Parameters used in chapter 2 - see Section 2.4. The first three of these parameters are not varied when fitting data. The parameters G_K and G_{KA} are used in the study of ${}^3P_1$ - ${}^1P_1$ mixing of strange axial-vector mesons. [See Eq.(2.8.1).] The parameter δ is used in the study of η - η' mixing.

$\mu = 0.010$ GeV
$\Lambda_3 = 0.622$ GeV
$m_u = 0.364$ GeV
$m_s = 0.565$ GeV
$\kappa = 0.055$ GeV^2
$G_V = 12.46$ GeV^{-2}
$G_S = 12.46$ GeV^{-2}
$\delta = 2.0$ GeV^{-2}
$G_K = 78.13$ GeV^{-2}, $G_{KA} = 8.00$ GeV^{-2}

Table 3

Vector mesons. Here $G_V = 12.46\ \text{GeV}^{-2}$, $m_u = 0.364$ GeV, $m_s = 0.565$ GeV, $\Lambda_3 = 0.622$ GeV, $\mu = 0.01$ GeV and $\kappa = 0.055\ \text{GeV}^2$.

Meson	Mass (Expt) [MeV]	Mass (Theory) [MeV]	Spectroscopic character
$\omega(782)^a$	781 ± 0.12	782	1^3S_1
$\omega(1420)^a$	1419 ± 31	1449	2^3S_1
$\omega(1600)$	1649 ± 24	1591	1^3D_1
---	-----	1766	3^3S_1
---	-----	1828	2^3D_1
$\phi(1020)^a$	1019.413 ± 0.008	1015	1^3S_1
$\phi(1680)$	1680 ± 20	1749	2^3S_1
$K^*(892)$	891.59 ± 0.24	870	1^3S_1
$K^*(1410)$	1412 ± 12	1590	2^3S_1
$K^*(1680)$	1714 ± 20	1732	1^3D_1
---	-----	1893	3^3S_1

a) These states are used to fix three parameters of the model: G_V, m_s and κ.

Table 4

Mass values of scalar mesons. See Table 2 for a list of parameters. No parameters are varied in these fits to the data.

Meson	Mass (Expt) [MeV]	Mass (Theory) [MeV]	Spectroscopic character
$K_0^*(1430)$	$1429 \pm 4 \pm 5$	1416	1^3P_0
---	-----	1738	2^3P_0
$K_0^*(1950)^a$	$1945 \pm 10 \pm 20$	1999	3^3P_0
$a_0(980)$	983.5 ± 0.9	1063	1^3P_0
$a_0(1450)^a$	1450 ± 50	1556	2^3P_0
---	-----	1857	3^3P_0

a) Needs confirmation.

Table 5

Mass values of the a_1 mesons.

Meson	Mass (Expt) [MeV]	Mass (Theory) [MeV]	Spectroscopic character
$a_1(1260)$	1230 ± 40	1220	1^3P_1
---	-----	1600	2^3P_1
---	-----	1895	3^3P_1

Table 6

Mass values for the b_1 mesons under the assumption of ideal mixing. [See Fig.13.] Here $m_a = m_b = 0.364$ GeV.

Meson	Mass (Expt) [MeV]	Mass (Theory) [MeV]	Spectroscopic character
$b_1(1235)$	1231 ± 10	1230[a]	1^1P_1
---	-----	1587	2^1P_1
---	-----	1876	3^1P_1

a) This state is used to fix $G_K = 78.13$ GeV^{-2}.

Table 7

Theoretical and experimental values of the masses of the axial-vector K_1 mesons. See Eqs.(2.8.30) and (2.8.31) for definitions of the coupling constant and mixing angle.

Meson	Mass (Expt) [MeV]	Mass (Theory) [MeV]	Mixing angle ϕ	g_1
$K_1(1270)$	1275 ± 10	1274[a]	-15.2^0	8.60
$K_1(1400)$	1402 ± 7	1483	40.9^0	3.13
$K_1(1650)$	1650 ± 50	1594[b]		
		1722		
---	-----	1772		
---		1838[b]		

a) Fit by the choice $G_{KA} = 8.0$ GeV^{-2}, when $M = 1.0$ GeV. [See Eq.(2.8.28).]

b) These are doublets weakly coupled to quarks.

Table 8

Mass values of $s\bar{s}$ axial-vector mesons in the case of ideal mixing. Here $m_a = m_b = 0.565$ GeV.

Meson	Mass (Theory) [MeV]	Spectroscopic character
f_1	1600	1^3P_1
	1902	2^3P_1
h_1	1468	1^1P_1
	1871	2^1P_1

Table 9

Experimental values for the mass and width of f_2 mesons [8]. The small dots in the first column denotes confirmed f_2 states as given in Ref.[8]. Reference [24] describes the observation of a $f_J(1750)$.

Meson	Mass (MeV)	Width (MeV)
$\cdot f_2(1270)$	1275 ± 5	185 ± 20
$f_2(1430)$	$\simeq 1430$	---
$\cdot f_2'(1525)$	1525 ± 5	76 ± 10
$f_2(1565)$	1565 ± 20	170 ± 40
$f_2(1640)$	1638 ± 6	200 ± 50
$f_J(1750)$	1770 ± 20	195 ± 22
$f_2(1810)$	1815 ± 12	250 ± 50
$f_2(1950)$	1950 ± 15	319^{+81}_{-69}
$\cdot f_2(2010)$	2011^{+62}_{-76}	202^{+67}_{-62}

Table 9 (continued)

Experimental values for the mass and width of f_2 mesons [8]. The small dots in the first column denotes confirmed f_2 states as given in Ref.[8]. Reference [24] describes the observation of a $f_J(1750)$.

Meson	Mass (MeV)	Width (MeV)
$f_2(2150)$	$\sim 2150 - 2226$	250
$f_J(2220)$	2225 ± 6	38^{+15}_{-13}
$\cdot f_2(2300)$	2297 ± 28	149 ± 41
$\cdot f_2(2340)$	2339 ± 55	319^{+81}_{-69}

Table 10

Values of the mass, g, g' and the mixing angles for the lowest five states of f_2 mesons obtained in chapter 3. Here, ideal mixing is seen, as expected. Additional $s\bar{s}$ states are found at 1745, 1767 and 1943 MeV and additional $(u\bar{u} + d\bar{d})$ states are found at 1913 and 1939 MeV. The six $(u\bar{u} + d\bar{d})$ states and the four $s\bar{s}$ states listed above correspond to the five states shown in Fig.15a, which have a degeneracy factor of 2. Here, $m_u = 0.364$ GeV, $m_s = 0.565$ GeV, $\kappa = 0.055$ GeV^2, $\Lambda_3 = 0.622$ GeV and $\mu = 0.010$ GeV [1-2, 17]. The two new parameters introduced in chapter 3 are $G_{T_1} = 47.00$ GeV^{-2} and $G_{T_2} = 6.80$ GeV^{-2}.

Mass [MeV]	Type	g	g'	$\hat{\theta}$ (degrees)	$\tilde{\theta}$ (degrees)
1254	$n\bar{n}$ 1S	7.82	-1.48	-35.26	-35.26
1429	$n\bar{n}$ 1S	4.62	2.12	-35.26	-35.26
1527	$n\bar{n}$ 2S	0.931	0.612	-35.26	-35.26
1551	$s\bar{s}$ 1S	-3.56	1.85	54.79	54.79
1685	$n\bar{n}$ 2S	0.972	-0.808	-35.26	-35.26

Table 11

Quark-antiquark states-bound of f_2 mesonsin the confining field at energies above 2 GeV. [See Fig.16.] Here, m_u = 0.364 GeV, m_s = 0.565 GeV and κ = 0.055 GeV^2.

Principal quantum number	$n\bar{n}$ Mass (GeV)	$s\bar{s}$ Mass (GeV)
3	----	2.205
4	2.155	2.373
5	2.319	2.517
6	2.455	2.653
7	2.570	2.760
8	----	2.860
9	----	2.970

Table 12

Mass values and wave functions of f_0 states calculated in chapter 4. In obtaining these results we have neglected $\mathrm{Im}K_{ij}(P^2)$. See Eq.(4.5.1) for the definition of c_1, c_2 and c_3 and Eq.(4.4.19) for the matrix of coupling constants.

Mass [MeV]	c_1	c_2	c_3	g
975	0.950	0.312	0.005	5.77
1370	0.0067	- 0.9997	- 0.003	8.15
1549	0.9946	-0.105	0.0046	2.10
1700	0.029	0.085	0.996	----
1843	0.980	- 0.198	0.0027	----
1864	- 0.064	- 0.998	- 0.0026	----
2064	0.994	- 0.106	0.0034	----
2108	0.0216	- 0.9998	- 0.0025	----

Table 13

Percentage of $n\bar{n}$, $s\bar{s}$ and glueball configurations in the $f_0(1710)$, $f_0(1500)$ and $f_0(1370)$ in the analysis of Lee and Weingarten [32-34].

	$f_0(1710)$	$f_0(1500)$	$f_0(1370)$
$n\bar{n}$	17.0	15.9	67.1
$s\bar{s}$	9.2	82.5	8.4
G	78.8	1.6	24.5

Table 14

Eigenvalues and wave functions for the matrix of Eq.(4.7.1). The wave functions are given in Eq.(4.7.3), with $|(n\bar{n})'\rangle$ being the 2^3P_0 $n\bar{n}$ state.

Eigenvalue [GeV]	a_1	a_2	a_3
1.643	0.725	0.180	0.664
1.485	- 0.561	- 0.403	0.722
1.370	- 0.398	0.897	0.192

Table 15

Eigenvalues and wave functions for the matrix of Eq.(4.7.3). Here $z = z_1$ = 0.075 GeV, m_{G_0} = 1.550 GeV, $m_{s\bar{s}}$ = 1.400 GeV, $m'_{n\bar{n}}$ = 1.550 GeV and $m_{n\bar{n}}$ = 1.000 GeV. The wave functions are of the form $|\Psi_n\rangle = b_1|G\rangle + b_2|s\bar{s}\rangle + b_3|(n\bar{n})'\rangle + b_4|n\bar{n}\rangle$.

Eigenvalue [GeV]	b_1	b_2	b_3	b_4
1.678	0.744	0.202	0.625	0.117
1.484	- 0.484	- 0.452	0.742	- 0.107
1.365	- 0.418	0.868	0.239	0.122
0.980	- 0.194	0.035	0.036	0.980

Figure Captions

Fig.1 Mass values for the mesons of the pseudoscalar and vector nonets are shown. The horizontal lines, rectangular boxes and crosshatched regions show experimental values taken from Ref.[8]. The dotted lines represent the mass values calculated in chapter 2. A small D is placed near those states that are calculated as D states or are so assigned in Table 12.2 of Ref.[8].

Fig.2 The eigenvalue of the largest magnitude for the T matrix calculated in our study of the $\eta - \eta'$ system. We find states with the energies 0.551, 1.039, 1.204, 1.406, 1.530, 1.543, 1.726, 1.749, 1.813 and 1.819 GeV, when the parameters of Table 2 are used.

Fig.3 The function $J_\omega(P^2)$ is shown. The horizontal line represents $G_V^{-1} = (12.46\ \text{GeV}^{-2})^{-1}$. The intersections of that line and the curve representing $J_\omega(P^2)$ provide the solutions of the equation $G_V^{-1} - J_\omega(P^2) = 0$.

Fig.4 The function $J_\phi(P^2)$ is shown. The horizontal line represents $G_V^{-1} = (12.46\ \text{GeV}^{-2})^{-1}$. (See caption to Fig.7.)

Fig. 5 The function $J^V_{us}(P^2)$ is shown. The vertical lines represent the energies of the bound states in the confining field. There is a 1^3D_1 sightly above the 2^3S_1 state and a 2^3D_1 state just above the 3^3S_1 state. The horizontal line represents $G_V^{-1} = (12.46\ \text{GeV}^{-2})^{-1}$. The intersections of that line with the curve representing $J^V_{us}(P^2)$ yields the solutions of the equation $G_V^{-1} - J^V_{us}(P^2) = 0$. (Note that the D states are hardly affected by the NJL interaction. For example, the 1^3D_1 state is found between the two vertical lines near $P^2 = 2.9\ \text{GeV}^2$ when the NJL interaction is taken into account.) The energies of the K^* mesons found in this manner are given in Table 3 and shown in Fig.5.

Fig.6 States of the scalar nonet are shown.

Fig.7 The function $J^S_{ud}(P^2)$ is shown. The horizontal line represents $G_S^{-1} = (12.46\ \text{GeV}^{-2})^{-1}$. (See Table 4 for masses of the a_0 mesons.)

Fig.8 The function $J^S_{us}(P^2)$ is shown. The horizontal line represents $G_S^{-1} = (12.46\ \text{GeV}^{-2})^{-1}$. (See Table 4 for masses of the K_0^* mesons.)

Fig.9 The $^3P_1$ and $^1P_1$ nonets of axial-vector mesons are shown.

Fig.10 The function $J^{A}_{us}(P^2)$ is shown. The first pair of vertical line at about 2.5 GeV^2 indicate the energies of the 1^3P_1 and 1^1P_1 states in the confining field with the 1^3P_1 state having a lower energy. The second pair of vertical lines show the positions of the 2^3P_1 and 2^1P_1 states in the confining field. The horizontal line represents $G_V^{-1} = (12.46\ \text{GeV}^{-2})^{-1}$. Note that only the $^3P_1$ states move down in energy to any significant degree, when the NJL interaction is taken into account.

Fig.11 The function $J^{A}_{11}(P^2)/M^2$ is shown. The intersection of that curve with the horizontal line representing $G_K^{-1} = (78.13\ \text{GeV}^{-2})^{-1}$ yields the (uncoupled) spectrum shown in Fig.14a. (Here $M = 1.0$ GeV.)

Fig.12 The function $J^{A}_{12}(P^2)/M$ is shown. (Here $M = 1.0$ GeV.)

Fig.13 The function $J^{A}_{11,ud}(P^2)$ is shown. Here $m_a = m_b = 0.364$ GeV. The horizontal line represents $G_K^{-1} = (78.13\ \text{GeV}^{-2})^{-1}$. The intersection of that line with curve representing $J^{A}_{11,ud}(P^2)$ yields the mass values for the b_1 mesons given in Table 6. Here we assume ideal mixing.

Fig.14 (a) The mass values obtained from the solution of the equation $G_K^{-1} - J^{A}_{11}(P^2) = 0$ are represented by dotted lines. Here $G_K = 78.13\ \text{GeV}^{-2}$. We find states with mass values of 1.35, 1.59, 1.73, 1.84 and 2.00 GeV.

(b) The mass values obtained from the solution of the equation $G_V^{-1} - J_{22}^A(P^2) = 0$ are shown as dotted lines. (Here G_V = 12.46 GeV^{-2}.) We find states with mass values of 1.43, 1.59, 1.75, 1.84 and 2.01 GeV. Note that $J_{22}^A(P^2)$ is the same as $J_{ss}^A(P^2)$ shown in Fig.10.

(c) The states of the K_1 meson, calculated with G_K = 78.13 GeV^{-2} and G_{KA} = 8.00 GeV^{-2}, are compared to the data. Here we include the mixing due to the polarization functions $J_{12}^A(P^2)$ and $J_{21}^A(P^2)$, as well as that due to the direct coupling parameterized by G_{KA}. (See Table 7.)

(d) Masses of the b_1 mesons. (See Table 6.)

Fig.15 (a) The levels in the confining field are shown for $m_u = m_d$ = 0.364 GeV, m_s = 0.565 GeV, κ = 0.055 GeV^2 and μ = 0.010 GeV. Here $\bar{n}n = (\bar{u}u + \bar{d}d)/\sqrt{2}$.

(b) Experimental values of the masses of the f_2 mesons. The $f_2'(1525)$ is assumed to have a $\bar{s}s$ configuration and it is possible that the $f_J(1750)$ is such a state [24].

(c) Theoretical mass values are shown for G_{T_1} = 47.00 GeV^{-2} and G_{T_2} = 6.80 GeV^{-2}. The mass values are 1254, 1429, 1527, 1551, 1685, 1745, 1767, 1913, 1939 and 1943 MeV.

Fig.16 The states of Fig.15a are put into correspondence with the states of Fig.15c. The dotted lines refer to the $s\bar{s}$ states. For each doublet, a state that is mainly $^3P_2$ lies lower in energy than the other member of the doublet, which is mainly of $^3F_2$ character.

Fig.17 (a) The diagram shows the basic vacuum polarization diagram of the NJL model which serves to define the function $-iJ^S(P^2)$.

(b) The diagram serves to define the function $-iJ^S(P^2)$ when confinement effects are included. The shaded triangular area represents the confining vertex shown in Fig.18. The right-hand side of the figure show a perturbative expansion for $-iJ^S(P^2)$.

Fig.18 (a) The figure shows the integral equation for the vertex $\bar{\Gamma}_S(P, k)$ [shaded triangular area]. The dashed line represents the confining interaction.

(b) A perturbative expansion for $\bar{\Gamma}_S(P, k)$ is shown.

Fig.19 The figure shows $J^S_{u\bar{d}}(P^2)$ which has singularities at the bound states in the confining field. The bound state energies are 1369, 1667, 1896, 2095, 2262, 2413, 2537 and 2651 MeV. The continuum starts at $2m_u + V_{max} = 2748$ MeV. Here $m_u = m_d = 0.364$ GeV, $\kappa = 0.055$ GeV^2 and $\mu = 0.01$ GeV. [See Fig.27a.]

Fig.20 The figure shows $J^S_{ss}(P^2)$. There are bound states in the confining field at 1693, 1945, 2154, 2331, 2485, 2625, 2744, 2855, 2955 and 3039 MeV. The continuum starts at $2m_u + V_{max} = 3150$ MeV. Here $m_s = 0.565$ GeV. [See Fig.27c.]

Fig.21 (a) The figure serves to define $-iK_{ij}(P^2)$ for intermediate two-meson states represented by wavy lines. The filled areas represent confinement vertex functions and the λ_i are Gell-Mann matrices.

(b) Contribution to $-iK_{ij}(P^2)$ from four-pion intermediate states are shown. (We neglect confinement in the case of the pion.)

Fig.22 (a) The amplitude $M_i^{\pi\pi}(P, \kappa)$ for a scalar $q\bar{q}$ state to decay to two pions is shown. The left-hand confinement vertex is represented by $\bar{\Gamma}_S(P, k) = \hat{a}_1(P, k) + \hat{k}\,\hat{a}_2(P, k)$ of Eq.(4.3.22). (The exchange diagram is not drawn.)

(b) The amplitude $M_i^{K\bar{K}}(P, \kappa)$ for a scalar $q\bar{q}$ state to decay to the K^+K^- or $K^0\bar{K}^0$ channels. The left-hand vertex is again given by $\bar{\Gamma}_S(P, k)$. Confinement vertices are included for the kaon.

Fig.23 The figure exhibits the values of $\mathrm{Im}K^{\pi\pi}_{88}(P^2)$ [solid line], $\mathrm{Im}K^{\pi\pi}_{08}(P^2)$ [dotted line] and $\mathrm{Im}K^{\pi\pi}_{00}(P^2)$ [dashed line]. The regulator of Eq.(4.3.24) is used in the calculation of the decay amplitude $M_i(P^2)$.

Fig.24 Values of $\mathrm{Im}K_{88}^{K\bar{K}}(P^2)$ [solid line], $\mathrm{Im}K_{08}^{K\bar{K}}(P^2)$ [dotted line] and $\mathrm{Im}K_{00}^{K\bar{K}}(P^2)$ [dashed line] are shown. (The regulator of Eq.(4.3.24) is used in these calculations.)

Fig.25 Values of $\mathrm{Re}K_{88}^{T}(P^2)$ [solid line], $\mathrm{Re}K_{08}^{T}(P^2)$ [dotted line] and $\mathrm{Re}K_{00}^{T}(P^2)$ [dashed line] are shown for the quantity defined in Eq.(4.4.4). (The regulator of Eq.(4.3.24) is used in these calculations.)

Fig.26 Values of $\mathrm{Re}K_{nn}^{T}(P^2)$ [solid line], $\mathrm{Re}K_{ss}^{T}(P^2)$ [dotted line] and $\mathrm{Re}K_{ns}^{T}(P^2)$ [dashed line] are shown. (The regulator of Eq.(4.3.24) is used in these calculations. These values are related to those of Fig.25 and do not contain the factor of 3 that appears in Eq.(4.4.6).)

Fig.27 (a) - (c) Figure (a) shows the energies of $n\bar{n}$ states bound in the confining field. Here $m_u = m_d = 0.364$ GeV, $\mu = 0.010$ GeV, and $\kappa = 0.055$ GeV^2. Figure (c) shows the energies of the $s\bar{s}$ states bound in the confining field. Here $m_s = 0.565$ GeV.

(b) In this figure we show how the energies of the states in (a) and (c) change when the short-range NJL interaction is included in the calculation. The letter G denotes the state we have chosen to be the scalar glueball. Here, dotted lines denote $s\bar{s}$ states.

(d) This figure shows the result of including $\mathrm{Re}K^T_{88}(P^2)$, $\mathrm{Re}K^T_{00}(P^2)$, $\mathrm{Re}K^T_{08}(P^2)$ and $\mathrm{Re}K^T_{80}(P^2)$ when calculating the energy levels. We are to close ideal mixing, with $s\bar{s}$ states denoted by dotted lines.

(e) Energy levels found in the data tables are shown [29]. The states at 2100 MeV and 2315 MeV have recently been seen by Bugg et *al.*.

Fig.28 The figure shows the calculated energies of the f_0 and a_0 mesons. Since the results are quite close to ideal mixing, we indicate $n\bar{n}$ states by a solid line and $s\bar{s}$ states by dotted lines. These results include the effects of $\mathrm{Re}K^T_{ij}(P^2)$ which was calculated with the regulator of Eq.(4.3.24). [See Fig.25.]

Fig.29 Values of $|T_{nn}|^2$ are shown as a function of $E=\sqrt{P^2}$. The resonance peaks are at 978, 1549, 1843 and 2064 MeV. [See Fig.28.] In the approximation based upon ideal mixing, the $f_0(980)$ resonance is elastic with a width $\Gamma_{f_0}(980)$ = 99 MeV. The other states have small widths for decay to two pions. Note the somewhat asymmetric form of the resonance representing the $f_0(980)$ which is due to the opening of the $K\bar{K}$ channel at 990 MeV.

Fig.30 Values of $|T_{ss}|^2$ are shown as a function of $E = \sqrt{P^2}$. The resonance peaks are at 1340, 1864 and 2108 MeV. The width for the $f_0(1370)$ to decay to the $K\bar{K}$ channel is $\Gamma_{f_0}(1370) = 225$ MeV. (The total width of the $f_0(1370)$ is given in the data tables as 200-500 MeV [29]). Inspection of region near the peak at 1864 MeV shows a small peak at 1843 MeV which represents the decay of our $f_0(1843)$ to the $K\bar{K}$ channel. (A tiny peak that is present at 2064 MeV is too small to be seen in this figure. See Fig.32.)

Fig.31 Schematic representation of $\pi - \pi$ scattering in our model. The factors of $\lambda_i/\sqrt{2}$ and $\lambda_j/\sqrt{2}$ arise from the representation of $t^S(P^2)$ given in Eq.(4.4.14). The amplitudes $M(P^2)$ are those defined in Fig.22a. [The amplitude $\mathrm{Im}K_{ij}^{\pi\pi}(P^2)$ contains a statistical factor $S = 2$ which has been divided out in Eq.(4.5.15).]

Fig.32 The values of $|T_{K\bar{K}}(E)|^2$ are shown as a solid line and are compared to $|T_{ss}(E)|^2$ of Fig.30 (dotted line). The three small peaks in $|T_{K\bar{K}}(E)|^2$ arise from the small $s\bar{s}$ component of the $n\bar{n}$ states at 1549, 1843 and 2064 MeV. [See Table 12.] The peak of the resonance representing the $f_0(1370)$ is at 1366 MeV for the function $|T_{K\bar{K}}(E)|^2$ (solid line). The corresponding width of the $f_0(1370)$ is $\Gamma_{f_0}(1370) = 192$ MeV for decay to the $\pi\pi$ plus $K\bar{K}$ channels.

Fig.33 The figure shows values of $\mathrm{Re}K_{00}^{\pi\pi}(P^2)$ and $\mathrm{Im}K_{00}^{\pi\pi}(P^2)$ calculated with the regulator $R(k_c^c) = \sqrt{2/3}\exp[k_c^2/\alpha_1]$ with $\alpha_1 = 0.325$ GeV. [See Fig.23, where the regulator of Eq.(4.3.24) was used.]

Fig.34 Values of $\mathrm{Re}K_{08}^{\pi\pi}(P^2)$ and $\mathrm{Im}K_{08}^{\pi\pi}(P^2)$ are shown. [See the caption of Fig.33.]

Fig.35 Values of $\mathrm{Re}K_{88}^{\pi\pi}(P^2)$ and $\mathrm{Im}K_{88}^{\pi\pi}(P^2)$ are shown. [See the caption of Fig.33.]

Fig.36 The figure shows $\mathrm{Re}K_{00}^{K\bar{K}}(P^2)$ and $\mathrm{Im}K_{00}^{K\bar{K}}(P^2)$ calculated with the regulator $R(k_c^c) = \sqrt{2/3}\exp[k_c^2/\alpha_1]$. Here $\alpha_1 = 0.325$ GeV.

Fig.37 The figure shows $\mathrm{Re}K_{08}^{K\bar{K}}(P^2)$ and $\mathrm{Im}K_{08}^{K\bar{K}}(P^2)$. (See the caption to Fig.36.)

Fig.38 The figure shows $\mathrm{Re}K_{88}^{K\bar{K}}(P^2)$ and $\mathrm{Im}K_{88}^{K\bar{K}}(P^2)$. (See the caption to Fig.36.)

Fig.39 The figure shows $|T_{\pi\pi}(E)|^2$, with peaks seen at 982, 1552, 1840 and 2062 MeV. The width of the $f_0(980)$ is 56 MeV in this calculation. (This figure represents s-channel effects in $\pi - \pi$ scattering, as obtained in our model.)

Fig.40 The figure shows values of $|T_{K\bar{K}}(E)|^2$, with resonance peaks at 1410, 1552, 1840, 1858, 2062 and 2102 MeV . The states at 1552, 1840 and 2062 MeV are the predominately $n\bar{n}$ states which were seen in Fig.36. The excitation with a peak at 1040 MeV is a feature of the $f_0(980)$ and arises from the process $K\bar{K} \to f_0(980) \to K\bar{K}$. The $f_0(1370)$, placed in correspondence with the peak at 1410 MeV, has a width of 192 MeV for decay to the $K\bar{K}$ channel.

Fig.41 The figure shows portions of Fig.39 [solid line] and Fig.40 [dotted line].

Fig.42 The eigenvalues of the matrix of Eq.(4.7.2) are shown as a function of z. Here $z_1 = z = 0.075$ GeV, $m_{G_0} = 1.550$ GeV, $m_{s\bar{s}} = 1.400$ GeV, $m'_{n\bar{n}} = 1.550$ GeV and $m_{n\bar{n}} = 1.000$ GeV. The horizontal dotted line are drawn at 1.000, 1.370, 1.500 and 1.700 GeV.

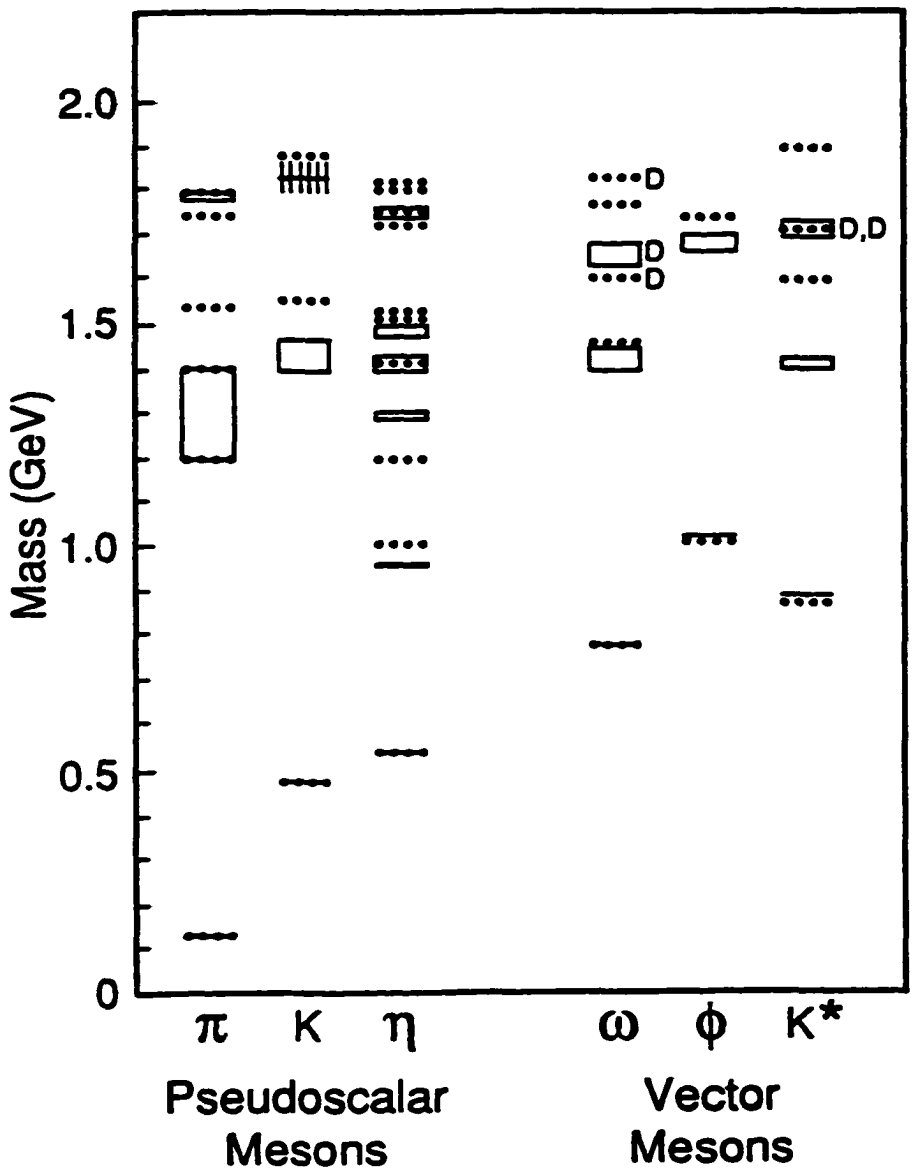

Figure 1

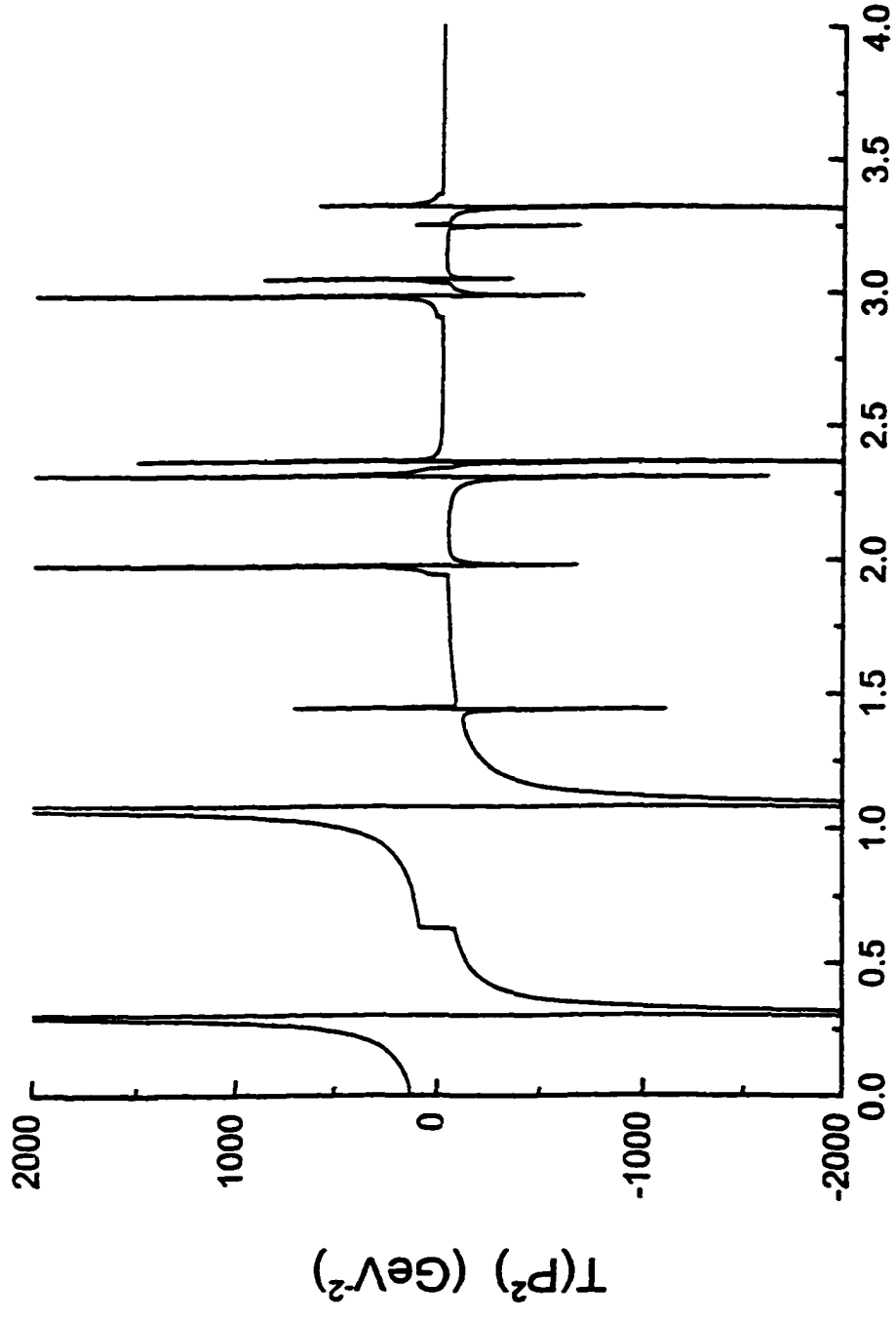

Figure 2

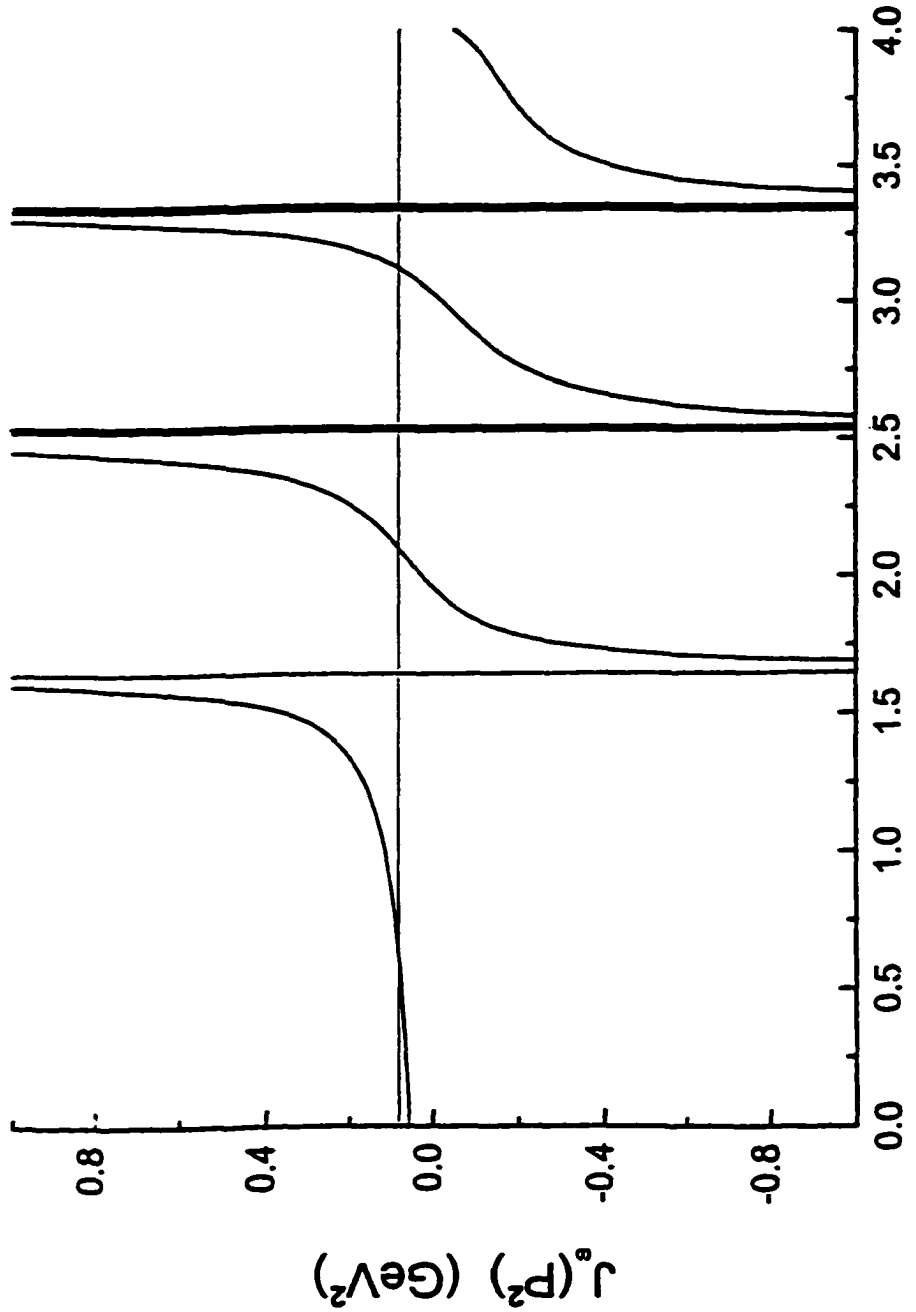

Figure 3

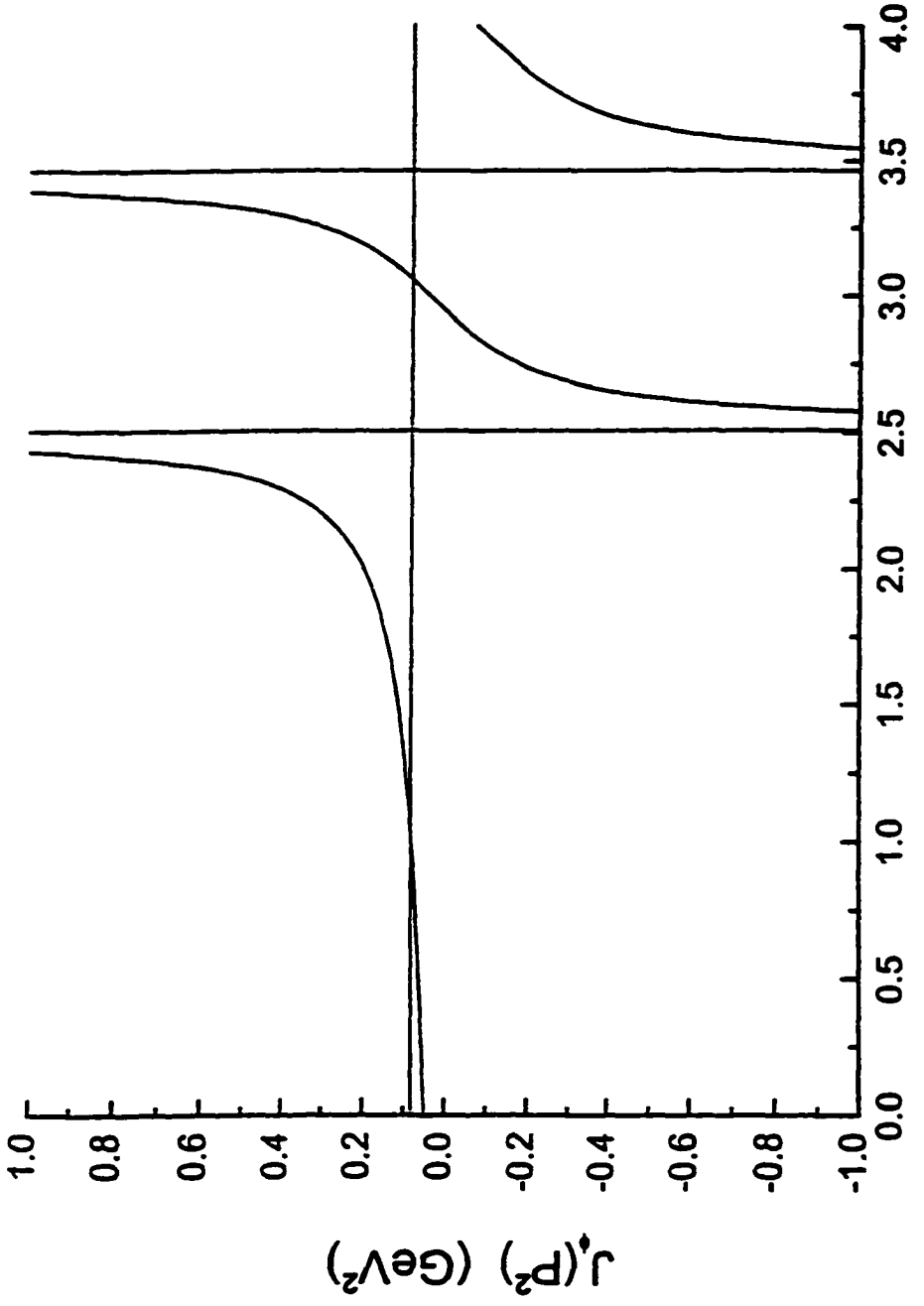

Figure 4

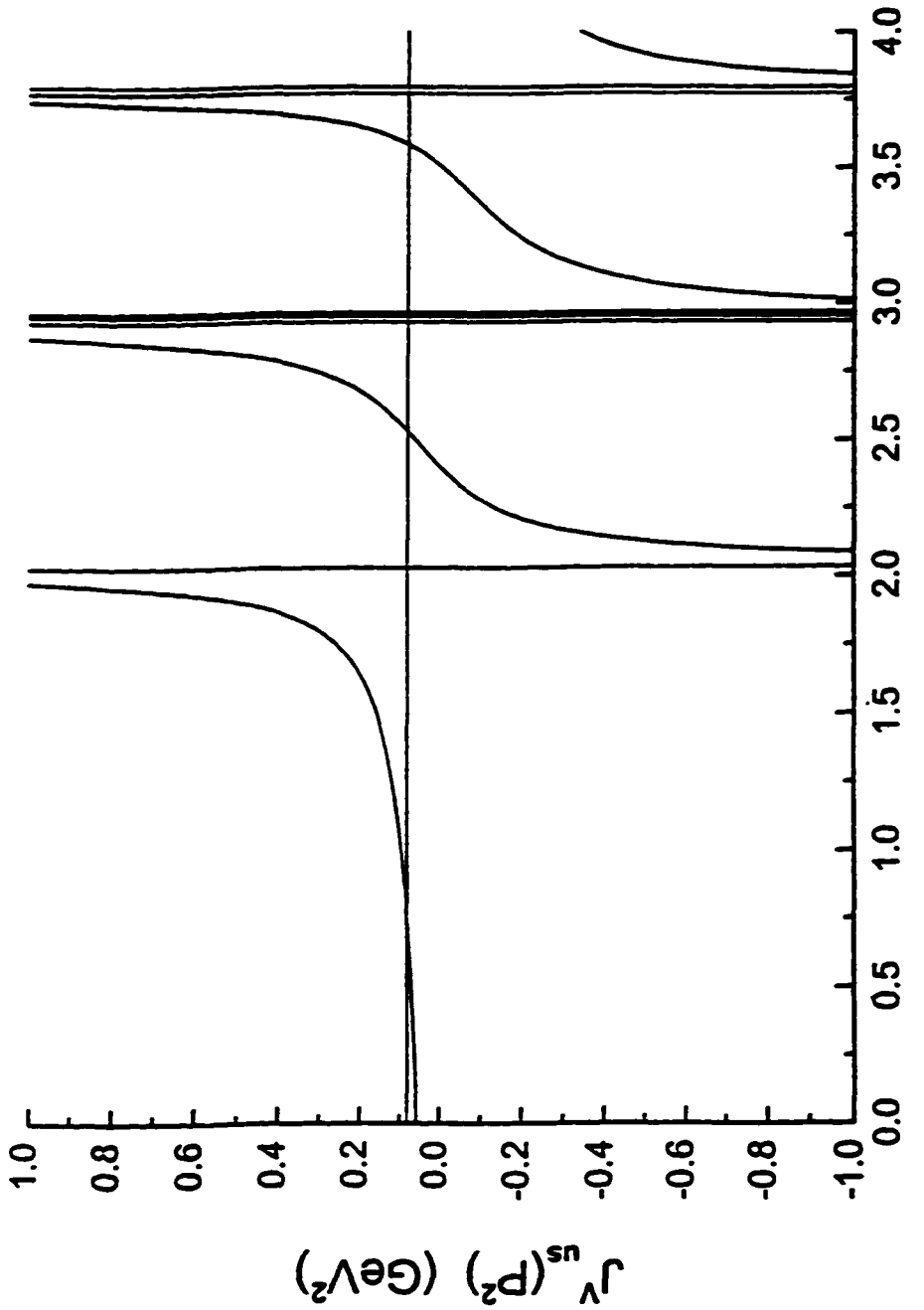

Figure 5

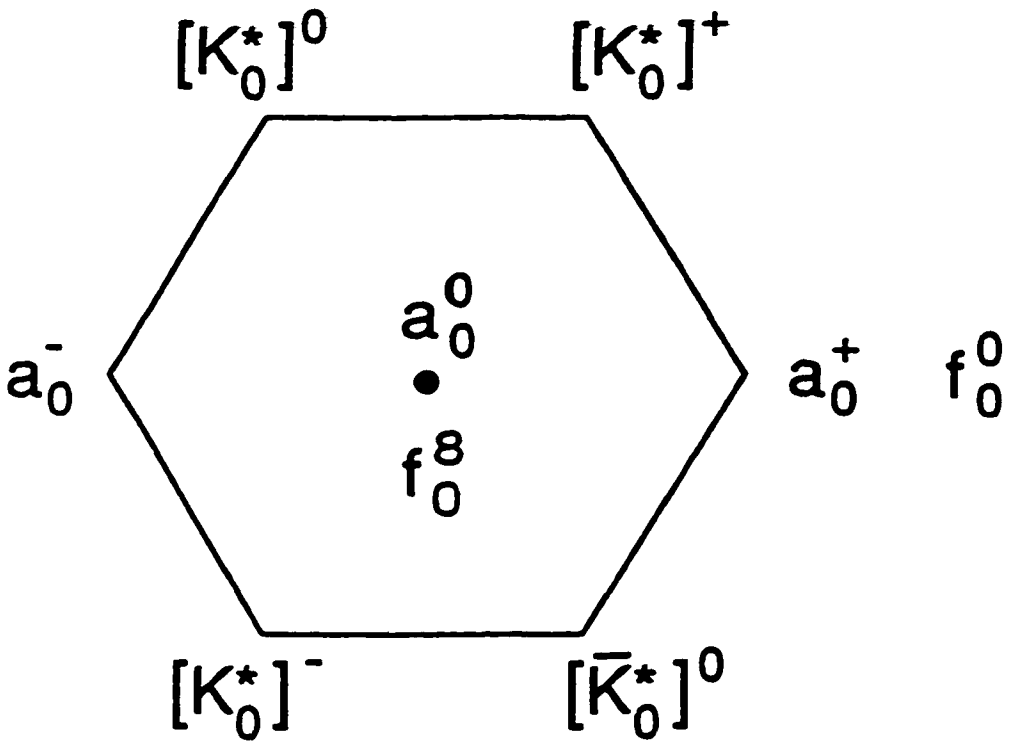

Figure 6

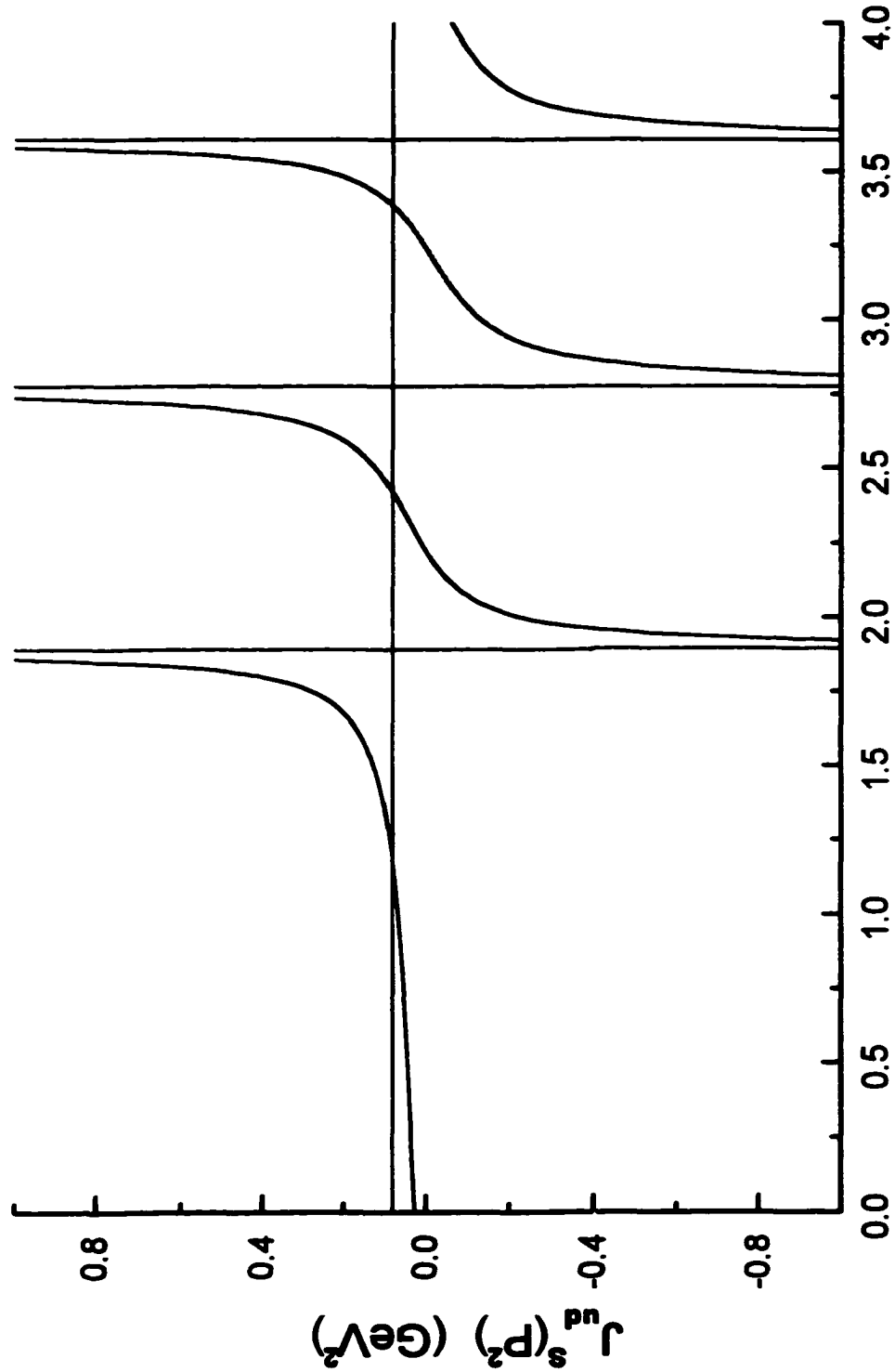

Figure 7

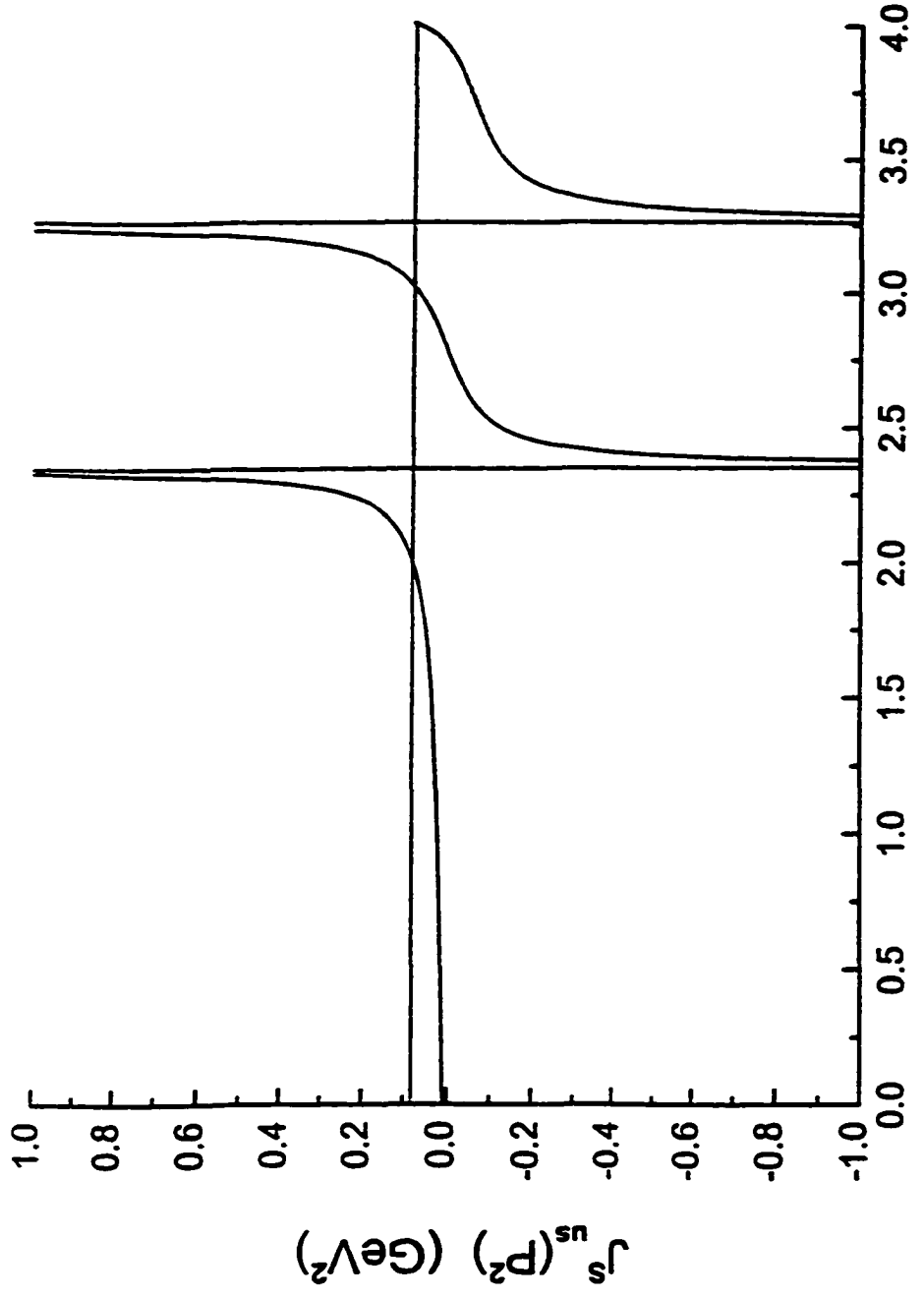

Figure 8

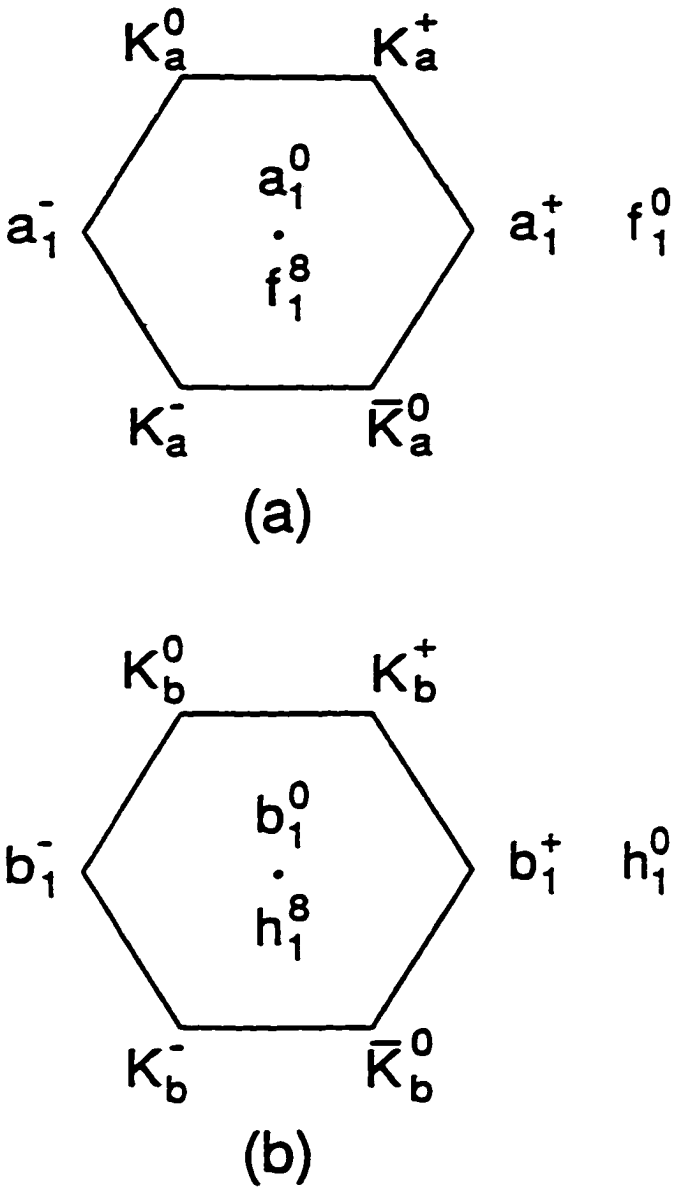

Figure 9

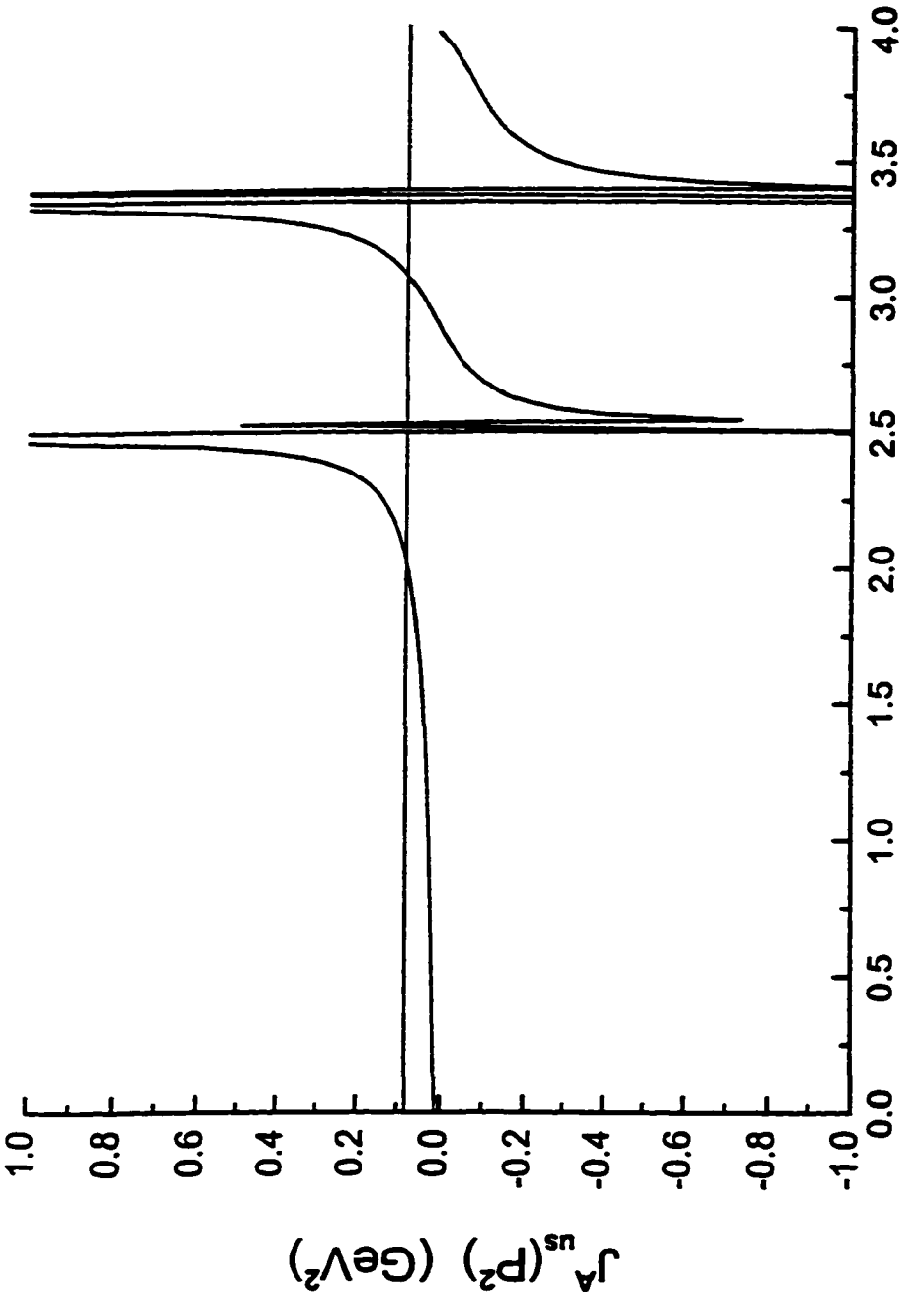

Figure 10

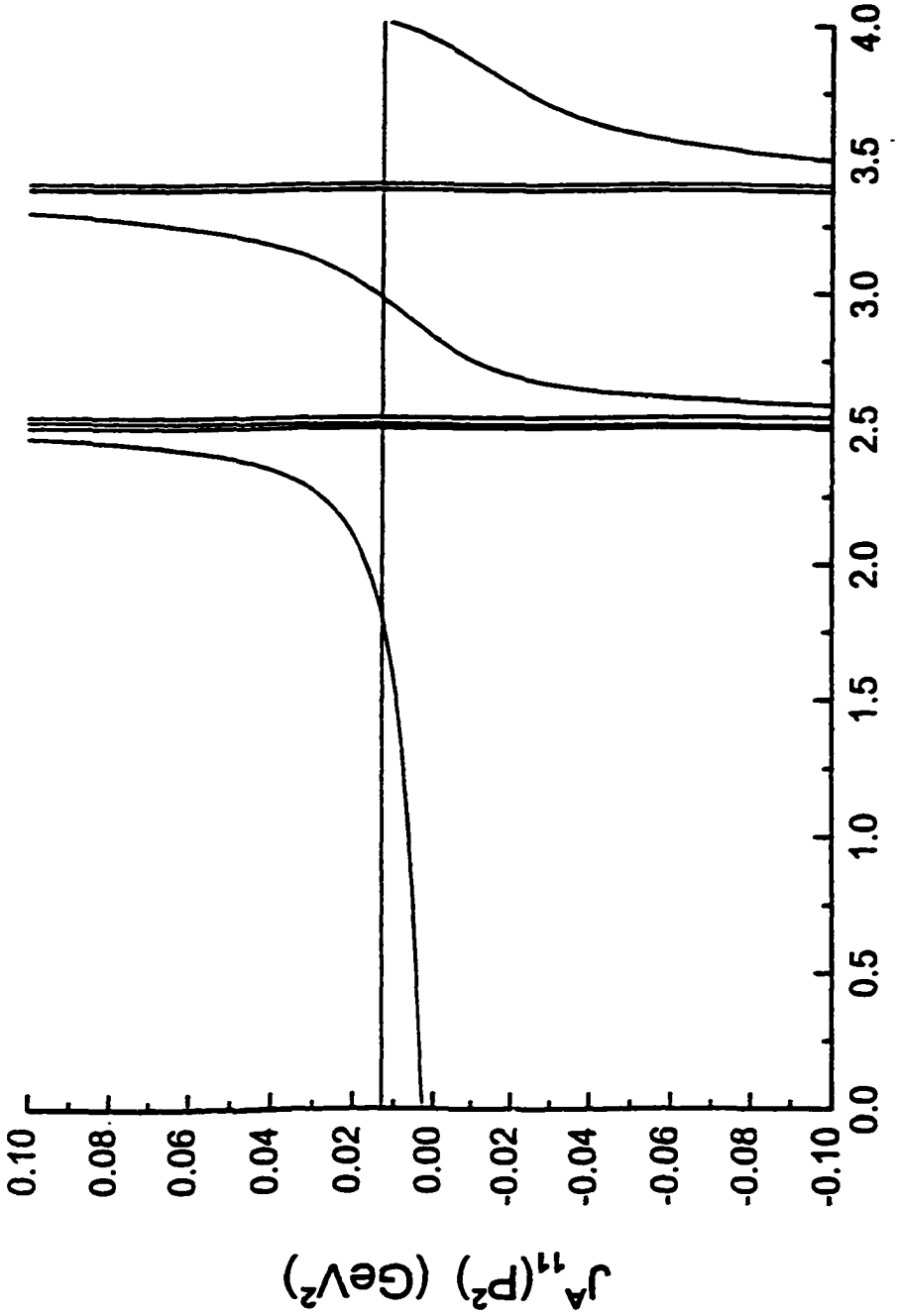

Figure 11

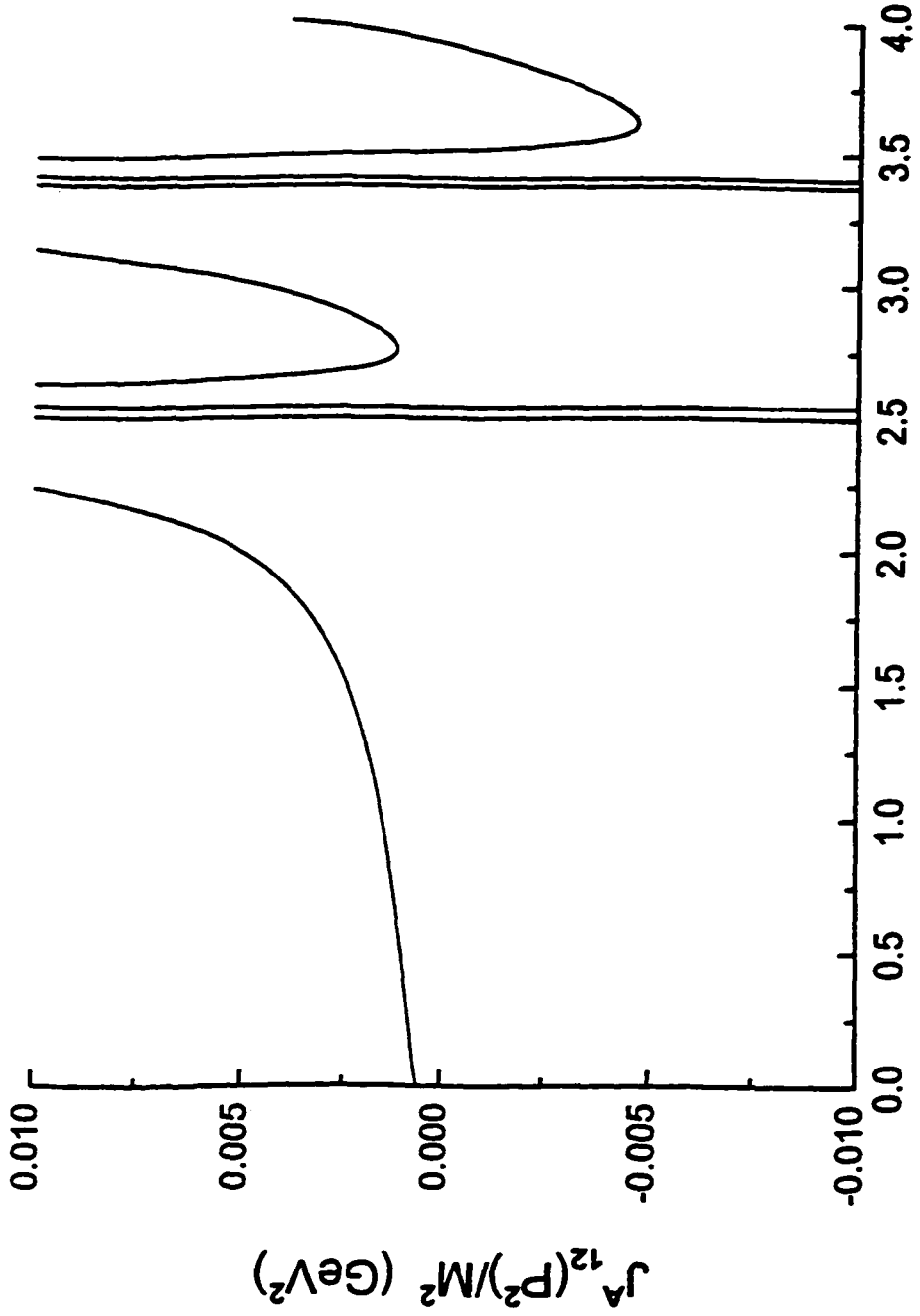

Figure 12

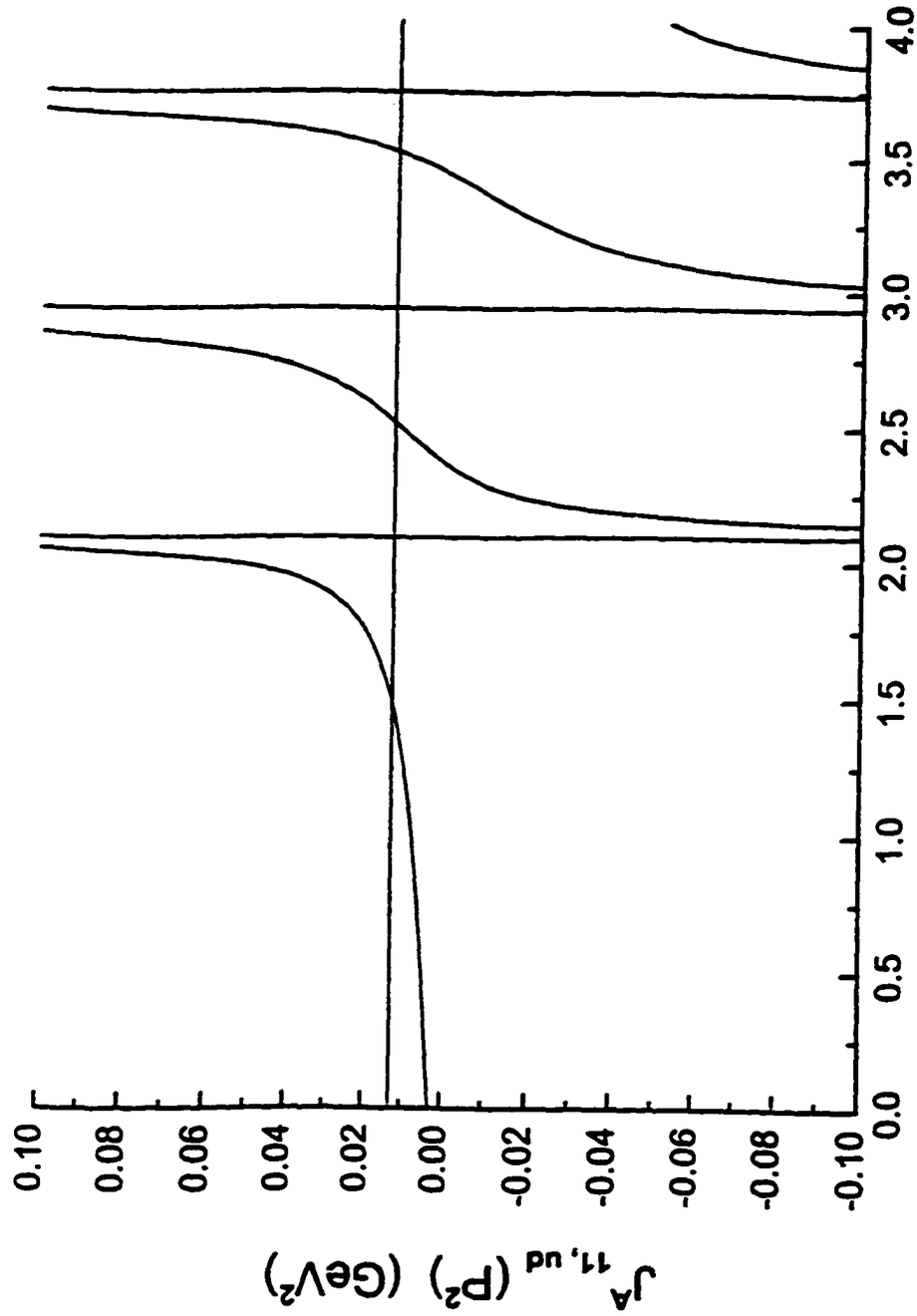

Figure 13

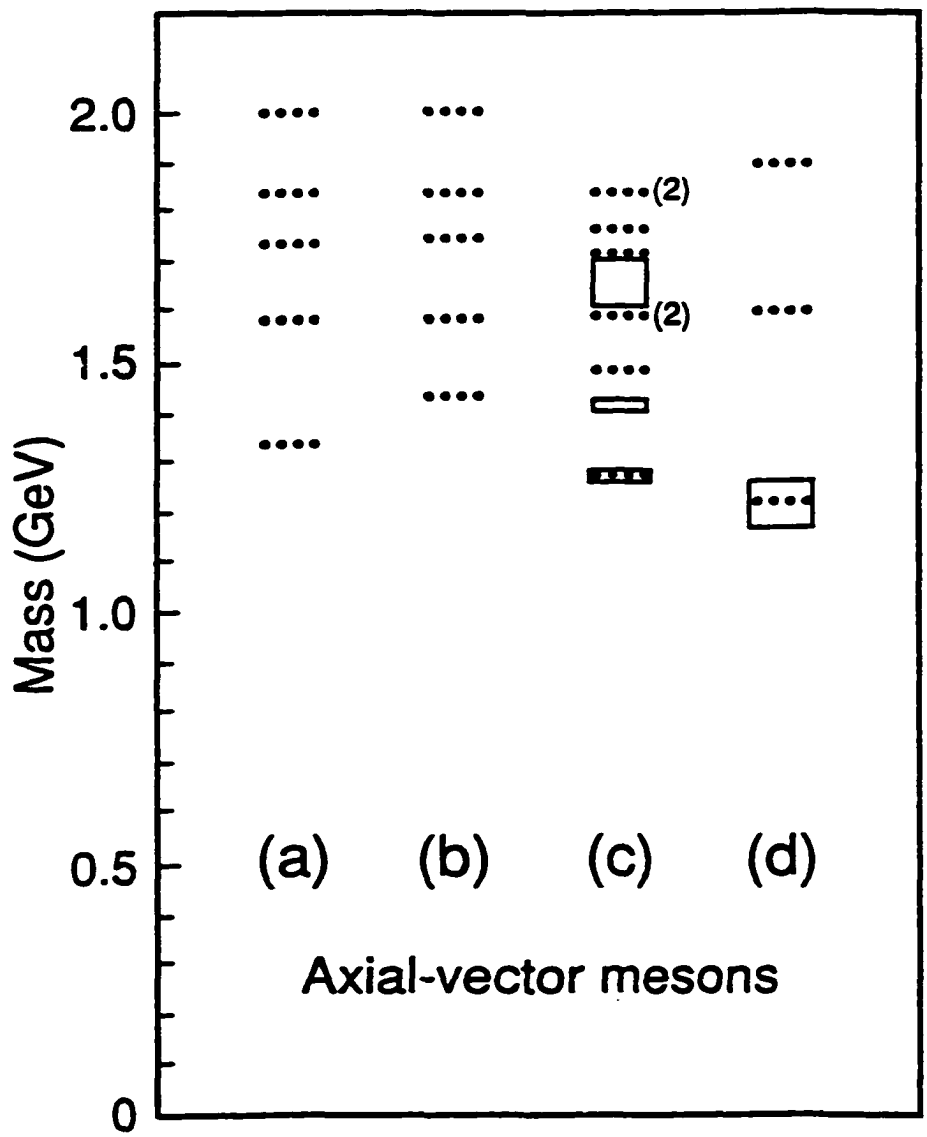

Figure 14

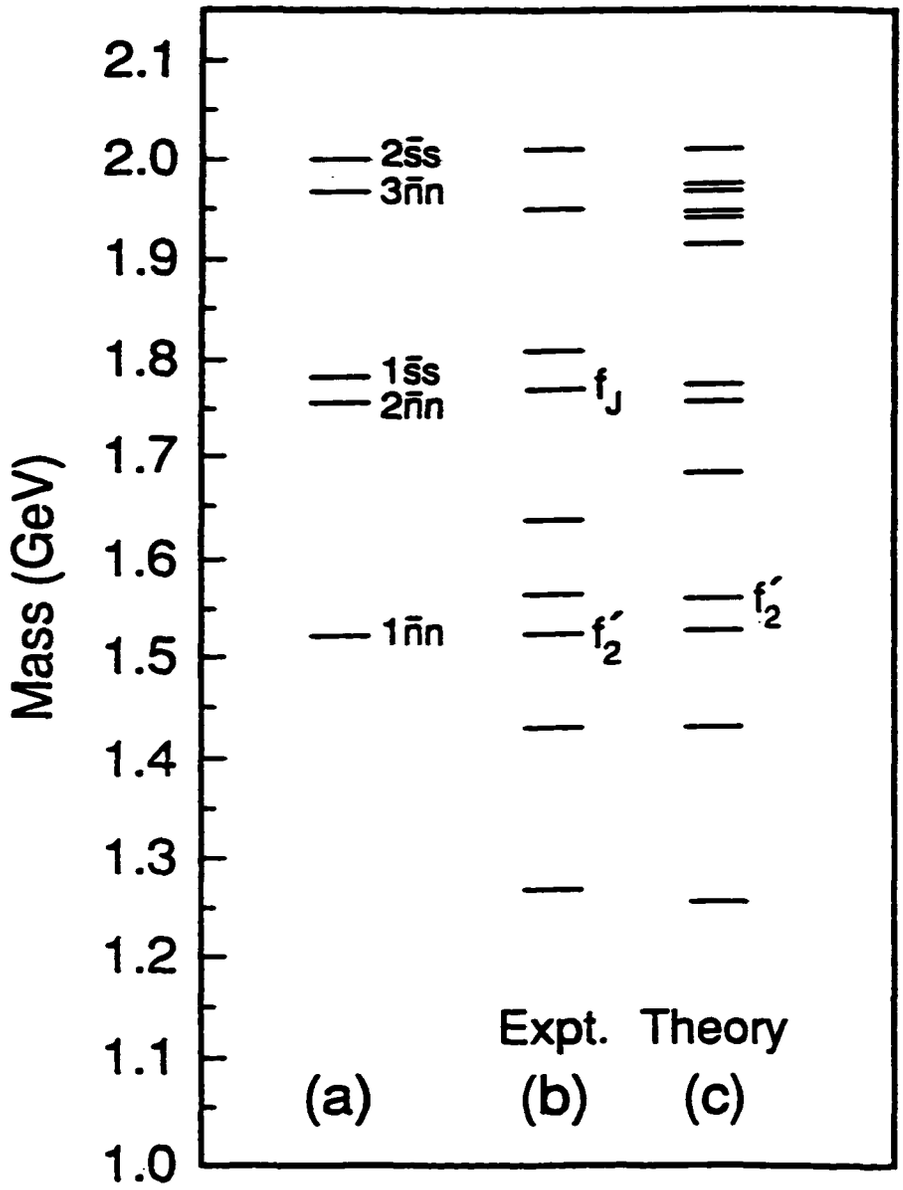

Figure 15

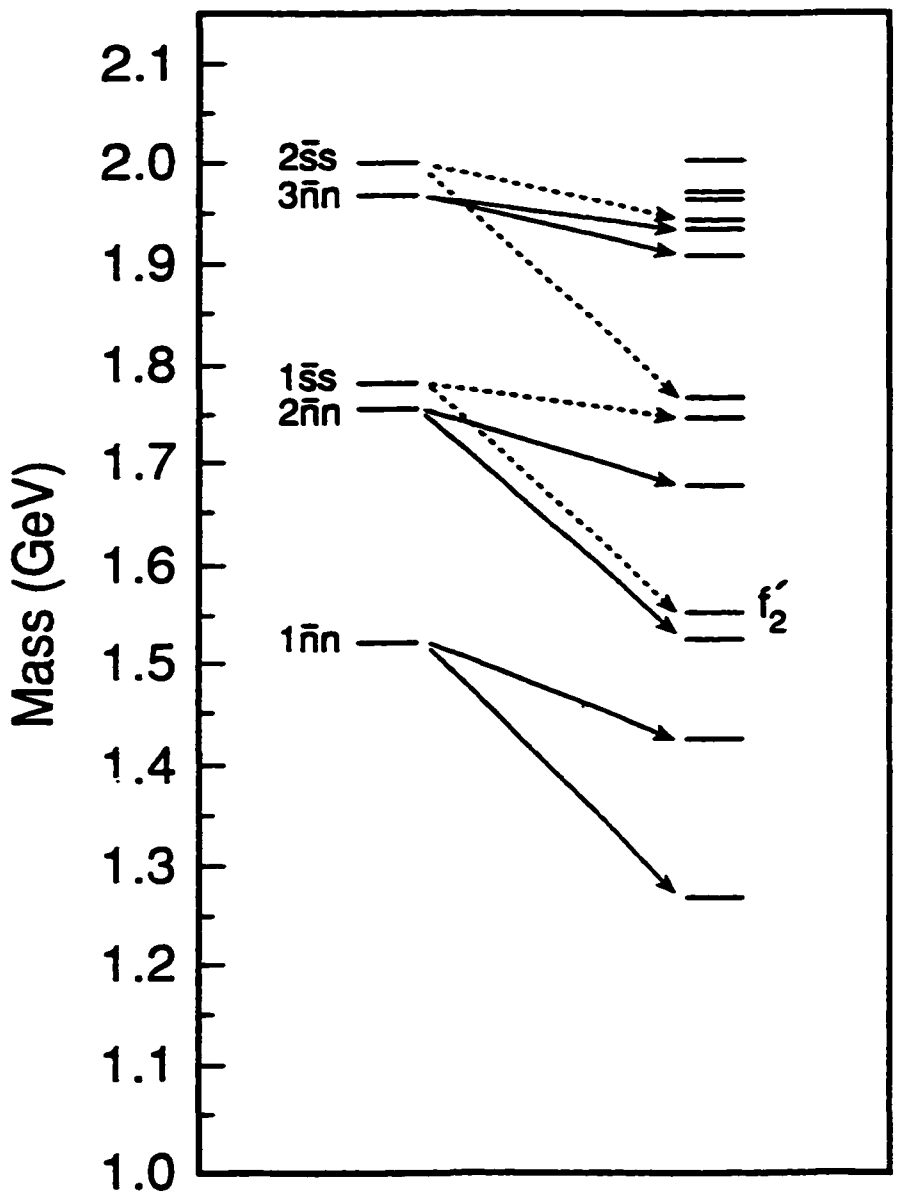

Figure 16

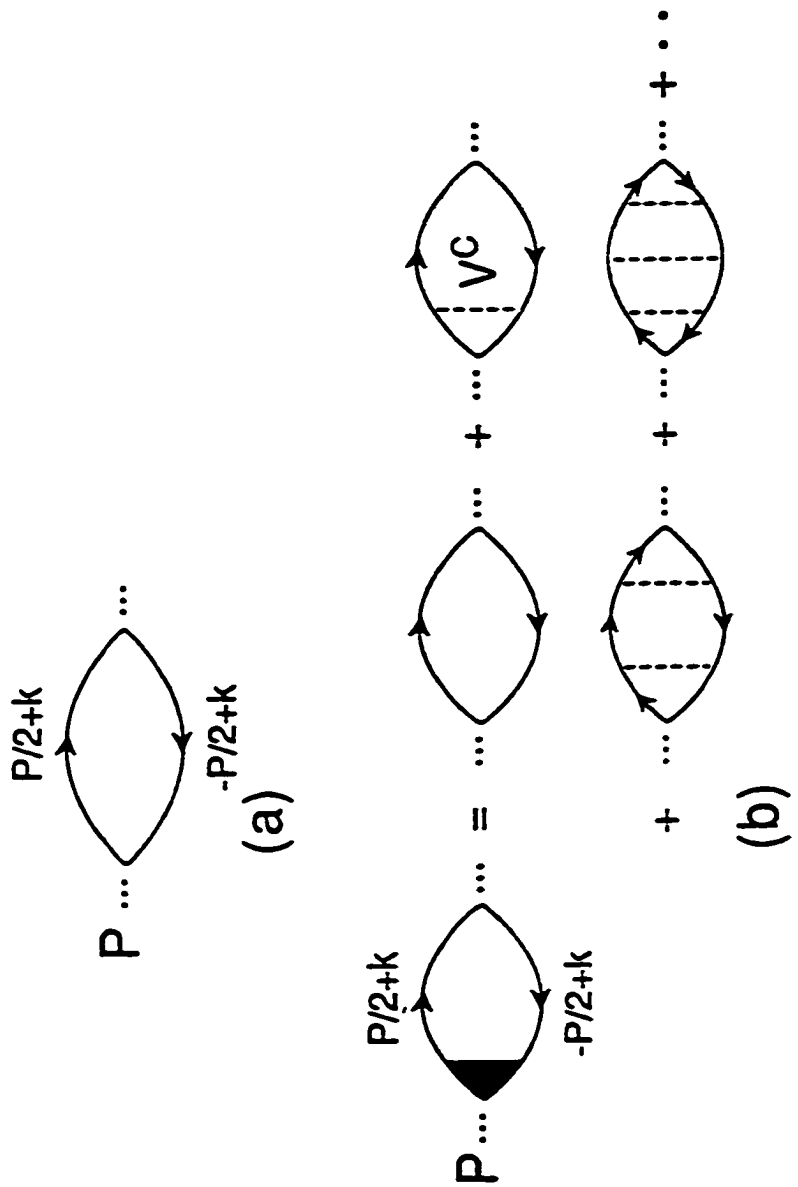

Figure 17

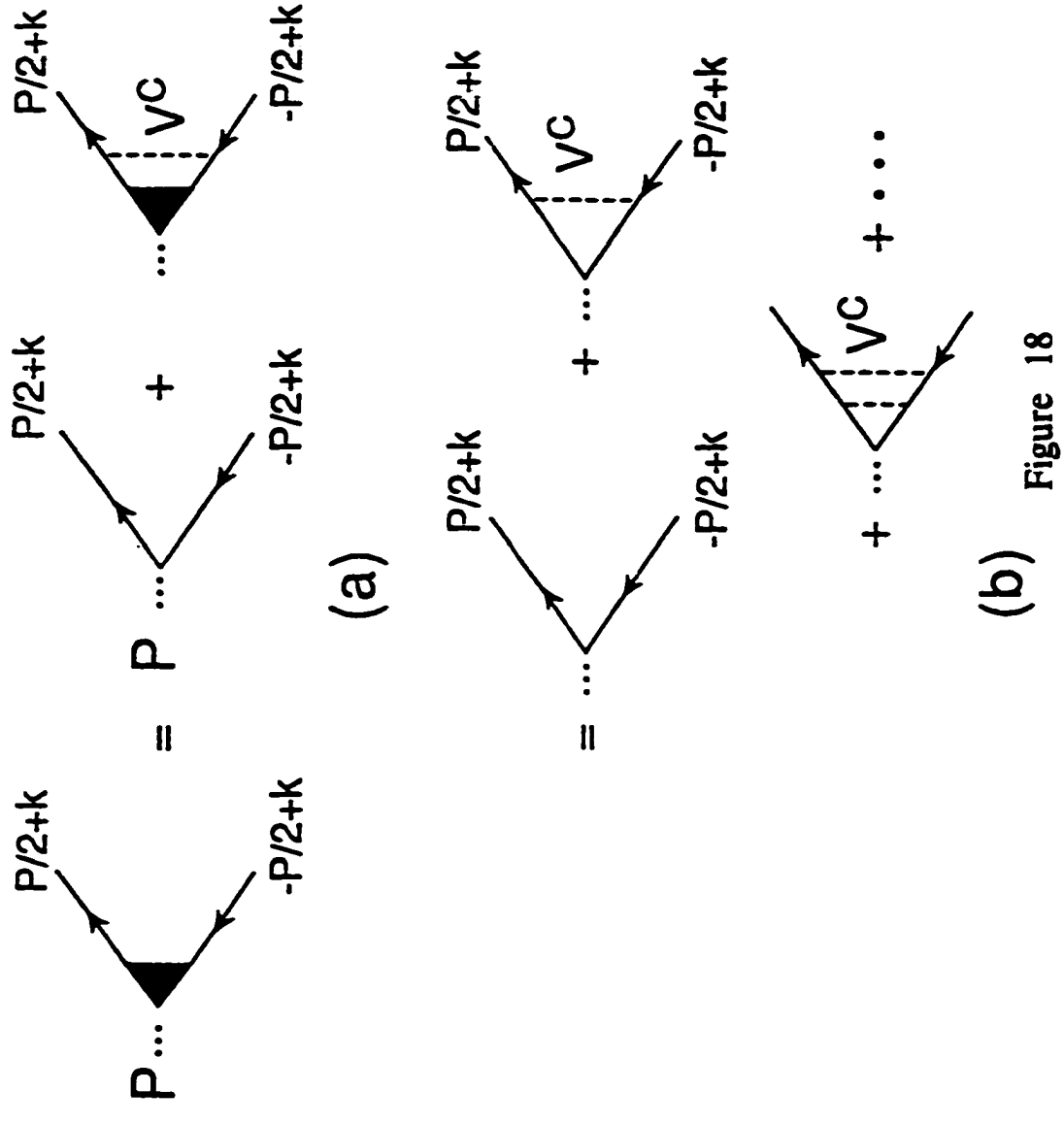

Figure 18

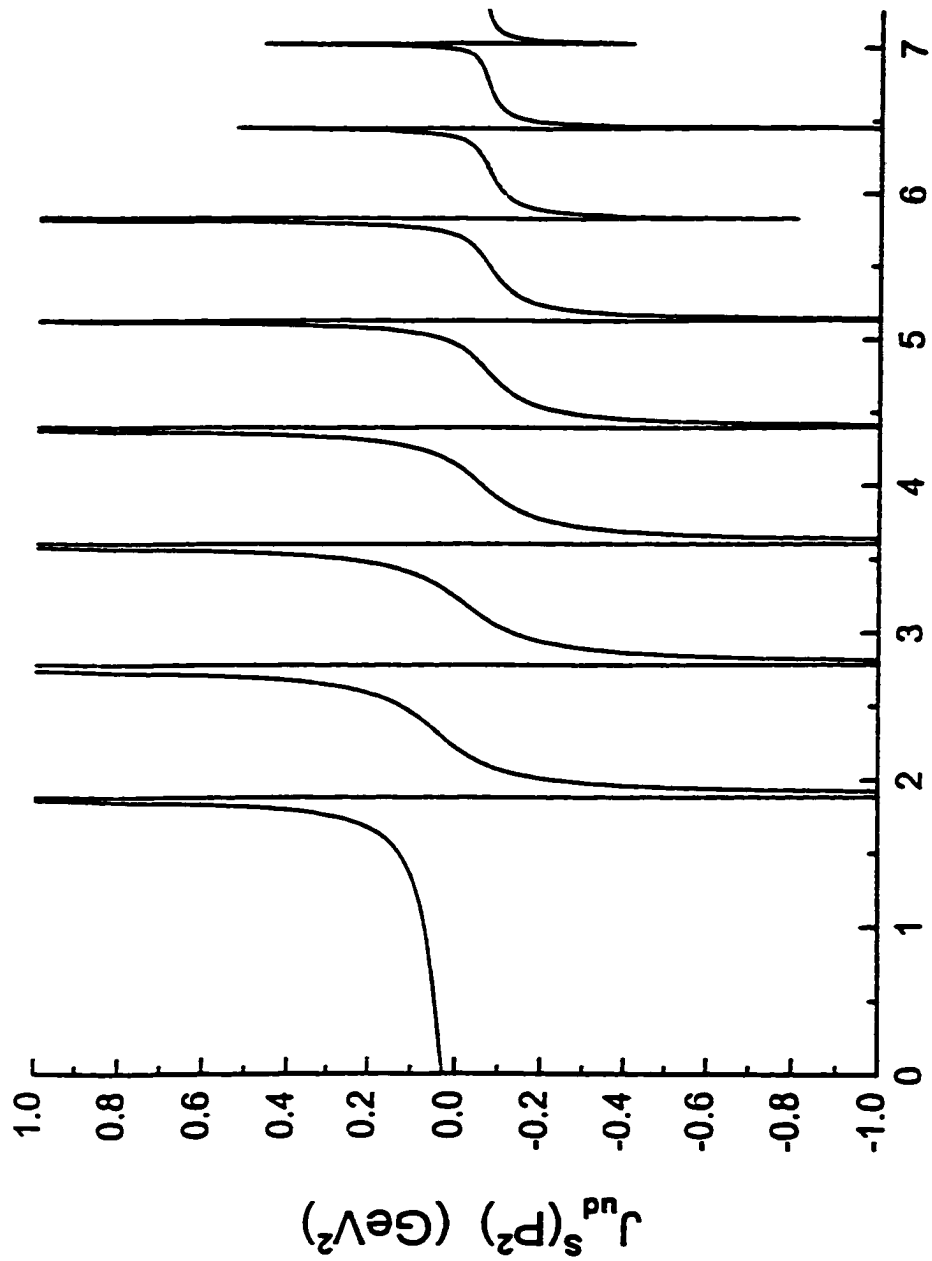

Figure 19

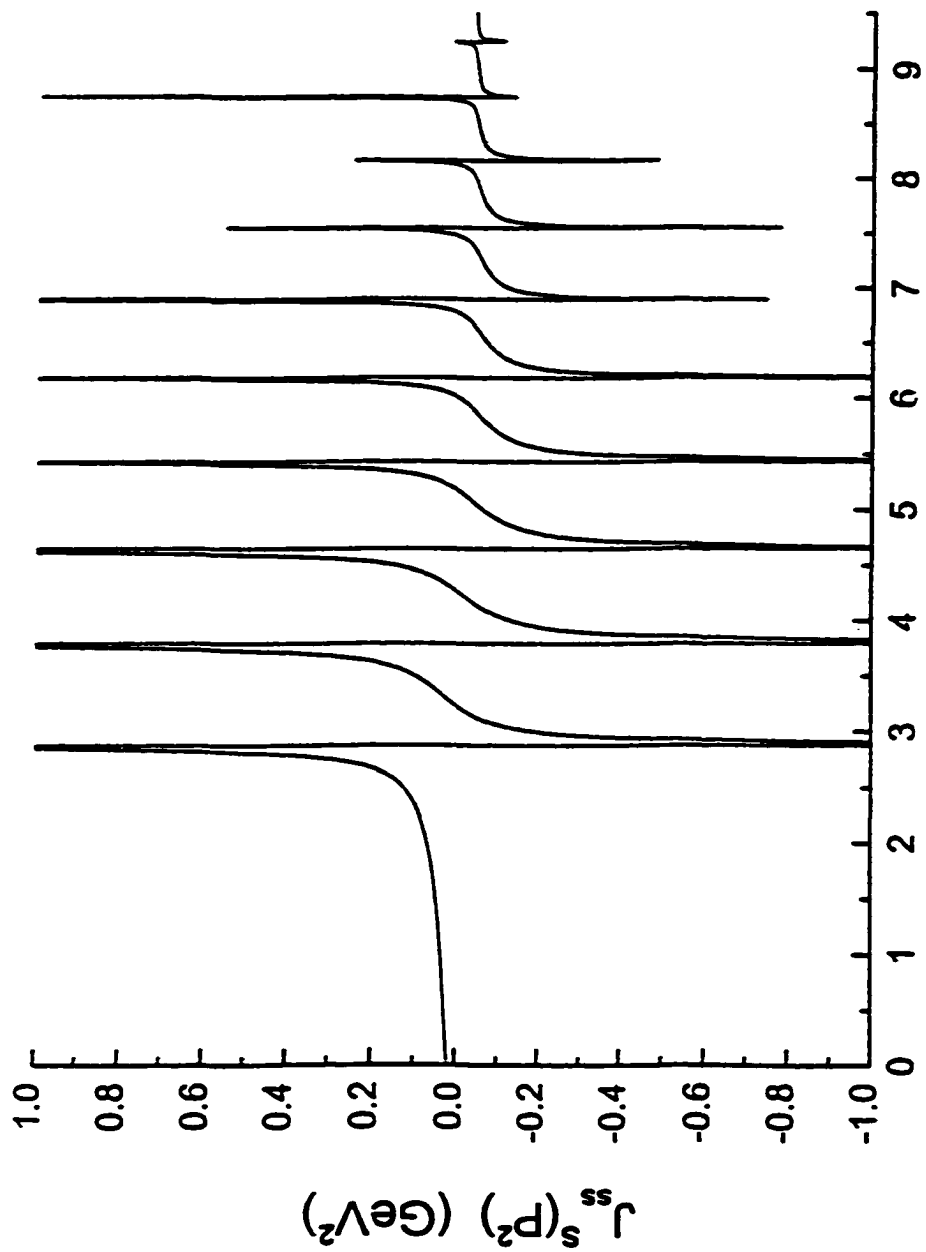

Figure 20

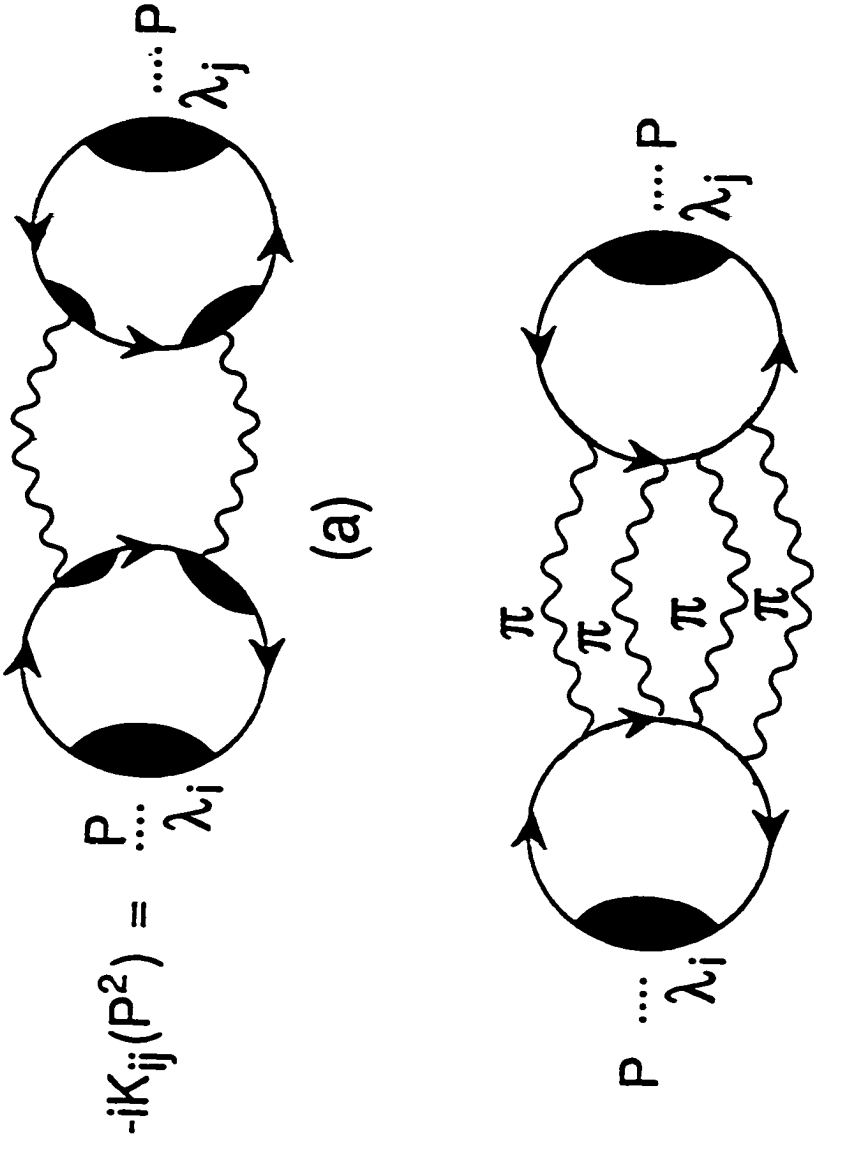

Figure 21

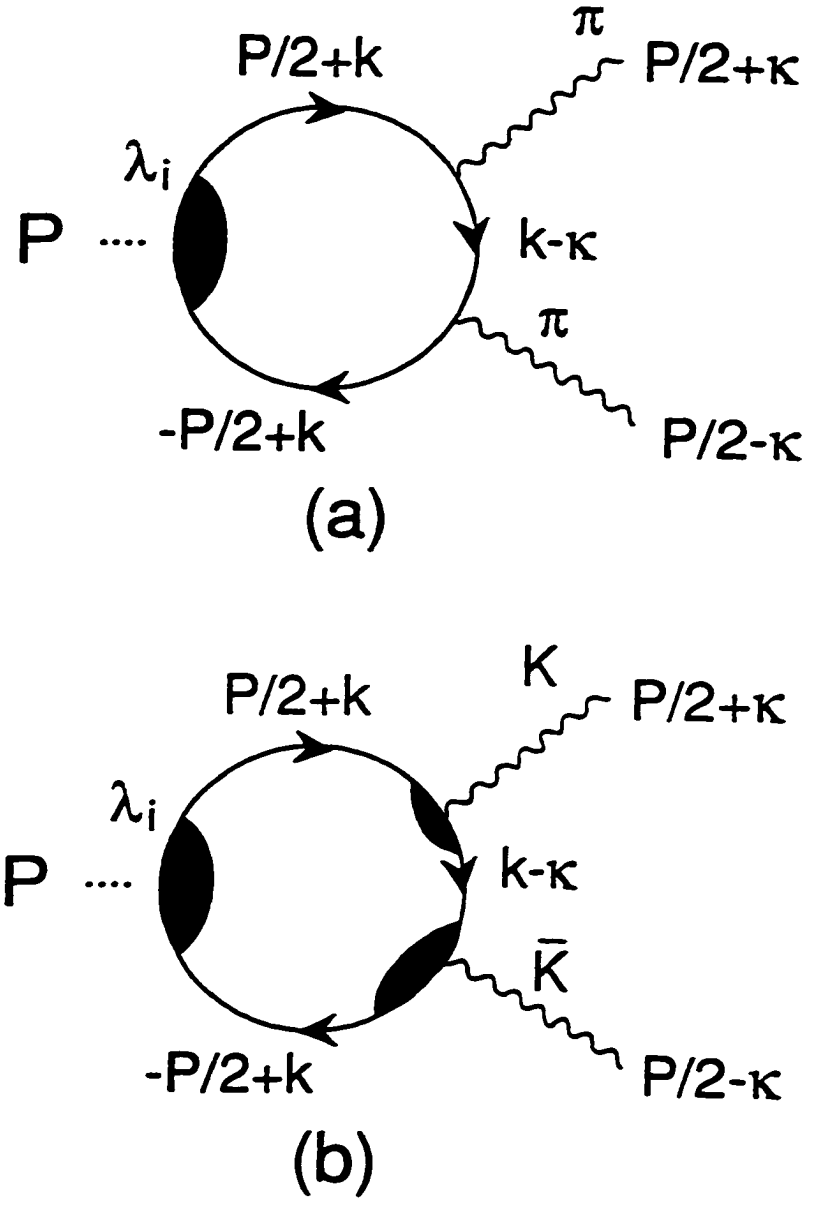

Figure 22

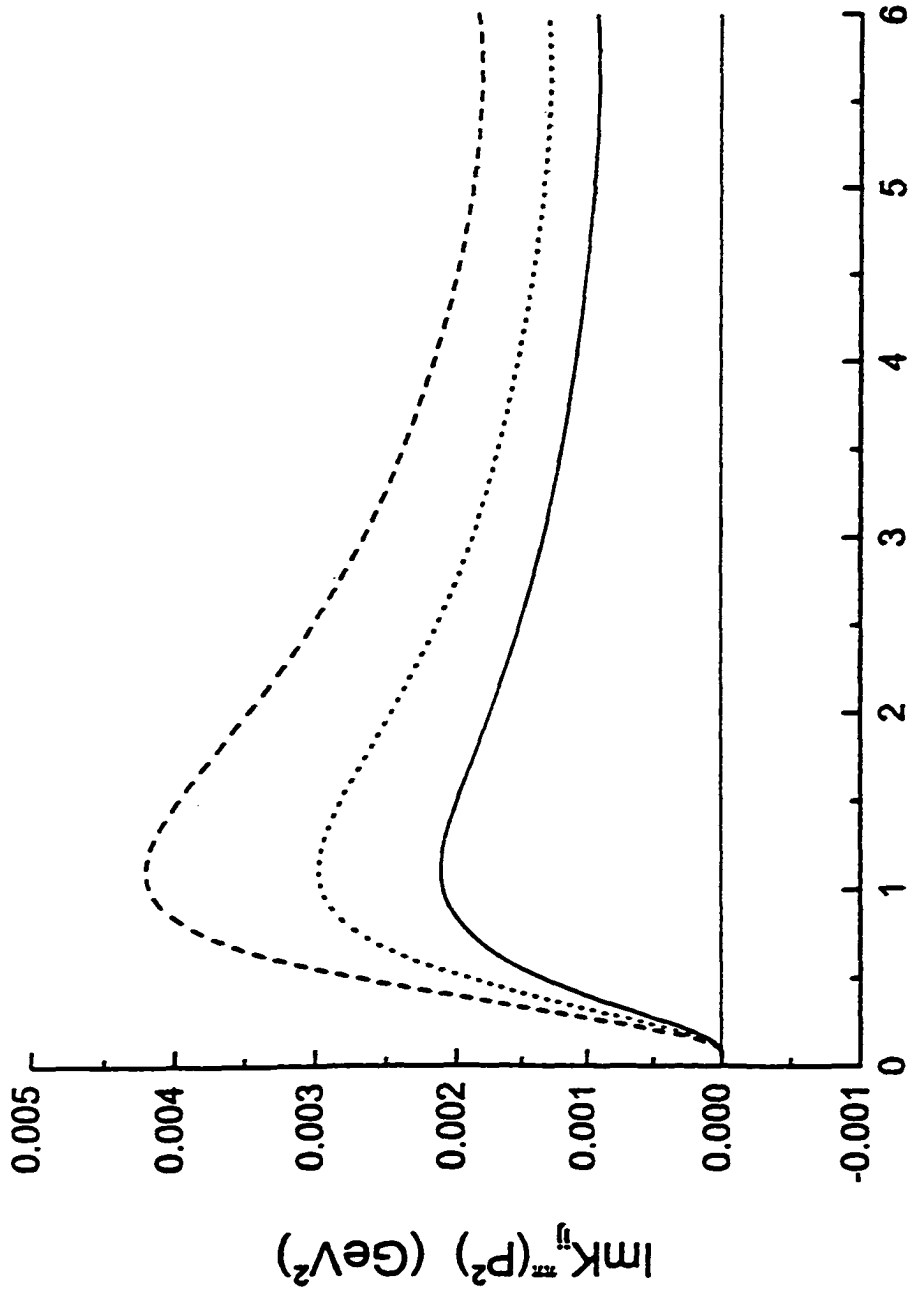

Figure 23

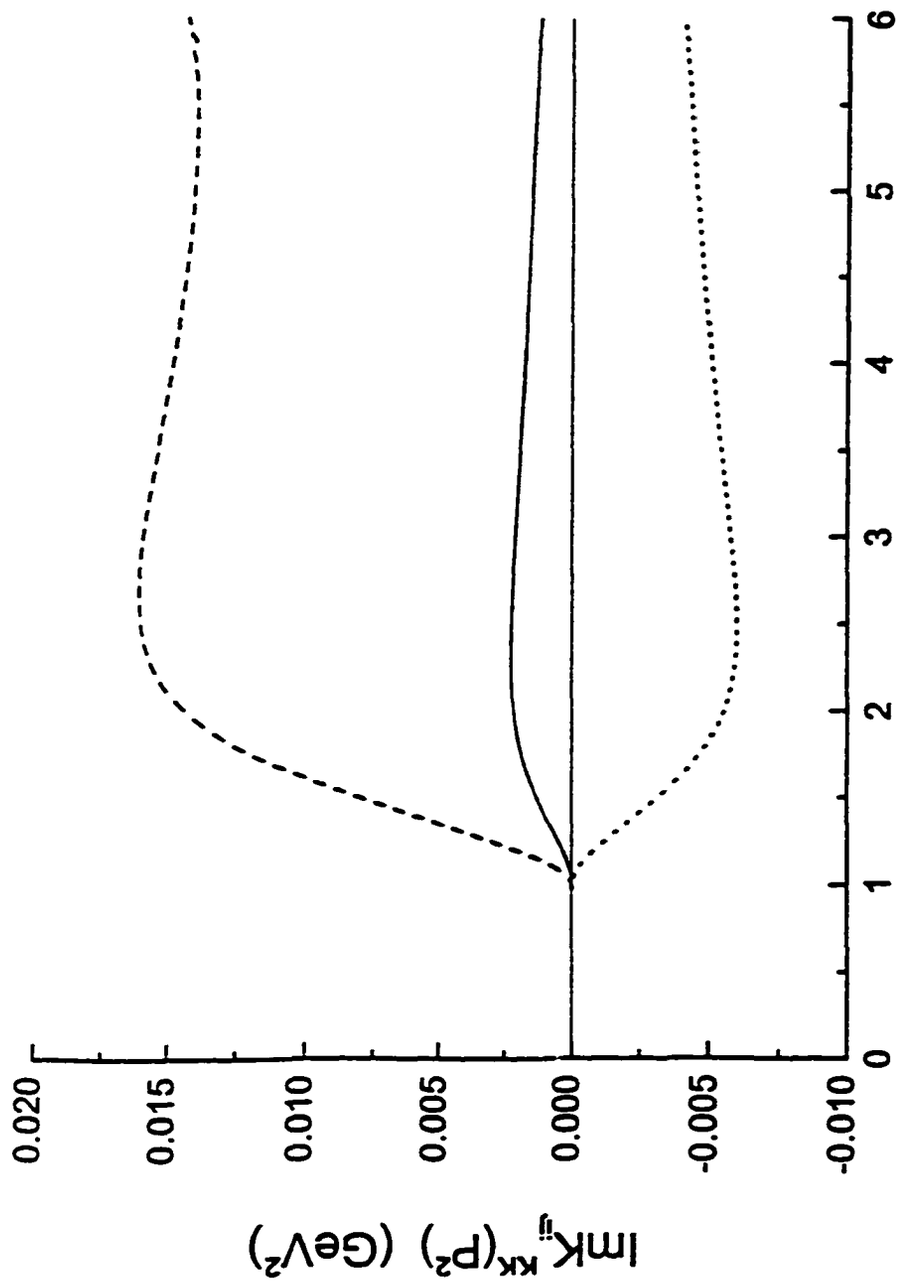

Figure 24

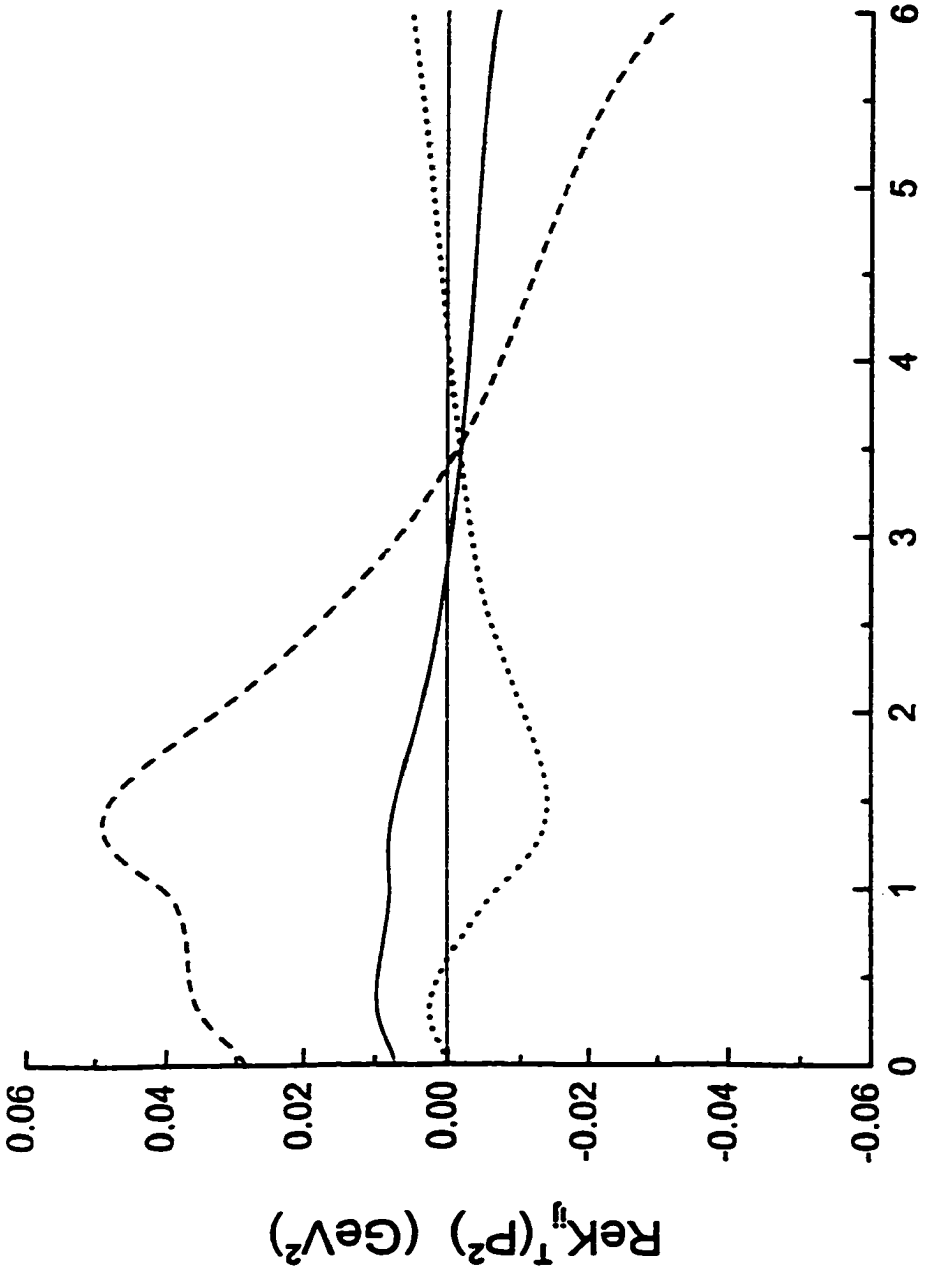

Figure 25

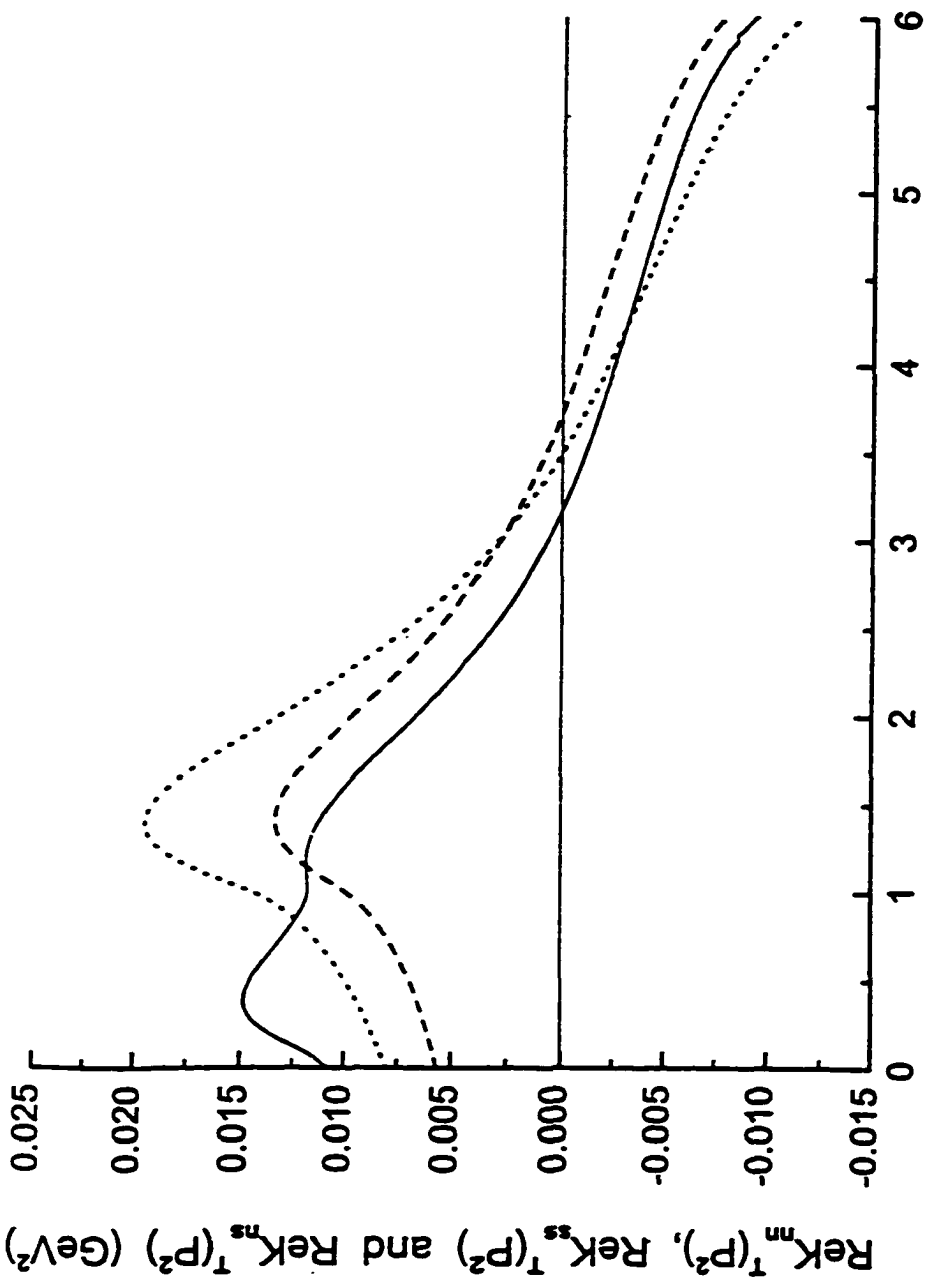

Figure 26

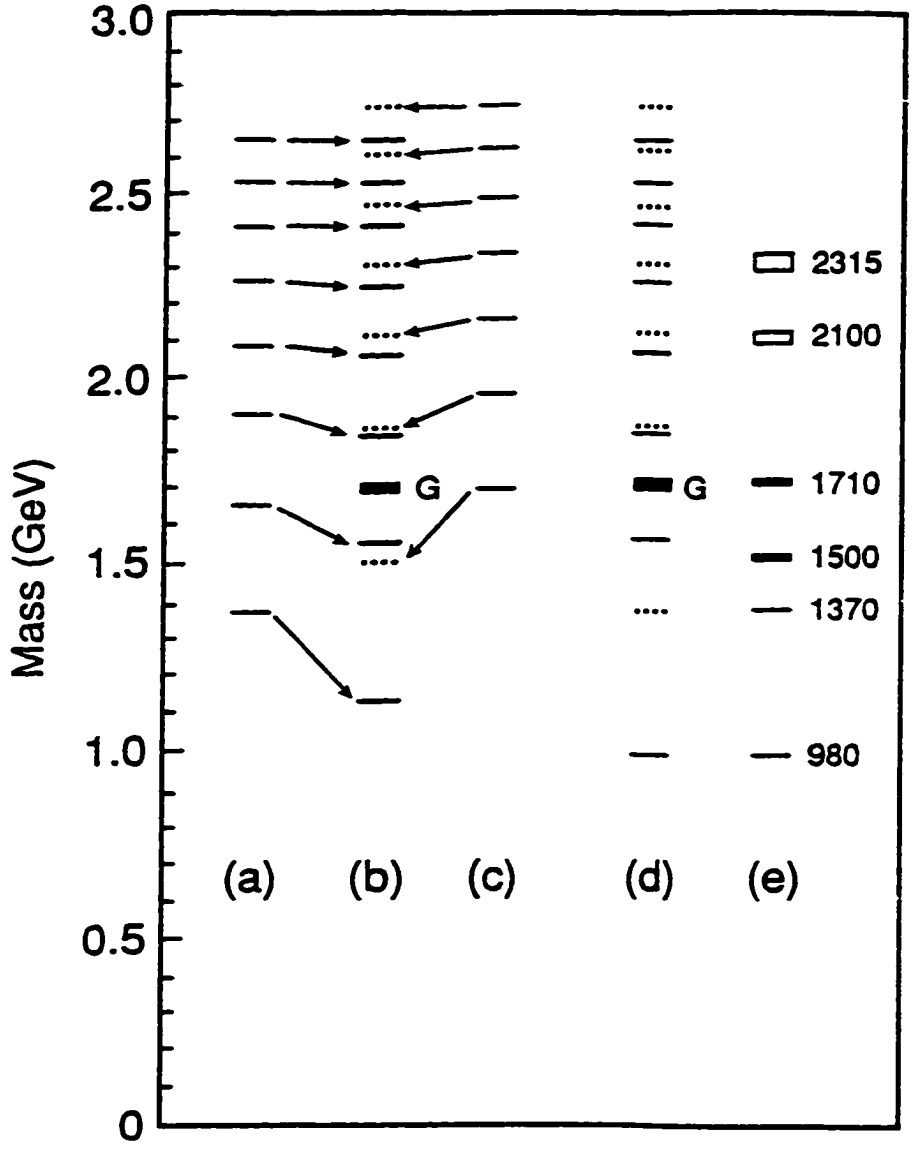

Figure 27

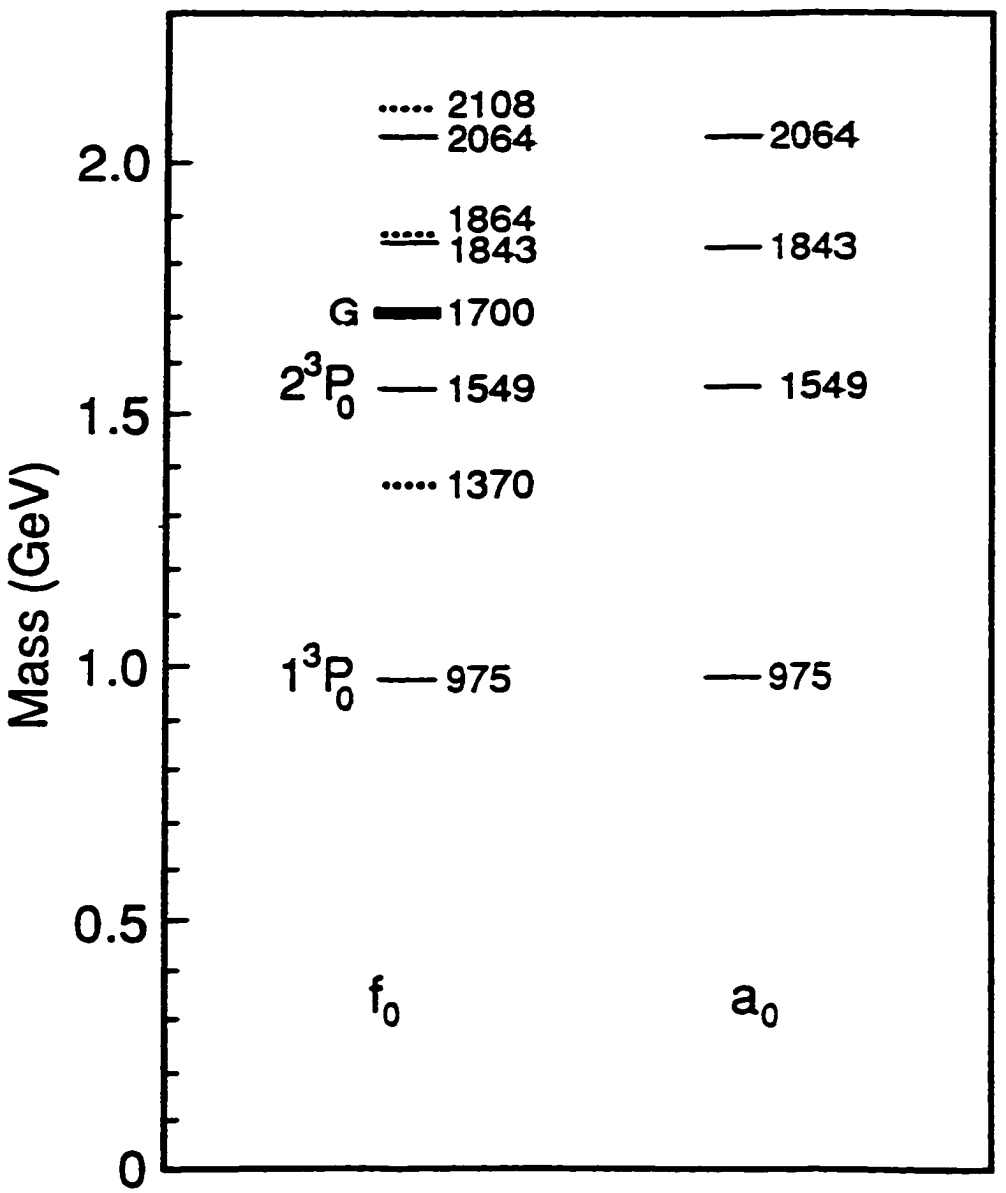

Figure 28

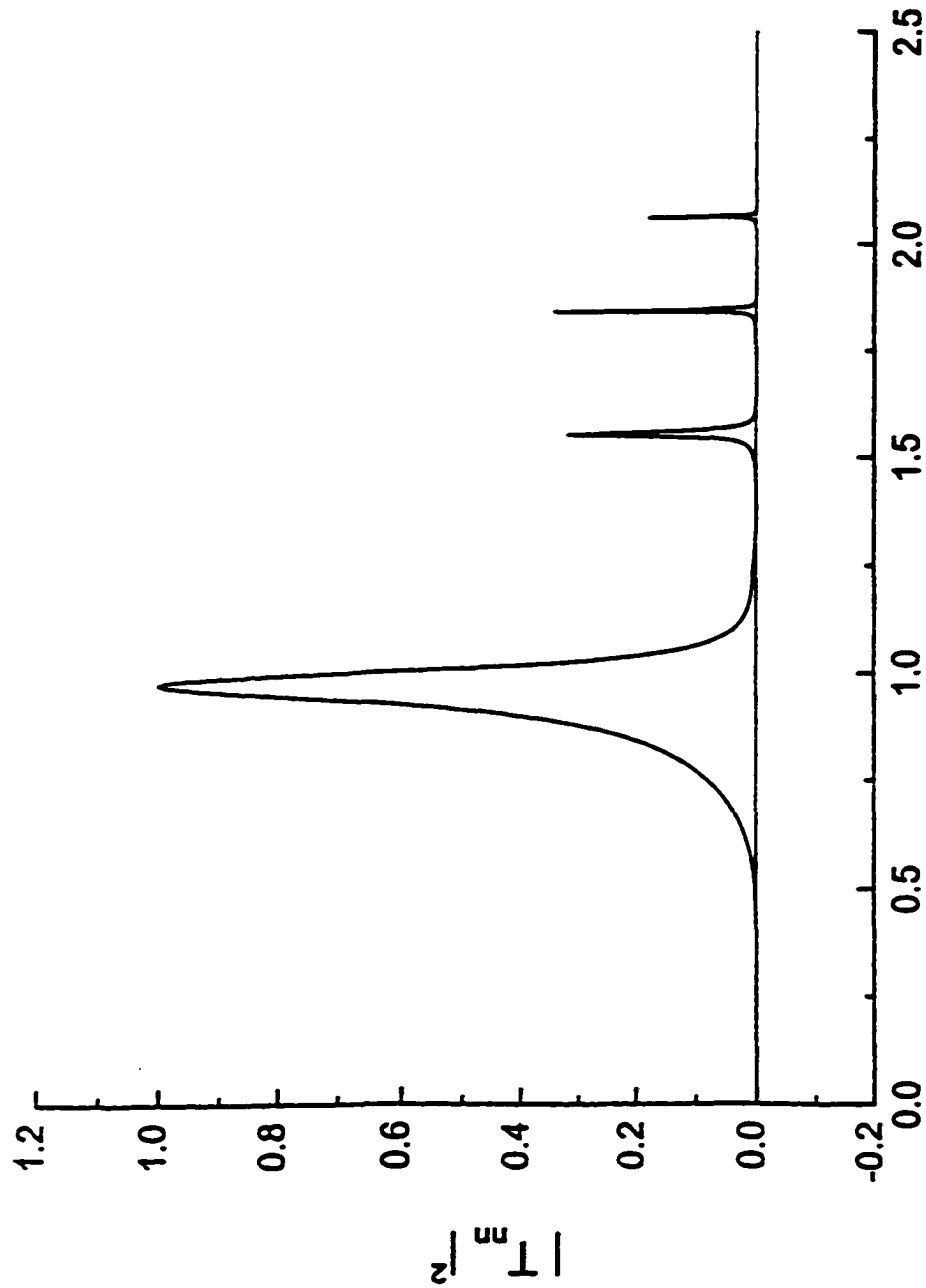

Figure 29

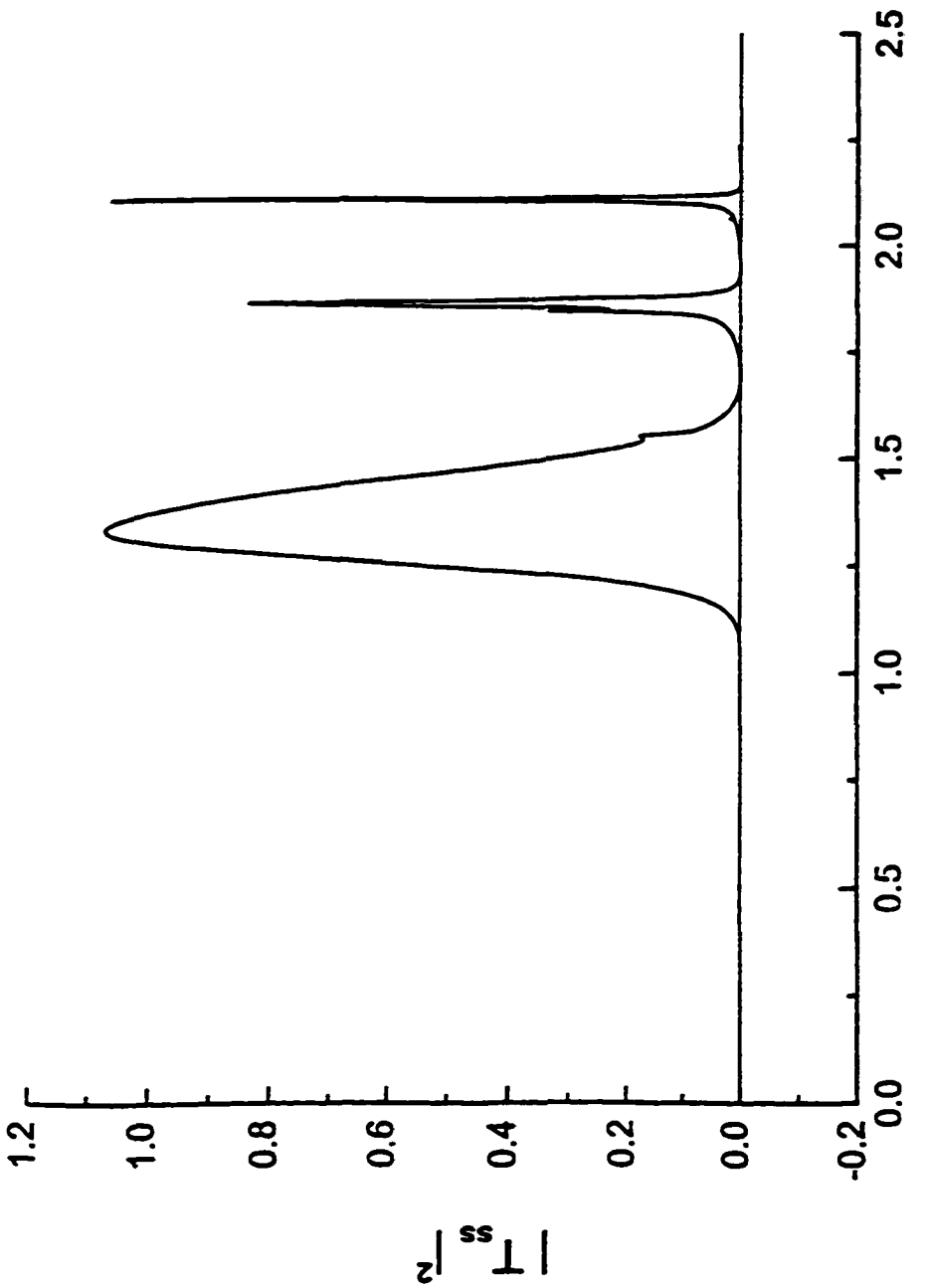

Figure 30

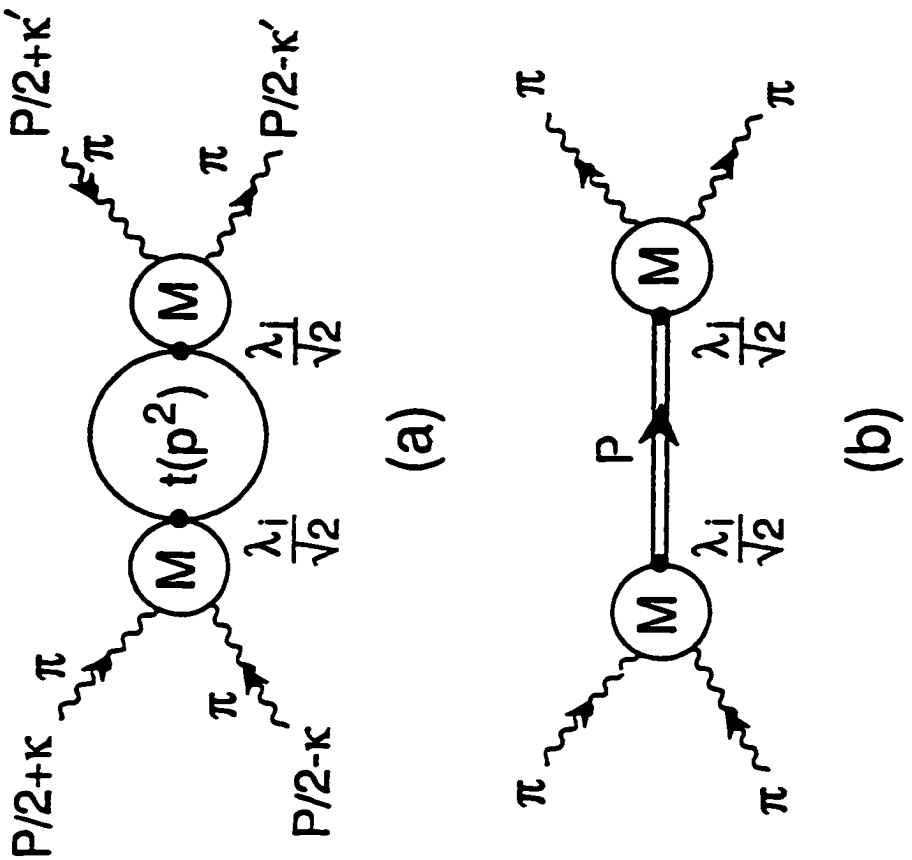

Figure 31

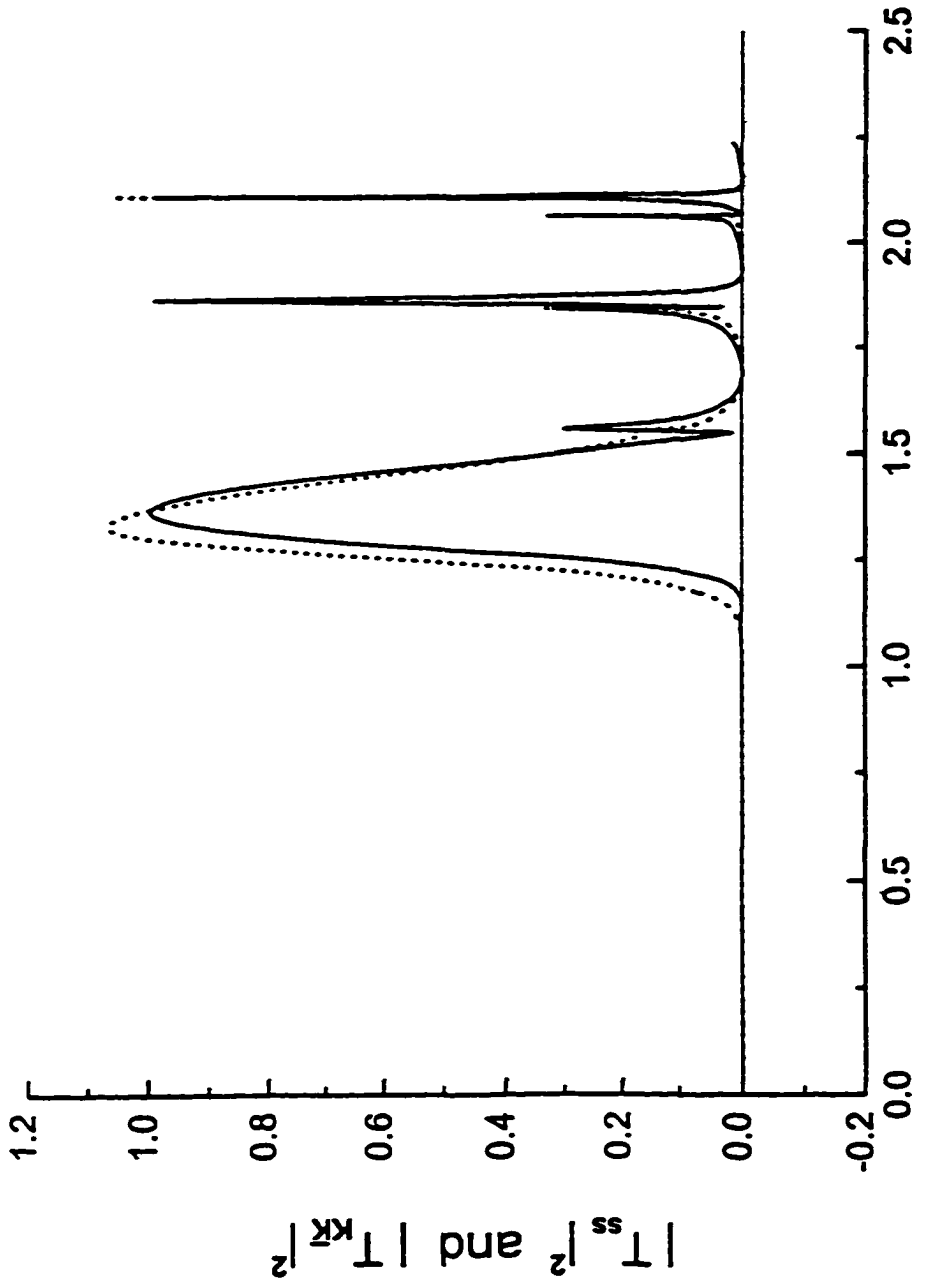

Figure 32

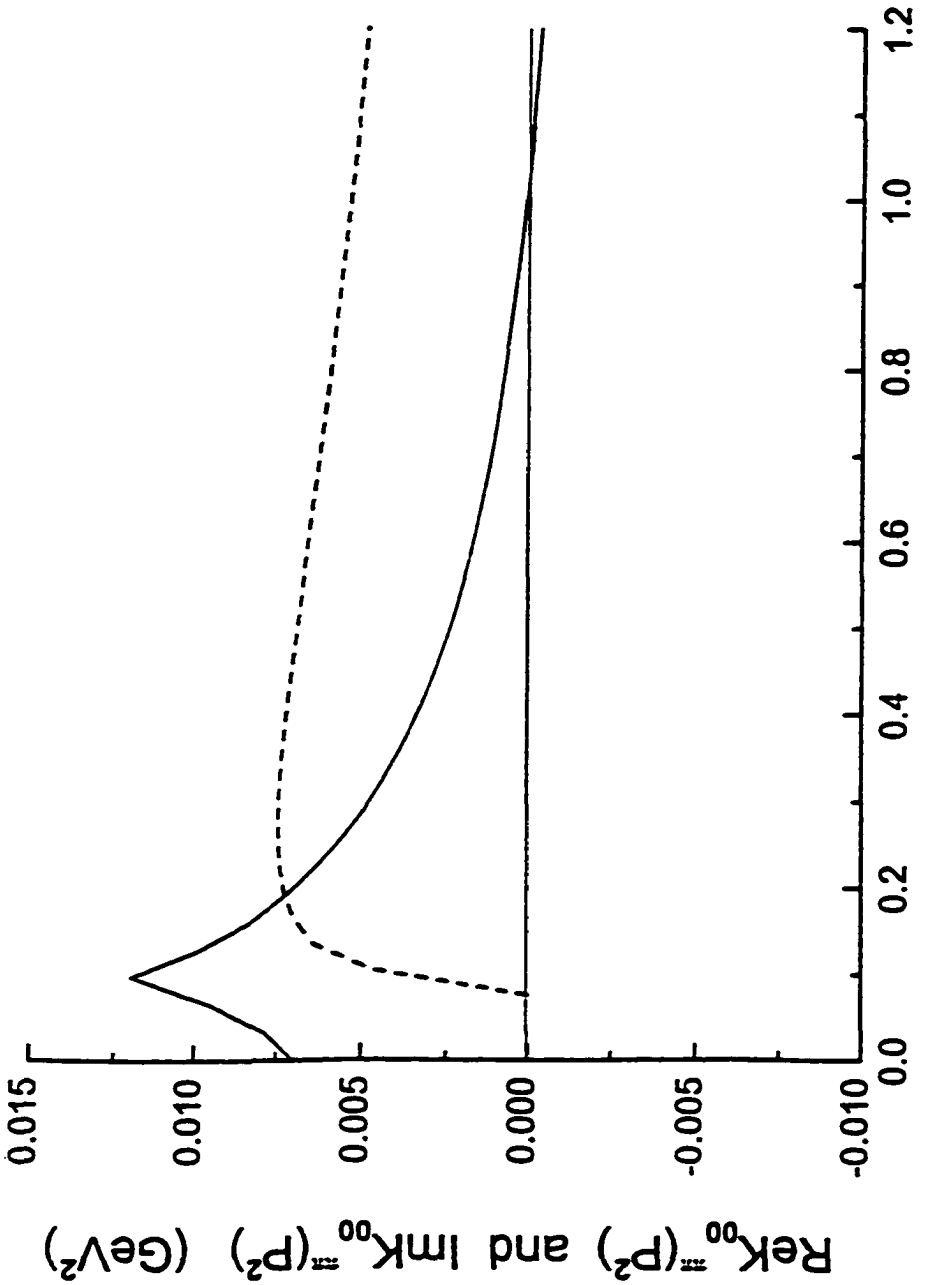

Figure 33

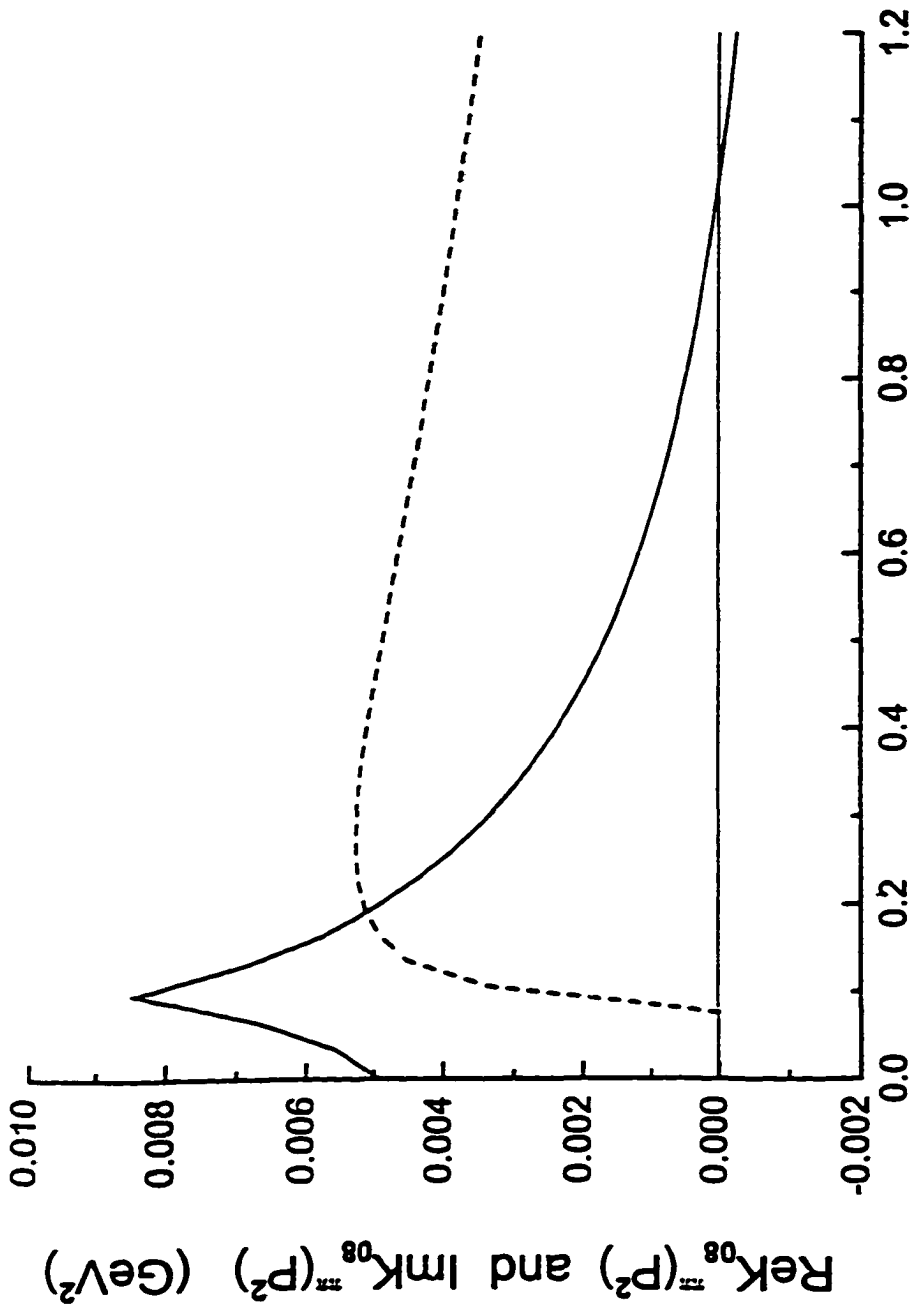

Figure 34

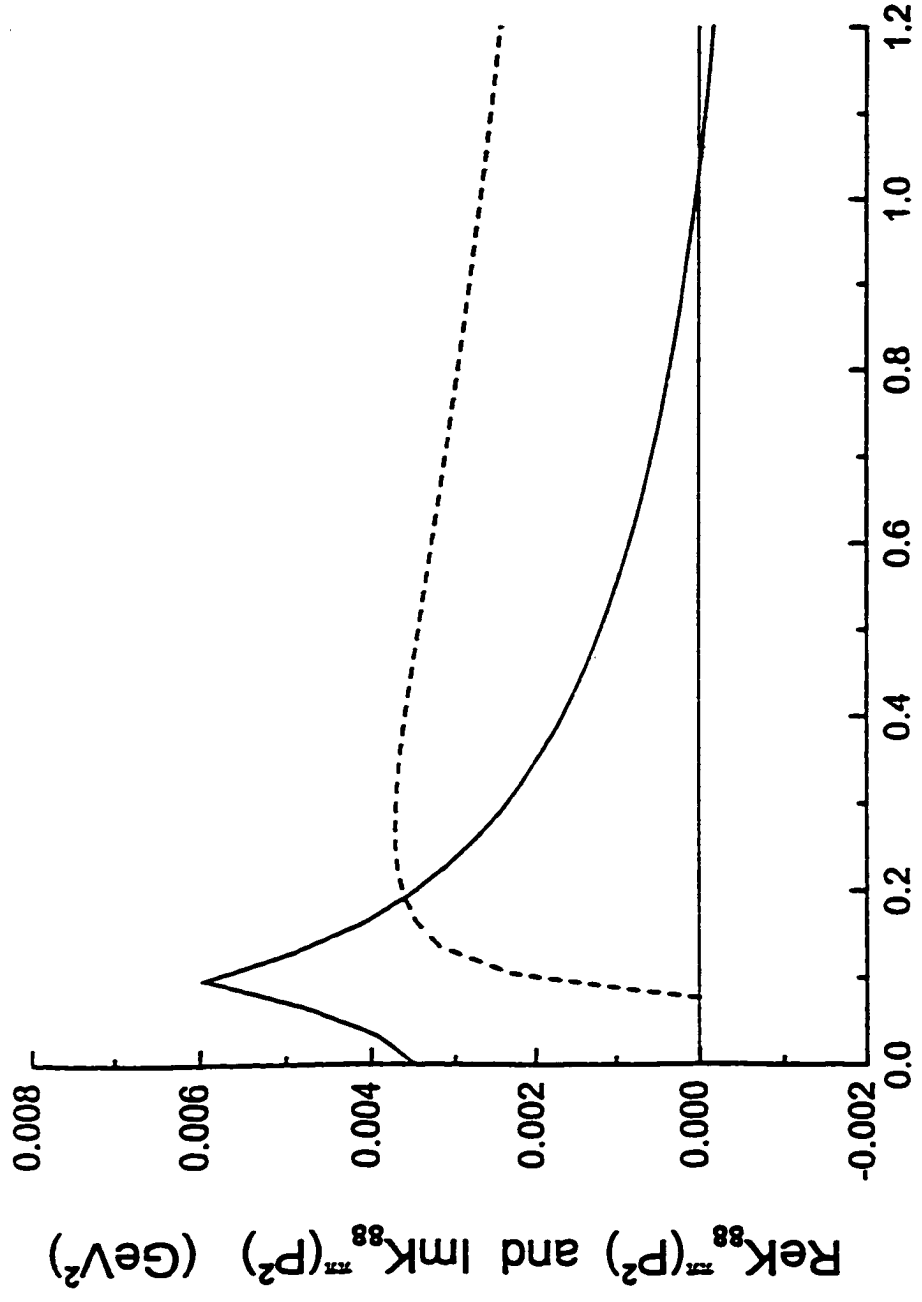

Figure 35

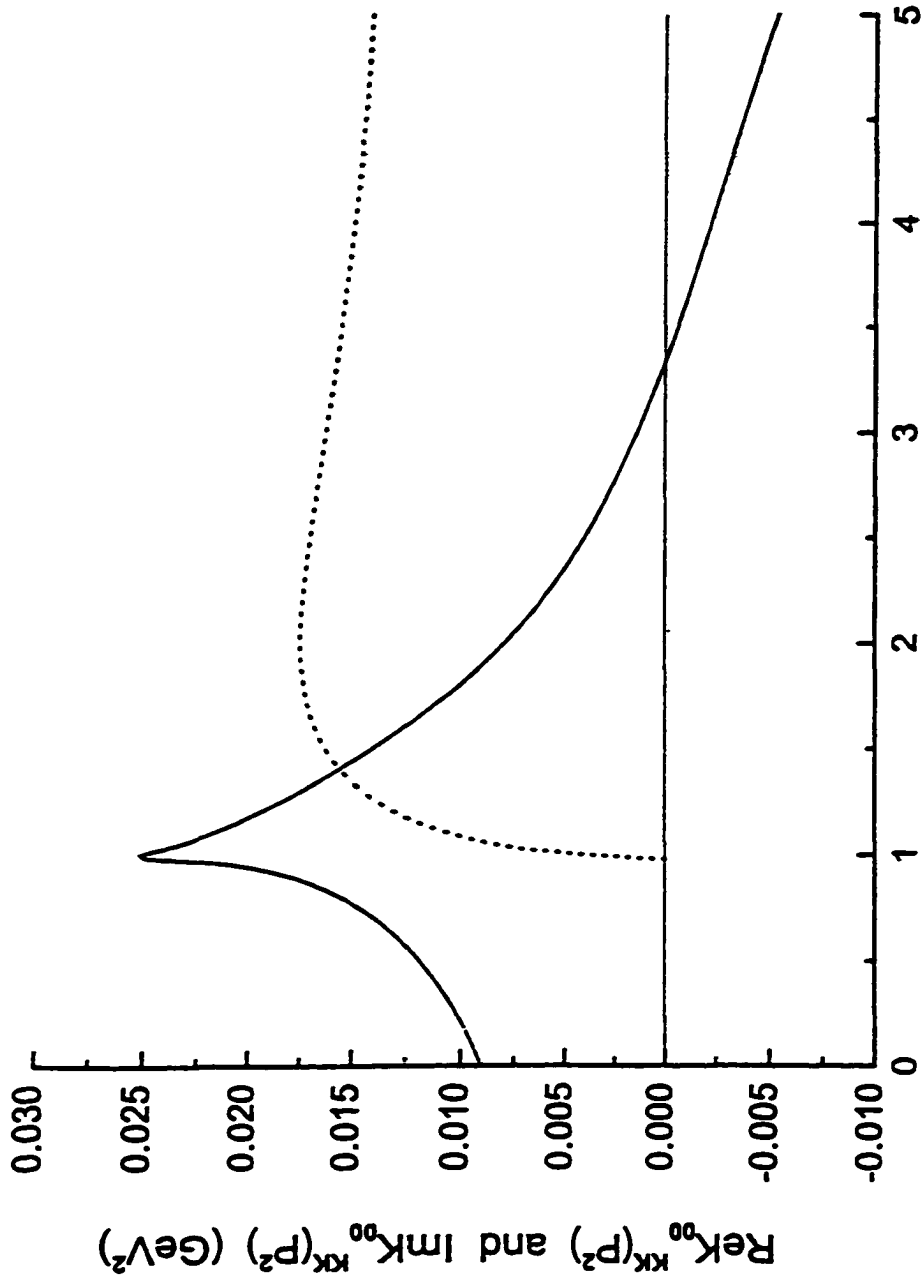

Figure 36

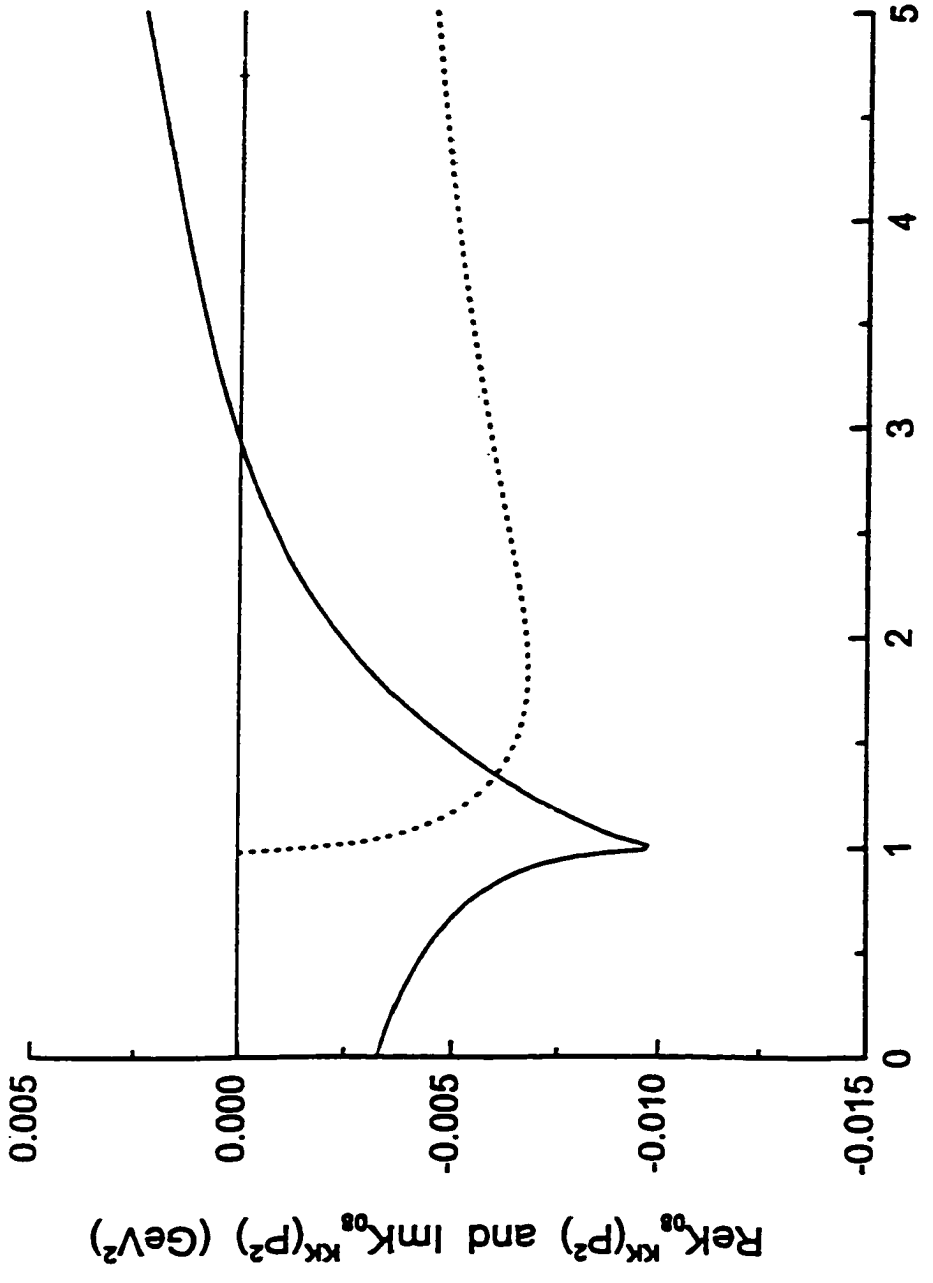

Figure 37

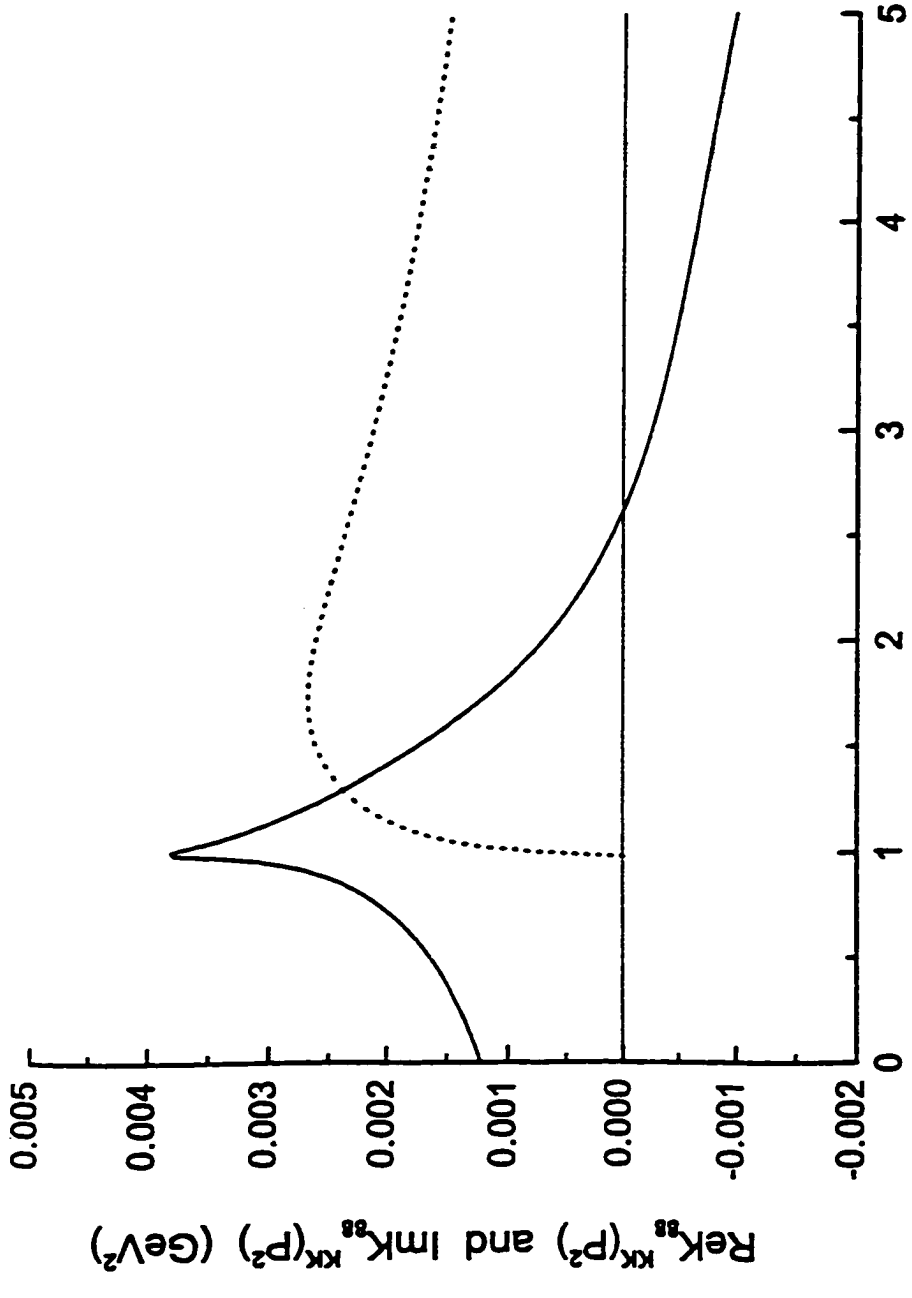

Figure 38

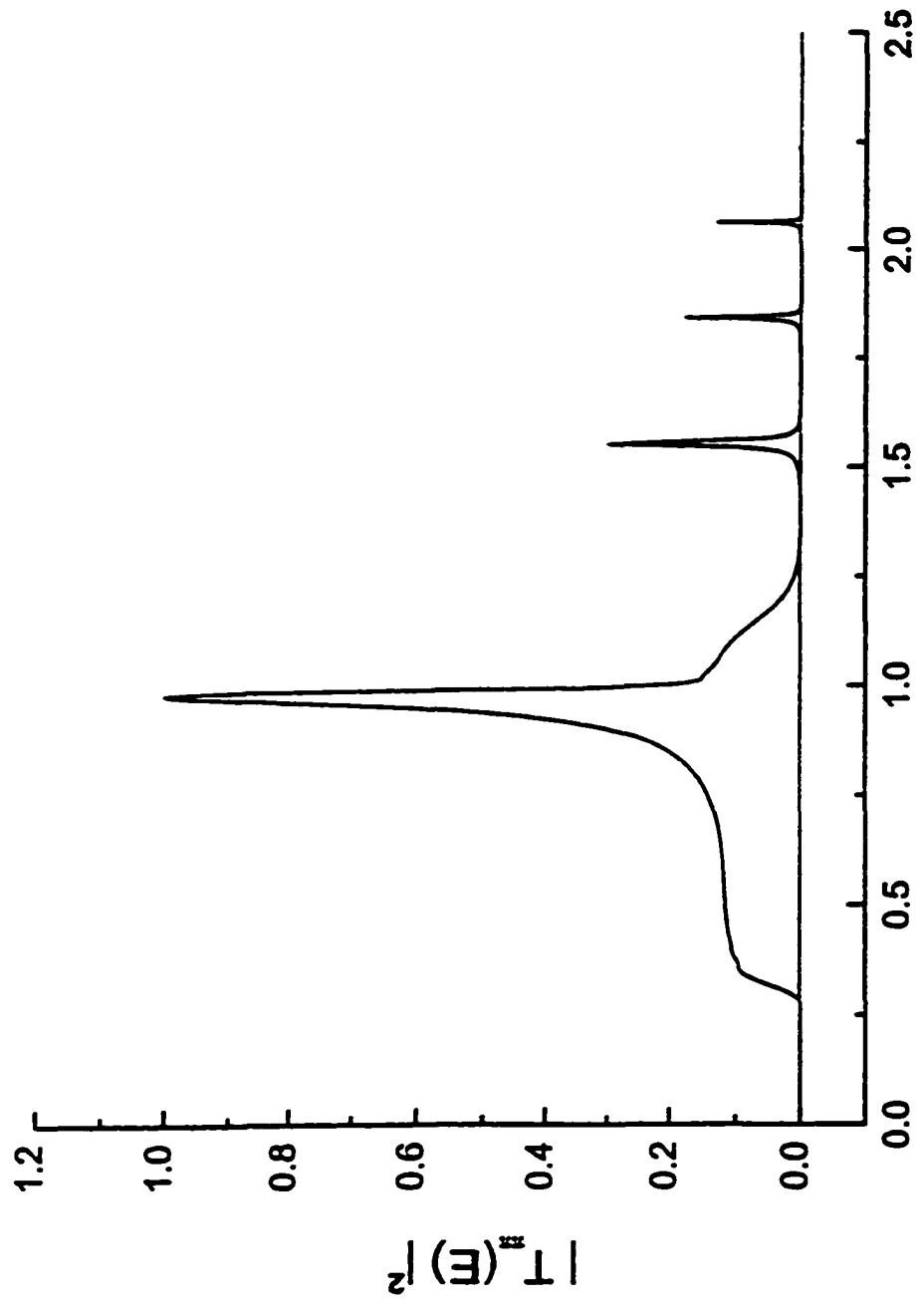

Figure 39

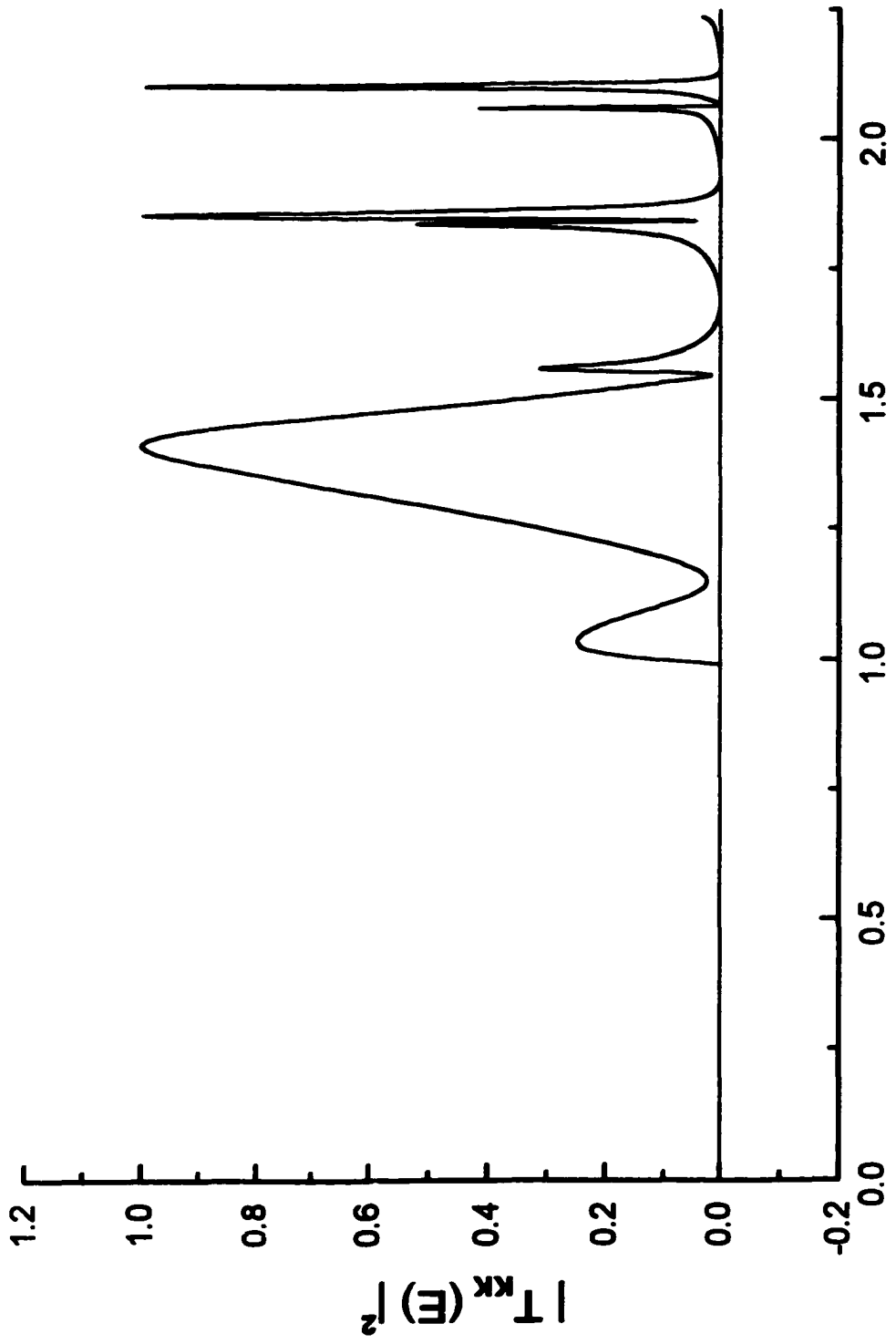

Figure 40

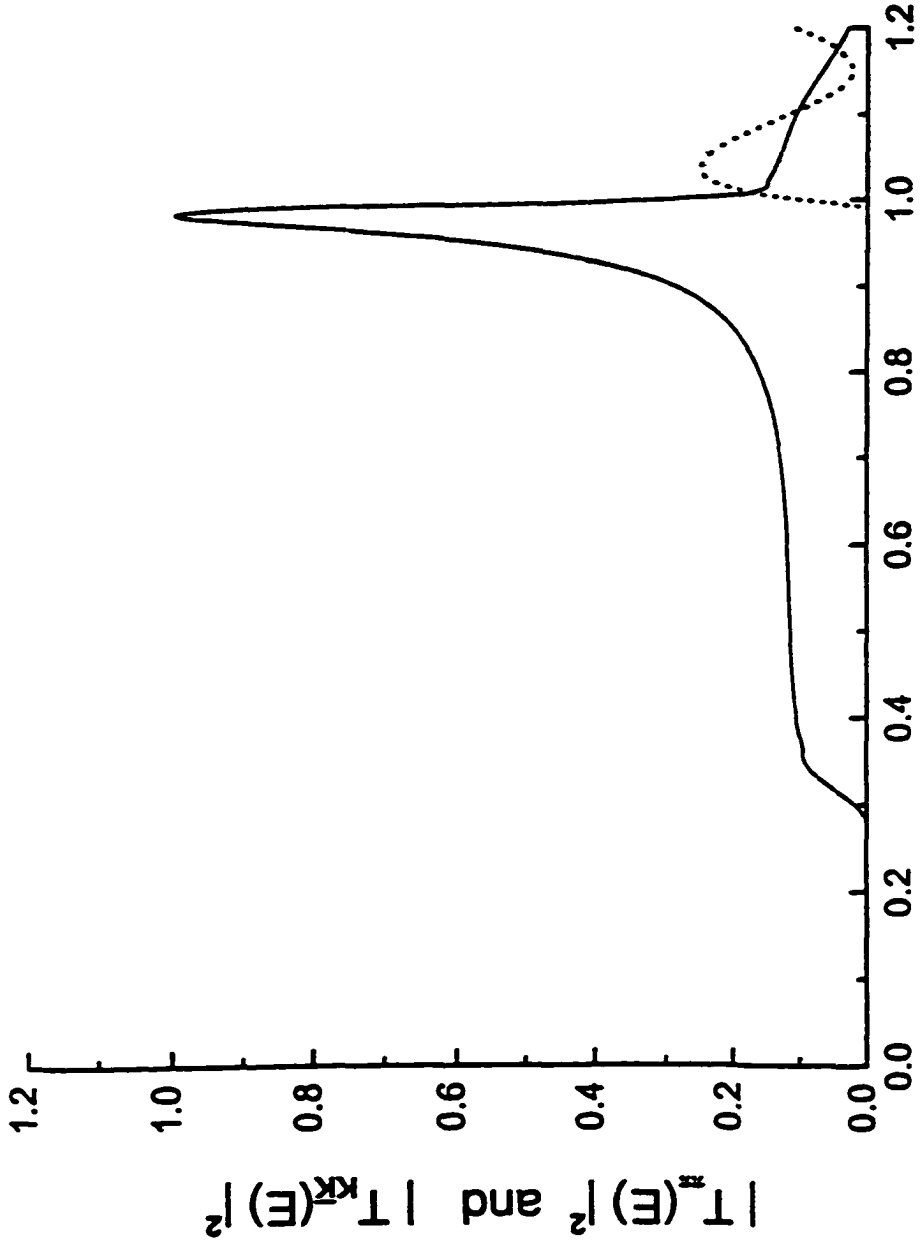

Figure 41

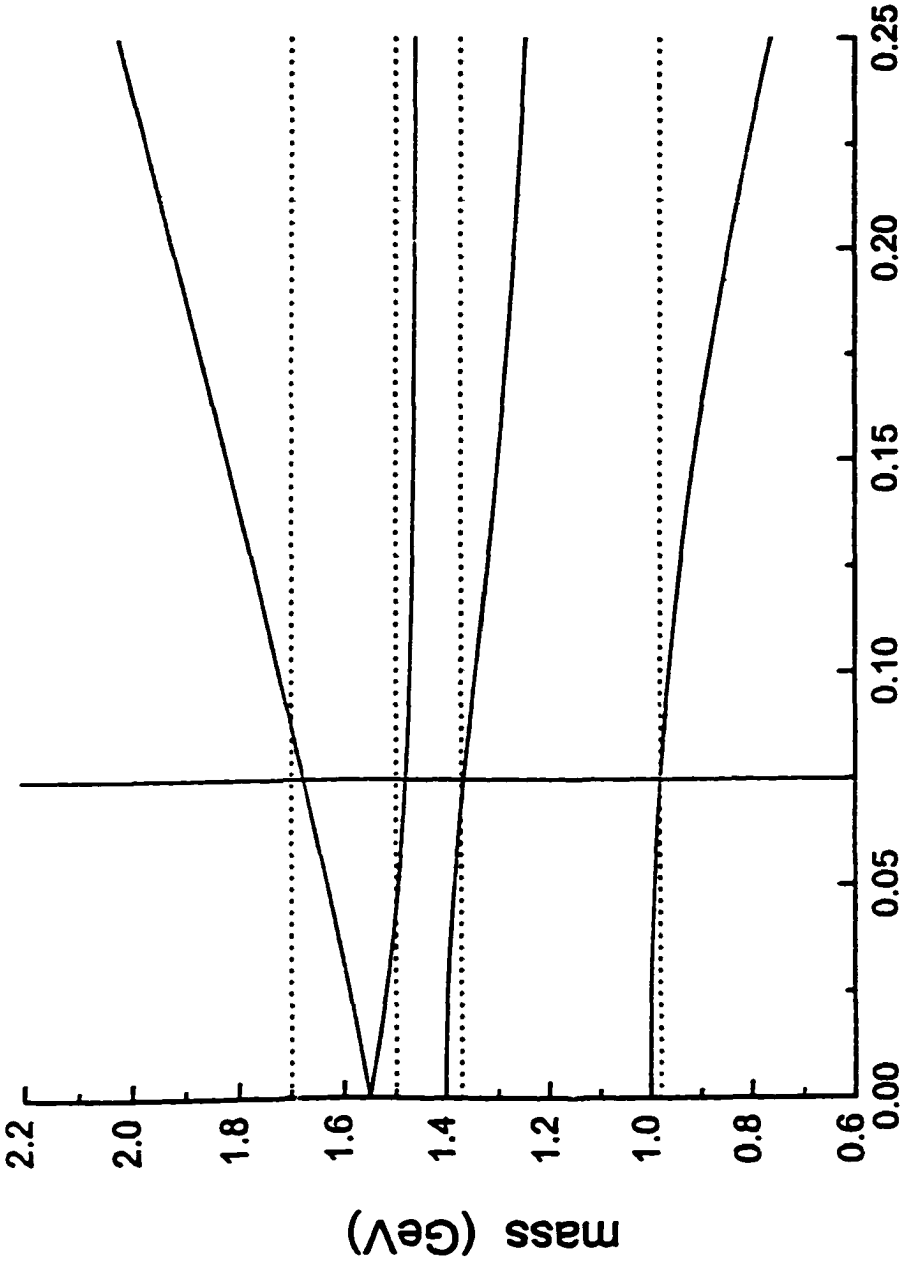

Figure 42

References

[1] Bo Huang, Xiang-Dong Li, and C.M.Shakin, Phys. Rev. C58, 3648 (1998).

[2] L. S. Celenza, Bo Huang, and C.M.Shakin, Phys. Rev. C59, 1041 (1999).

[3] L. S. Celenza, Bo Huang, and C.M.Shakin, Phys. Rev. C59, 1030 (1999).

[4] L. S. Celenza, Bo Huang, and C.M.Shakin, Phys. Rev. C59, 1700 (1999).

[5] L. S. Celenza, Bo Huang, and C.M.Shakin, Phys. Rev. C59, 2814 (1999).

[6] For reviews of the NJL model, supplemented by the 't Hooft interaction, see, S. P. Klevansky, Rev. Mod. Phys. 64, 649(1992); U. Vogl and W. Weise, Prog. Part. Nucl. Phys. 27, 195(1991).

[7] S. Klimt, M. Lutz, U. Vogl, and W. Weise, Nucl. Phys. A516, 429(1990).

[8] Particle Data Group, R. M. Barnett *et al*, Phys. Rev. D54, 1(1996).

[9] L.S. Celenza, Xiang-Dong Li, and C.M. Shakin, Phys. Rev. C 55, 1492(1997).

[10] P. Jain and H. J. Munczek, Phys. Rev. D48, 5403(1993); H. J. Munczek and P. Jain, Phys. Rev. D46, 438(1992); J. Praschifka, C. D. Roberts, and R. T.Cahill, Phys. Rev. D36, 209(1987); P. C. Tandy, Prog. Part. Nucl. Phys.39, 117(1994).

[11] L.S. Celenza, Xiang-Dong Li, and C.M. Shakin, Phys. Rev. C 55, 3083(1997); *ibid.* 56, 3326(1997).

[12] M. Suzuki, Phys. Rev. D47, 1252(1993).

[13] N. A. Törnquist, Zeit. f. Physik C68, 647(1995).

[14] M. K. Volkov and C. Weiss, Phys. Rev. D56, 221(1997).

[15] P. Maris and C. D. Roberts, Phys. Rev. C56, 3369(1997); P. Maris, C. D. Roberts, and P. Tandy, Phys. Lett. B420, 267(1998); C. J. Burden, Lu Qian, C. D. Roberts, P. Tandy, and M. J. Thompson, Phys. Rev. C55, 2649(1997); M. R. Frank and C. D. Roberts, Phys. Rev. C53, 390(1996); C. D. Roberts, Nucl. Phys. A605, 475(1996); C. D. Roberts and A. G. Williams, Prog. Part. Nucl. Phys. 33, 477(1994).

[16] S. Godfrey and J. Napolitano, Light Meson Spectroscopy, LANL archive:hep-ph/9811410(1998)-submitted to Reviews of Modern Physics.

[17] L. S. Celenza, Bo Huang, Huangsheng Wang, and C.M.Shakin, Phys. Rev. C60, 025202 (1999).

[18] C. R. Münz, J. Resag, B. C. Metsch, and H. R. Petry, Nucl. Phys. A578, 418(1994); J. Resag, C. R. Münz, B.C. Metsch, and H. R. Petry, Nucl. Phys. A578, 397(1994).

[19] C. R. Münz, Nucl. Phys. A609, 364(1996).

[20] C. Ritter, B. C. Metsch, C. R. Münz and H. R. Petry, Phys. Lett. B380, 431(1996).

[21] E. Klempt, B. C. Metsch, C. R. Münz and H. R. Petry, Phys. Lett. B361, 160(1995).

[22] C. R. Münz, B. C. Metsch and H. R. Petry, Phys. Rev. C52, 2110(1995).

[23] T. Meissner and L. S. Kisslinger, Phys. Rev. C57, 1528(1998).

[24] T. Van Rhee, Acta Phys. Polonica, B29, 3401(1998); S. Braccini, Contribution to LEAP98, Villasimus, Italy (Sept. 1998)-LANL archive hep-ex/9811017.

[25] L. S. Celenza, Bo Huang, Huangsheng Wang, and C.M.Shakin, Phys. Rev. C60, 035206 (1999).

[26] L. S. Celenza, Bo Huang, Huangsheng Wang and C.M.Shakin, Brooklyn College Report: BCCNT99/031/279 (1999).

[27] L. S. Celenza, Bo Huang, Huangsheng Wang and C.M.Shakin, Brooklyn College Report: BCCNT99/062/280R1 (1999) - submitted for publication.

[28] L. S. Celenza, Bo Huang, Huangsheng Wang and C.M.Shakin, Brooklyn College Report: BCCNT99/061/281R1 (1999) - submitted for publication.

[29] C. Caso *et al.* (Particle Data Group), Eqr. Phys. Jour. C3, 1(1998).

[30] C. Amsler and F. Close, Phys. Rev. D53, 295(1996).

[31] C. Amsler, Rev. Mod. Phys. 70, 1293(1998) - See Section X.

[32] W. Lee and D. Weingarten, Nucl. Phys. Proc. Suppl. 53, 232(1997).

[33] W. Lee and D. Weingarten, LANL archive:hep-lat/9805029(1998).

[34] W. Lee and D. Weingarten, Nucl. Phys. Proc. Suppl. 73, 249(1999).

[35] T. Barnes, Radial Excitations-Summary Session, WHS99-Frascati, 8-12(March 1999).

[36] M. Strohmeier-Prešiček, T. Gutscke, R. Vink Mau and Amand Faesler, Phys. Rev. D60, 054010(1999).

[37] S. Narison, Nucl. Phys. B509, 312(1998).

[38] J. Sexton, A. Vaccarino and D. Weingarten, Nucl. Phys. Suppl. 47, 128(1996).